27

THE BEHAVIOUR OF ELECTRON SWARMS IN POLYATOMIC GASES

COLIN W. DUNCAN

Ph.D. Thesis

University of Stirling

December 1971

ProQuest LLC.
789 East Eisenhower Parkway
P.O. Box 1346
Ann Arbor, MI 48106 – 1346

ABSTRACT

This work is concerned with collision processes occurring between simple polyatomic gas molecules and electrons of low incident kinetic energy (0-5 eV).

The principal methods of experimental investigation and previous work in the field are reviewed. An outline of fundamental concepts of wave-mechanical scattering theory is presented and applications of theory to low energy electron-molecule collisions are reviewed and discussed. After consideration of the shortcomings of existing theories in relation to triatomic and larger molecules it is concluded that appreciable direct excitation of infrared-active vibrational modes is to be expected.

A description is given of the design and construction of a Townsend-Huxley type diffusion apparatus to measure the ratio of diffusion coefficient to mobility (D/μ) for electrons in gases. The principal feature of this apparatus is its suitability for accurate measurement in low-energy swarms achieved by choice of geometry, mechanical accuracy, uniformity of electric field and use of ultra-high vacuum techniques.

The results obtained using this apparatus are presented as D/μ values in methane, ethylene, acetylene, cyclopropane and hydrogen

sulphide. In each case the measurements extend to considerably lower values of field strength/pressure ratio than hitherto published results.

An account is given of the method of swarm transport coefficient analysis by solution of the Boltzmann equation for trial cross-section values. A computer program is described which automatically adjusts the cross-sections until they are consistent with experimental data.

For each gas studied, the results of the analysis are given. For methane and ethylene, the momentum-transfer cross-section is derived along with two inelastic cross-sections corresponding to excitation of infrared-active vibrational modes. For acetylene and cyclopropane only one vibrational cross-section is used. The likely contributions from other inelastic processes are discussed.

The results suggest that the large inelastic energy losses in these molecules can be explained by vibrational excitation cross-sections peaking just above threshold energy with magnitudes of the order of 10^{-16} cm^2. No evidence is found to support the idea that this excitation may occur via an intermediate negative ion "resonance".

CONTENTS

CHAPTER I

REVIEW OF ELECTRON-MOLECULE COLLISIONS

I.1. INTRODUCTION

The study of electron-molecule collisions can be considered to affect two principal areas of scientific understanding. Firstly, it can give important information on molecular structure, both in the ground electronic state and in excited and ionic states. Secondly, it gives insight into the dynamics of molecular processes. The former effects have been exploited by the development of standard techniques for structural investigation, such as electron diffraction, mass spectrometry, and electron-impact spectrometry, while the latter have stimulated the development of a vast new field of theoretical physics, with important consequences to the understanding of all fundamental processes.

The possible consequences to an electron molecule encounter may be classified as follows.

(a) Elastic scattering, in which there is no change in the internal energy state of the molecule.

(b) Inelastic scattering with excitation of the molecule to a state differing in one or more of its rotational, vibrational, or electronic quantum numbers. The reverse of this process (i.e. de-excitation) is often referred to as superelastic

scattering.

(c) Ionisation to either a positive or negative ion, this being a special case of (b). As with electronic excitation, ionisation may lead to molecular dissociation.

The above classification is somewhat empirical as it depends to a certain extent on the experimental system. Thus, if a negative ion formed lives long enough to be detected as such, the collision will be classified as an electron attachment, whereas if the lifetime is short and the ion undetected, the collision will usually be described as elastic or inelastic according to the kinetic energy of the emitted electron.

Quantitative description of collisions is made in terms of the collision cross-section[1]. The total cross-section Q is defined as the probability of the projectile colliding in travelling unit distance through a gas of unit density. Hence the number of electrons scattered from a beam of current density I in travelling a distance dx is given by

$$-dI = NQIdx \qquad (I.1)$$

As it is often possible to measure the angular distribution of scattered electrons, the scattering phenomenon is further described in terms of the differential cross-section $\sigma(\theta)$, which is the probability per unit solid angle of scattering through an angle θ. This is related to the total cross-section by

$$Q = \int_{\omega} \sigma(\theta) d\omega = \int_0^{2\pi}\int_0^{\pi} \sigma(\theta) d\theta d\phi \qquad (I.2)$$

using a spherical polar co-ordinate system centred on the target.

If the collisions are classified into distinct processes, the total cross-section is the sum of the individual cross-sections for each process:

$$Q = \sum_{i=0}^{n} Q_i \qquad (I.3)$$

A similar relationship holds for the differential cross-sections.

A cross-section definition of particular importance in electron swarm analysis is the momentum-transfer cross-section Q_m (also called the diffusion cross-section). For elastic scattering of an electron of mass m through an angle θ by a molecule of mass M, where $M \gg m$, the fractional loss of kinetic energy by the electron is[2]

$$\lambda \simeq 2(1 - \cos\theta)\, m/M \qquad (I.4)$$

In terms of the differential elastic cross-section $\sigma_o(\theta)$, the average fractional energy loss per collision is therefore

$$\bar{\lambda} = \frac{2m/M}{Q_o} \int_0^{\pi}\int_0^{2\pi} (1-\cos\theta)\, \sigma_o(\theta) \sin\theta d\theta d\phi \qquad (I.5)$$

The total momentum-transfer cross-section is defined as

$$Q_m = \int_0^{\pi}\int_0^{2\pi} (1-\cos\theta)\, \sigma(\theta) \sin\theta d\theta d\phi \qquad (I.6)$$

so the mean fractional energy loss for elastic collisions becomes

$$\bar{\lambda} = \frac{2m}{M} \cdot \frac{Q_m}{Q_o} \qquad (I.7)$$

Q_m is therefore the probability, per unit distance and unit target density, of collisional transfer of a fraction $2m/M$ of electron energy to target kinetic energy. It is thus similar to the total cross-section but weighted according to the anistropy of the collisions.

The above definitions are purely phenomenological, no assumptions being made about the mechanisms of scattering or any intermediate states formed.

This work is concerned almost entirely with collisions by electrons of incident energy ranging from thermal (.037 eV at 300°K) to a maximum of around 5 eV. This is well below the first ionisation potential for most simple molecules, and little attention will be paid to electronic excitation. The chief processes involved, besides elastic scattering, are vibrational and rotational excitation and de-excitation of the molecules. In this chapter the experimental and theoretical methods for investigating such processes are reviewed, to provide a background for the interpretation of the results of this work.

I.2. EXPERIMENTAL METHODS

A comprehensive review of the experimental methods is included in the works by Massey and Burhop[2,3]. The experiments fall into two main categories: direct single collision beam experiments; and a variety of multiple-collision experiments, of which those generally referred to as "electron swarm" experiments constitute the most important group at low energies. Although the present work is not concerned with electron

beams, experiments of this type approach closest to giving a detailed view of the scattering process, and their results must constantly be borne in mind when interpreting swarm work. A brief description of beam experiments will therefore be given in I.2.1. Historically, both types of experiment originated at roughly the same time, and have been developed in parallel as technological and theoretical advances have enabled an increasing amount of information to be extracted from their execution.

I.2.1. Electron beam experiments

The first quantitative measurements of scattering were performed by Ramsauer[2] in 1921, who simply measured total cross-sections by the attenuation of a beam in passing through a gas. The method was later adapted by Golden and Bandel[4]. Although sharp structure is not generally observed in total cross-sections several interesting features were apparent, one being the observation of a marked transparency in the inert gases Ar, Kr, and Xe at low impact energies ($\sim$1 eV). This phenomenon was discovered independently by Townsend[5], and became known as the Ramsauer-Townsend effect. The quantum mechanical prediction of this effect, which remained unexplained classically, was held to be a convincing early proof of the theories of wave mechanics. Another unexpected effect was the presence of quite sharp maxima in the cross-sections of N_2, CO, and N_2O at around 2 eV. More easily explained however were the steep rises as low impact energies were approached in

the cross-sections of dipolar molecules, a consequence of the velocity dependence of electron-dipole scattering[3].

The advent of electrostatic analysers and improved electron-optical systems increased energy resolution and encouraged the study of inelastic processes by energy analysis of the scattered electrons. Many experiments of this type have been performed[2,3,6], using one or more electrostatic analysers to measure fixed or variable angle scattering. One experimental difficulty encountered is that as resolution is increased and energy lowered, intensity falls off rapidly and experiments become increasingly difficult to perform. Nevertheless, recent experiments have produced good energy-loss spectra at impact energies of a volt or two and in one extreme case Ehrhardt and Linder[7] have resolved the structure due to excitation of discrete rotational levels accompanying the vibrational excitation of H_2.

In general, however, observation of near-threshold excitation of molecular vibration is beyond the scope of most beam techniques, and attention has been concentrated on electronic transitions. At high impact energies ($>$ 200 eV) the principal feature is the observation of optically allowed (dipole) transitions[8], in accordance with the general principle that high-energy electrons resemble electromagnetic radiation in behaviour. At intermediate energies (50 - 200 eV) electric quadrupole transitions also occur[9], and at still lower energies spin-forbidden (singlet-triplet) transitions appear[6,10]. The latter are interpreted as occurring through the mechanism of electron exchange; the probability

of excitation increases as impact energy decreases to threshold and as scattering angle increases. This phenomenon is of great importance to the study of molecular electronic structure as it permits the identification of states not normally observed in electromagnetic spectra.

A rather different type of beam technique which has yielded valuable results is the "electron trap" introduced by Schulz[11]. This involves trapping and collecting inelastically scattered electrons which have lost practically all of their kinetic energy in a shallow electrostatic potential well of around 100 mV depth. Scanning the incident energy at fixed well depth produces a threshold spectrum in which the peaks are proportional to the magnitudes of the total inelastic cross-sections in the region immediately above threshold. The technique detects both optically allowed and spin-forbidden transitions with similar intensities, and also extends into the region of pure vibrational excitation. Many simple molecules, including several hydrocarbons[12], have been studied by this method.

A consequence of the improvement in beam resolution over that of early experiments was the discovery of "resonances" in the early 1960's[13]. These were attributed to the formation of short-lived negative ion states and manifested themselves as marked structure in both elastic and inelastic cross-sections. Some discussion of molecular resonances will be presented in sections I.3.4. and I.4.

Low-energy electron beam experiments tend to be limited by uncertainty in both the energy scale and the absolute magnitude of the

cross-sections. In this respect they are complemented by swarm experiments, which although inherently incapable of resolving rapid variations in cross-section magnitude and type, do have an established energy scale and are capable of giving absolute magnitude with high accuracy.

I.2.2. Electron swarm experiments: Introduction

An electron swarm may be defined as a current of electrons moving through a gas in an electric field under such conditions that the electron mean free path is much smaller than the apparatus dimensions. Each electron therefore undergoes many collisions and its motion is essentially random, modified only by an overall drift in the field direction. This causes a broad distribution of electron velocities, and so electrons of a specific energy cannot be studied as in beam experiments, it being only possible to observe averaged macroscopic properties. Typical conditions for swarms are gas pressures from ~ 1 torr to greater than atmospheric, and fields of up to several hundred V cm^{-1}.

Although information on collisions has been gained from swarms in A.C. fields[2], the present work is concerned only with swarms moving in uniform D.C. fields. Under this condition a swarm has two useful measurable properties ("transport coefficients"): the drift velocity (W) and the diffusion coefficient (D). These are defined as follows.

$$W = \int_0^\infty \underline{v}_z \, f(\underline{v}) \, d\underline{v} \qquad \text{(I.8)}$$

where $f(\underline{v})$ = fraction of electrons having velocity $\underline{v}$.

$$D = -\underline{J} / \underline{\nabla} n \qquad (I.9)$$

(in the absence of external forces),

where $\underline{J}$ = electron current density, n = electron density.

I.2.3. Measurement of transport coefficients

(a) Drift velocity W: The first drift velocity measurements were made indirectly by observing the deflection of a swarm in a transverse magnetic field[5], but this method was later superceded by direct time-of-flight techniques, of which the Bradbury-Nielson shutter method[14] has yielded most of the available accurate data. The method employs two electron-shutter grids, spaced widely apart along the drift path, and switched in phase by a variable frequency A.C. signal. Current is transmitted only when the period of the signal is an integral sub-multiple of the swarm drift time; thus observation of current variation with switching frequency gives an accurate measure of the drift velocity.

Another well-established method[15] utilises a pulsed source and electronically measures the drift time as the delay between source and collected pulses.

(b) Diffusion coefficient D: A few experiments have measured D directly[15,16,47] but most have measured the ratio D/W, which is of great significance in the interpretation of swarm behaviour. The most widely used technique is derived from Townsend's original apparatus[5]

and is commonly called the Townsend-Huxley experiment[31]. A full description of such an apparatus, as used in the present research, is given in Chapter II. Basically the technique consists of determining the lateral spread of a swarm issuing from a small aperture by measuring the current distribution on a divided collector. This distribution is related to the ratio D/W through the appropriate solution of the diffusion equation for an applied field in the z direction.

$$D \nabla_{-n}^2 - W \frac{dn}{dz} = 0 \qquad (I.10)$$

I.2.4. Significance of transport coefficients

The relationship between the transport coefficients and the collision cross-sections can be seen from a crude semi-quantitative description[17]. For a swarm moving in a uniform field E with mean drift velocity W, the mean displacement of an electron in the field direction between collisions is

$$Wt = \frac{Eet^2}{2m} \qquad (I.11)$$

assuming isotropic scattering. Under the usual swarm condition that the mean electron speed $v \gg W$, the time between collisions t is equal to l/v, where l is the mean free path. This gives

$$W = \frac{Eel}{2mv} \qquad (I.12)$$

If λ is the mean fractional kinetic energy loss per collision,

the energy lost in travelling a distance z in the field direction is given by

$$-\Delta\epsilon = \frac{\lambda m v^3 z}{2W\overline{1}} = Eez \qquad (I.13)$$

since in a steady state the power loss is balanced by the power input from the field (Eez). Combining (I.12) and (I.13) gives

$$\lambda = 4W^2/v^2 \qquad (I.14)$$

and introducing the total cross-section $Q = 1/\overline{1}N$ (where N = gas density) yields the expression

$$W^2 = \tfrac{1}{4}(e/m)\frac{\sqrt{\lambda}}{Q}(E/N) \qquad (I.15)$$

Evidently if v can be measured, both λ and Q may be calculated. Turning to Einstein's formula for the diffusion coefficient -

$$D = \overline{v}\overline{1}/3 \qquad (I.16)$$

and using (I.12)

$$D/W \propto v^2/E \qquad (I.17)$$

If the mobility is defined as $\mu = W/E$, then

$$D/\mu \propto v^2 \quad (\propto \epsilon) \qquad (I.18)$$

Thus by combining measurements of W and D/μ, Q and λ may be at least estimated. Since for elastic collisions only, $\lambda \simeq 2m/M$, any

increase in λ over this value is a measure of the relative importance of inelastic collisions.

The foregoing expressions give both W and D/μ to be functions of E/N (and hence E/P, where P = gas pressure). This remains true even in rigorous swarm theory, except at very high pressures ($\gg 1$ atmosphere) where the mean free path becomes so short that the molecular dimensions are relatively significant[18]. Thus the chief experimental variable (apart from temperature) is E/P, usually expressed in V cm^{-1} $torr^{-1}$, and transport coefficients are normally measured as a function of this.

Variation of E/P gives control over the mean swarm energy. At zero E/P, the swarm is in thermal equilibrium with the gas,

$$\text{i.e.} \quad \tfrac{1}{2}mv^2 = 3kT/2 \tag{I.19}$$

which leads to

$$D/\mu = kT/e \tag{I.20}$$

As E/P is raised, the mean swarm energy increases, and since D/μ is a measure of this it has been called the "characteristic temperature" of the swarm. Another quantity sometimes referred to is the Townsend energy coefficient k_1, defined as

$$k_1 = \frac{D/\mu}{kT/e} \tag{I.21}$$

For a swarm with a Maxwellian velocity distribution this is simply the ratio of swarm kinetic energy to gas kinetic energy. However

the uncertainty associated with the velocity distribution and the likely confusion arising from different definitions of k_1 give it little advantage in use over D/μ, which will therefore be used throughout this work.

It is instructive to notice how the transport coefficients vary. Other things being equal, both W and D/μ increase with E/P and decrease with Q. However although D/μ decreases with λ , W increases. This is because inelastic collisions serve to reduce the random velocity of the swarm, consequently the time interval between collisions is greater and the electrons drift further in the field direction between collisions. It is this opposite polarity in the variation of W with Q and λ that allows the separation of elastic and inelastic effects.

I.2.5. Interpretation of swarm experiments

The preceding analysis is extremely crude in that it numerically combines various different averages. A correct statistical analysis has been performed which gives the following formulae:

$$W = -\frac{4\pi}{3} \cdot \frac{e}{m} \cdot \frac{E}{N} \cdot \int_0^\infty \frac{v^2}{Q_m(v)} \cdot \frac{df_o}{dv} \cdot dv \qquad (I.22)$$

$$D = \frac{4\pi}{3} \cdot \frac{1}{N} \cdot \int_0^\infty f_o \frac{v^3}{Q_m(v)} \cdot dv \qquad (I.23)$$

where f_o is the spherically symmetric term in the expansion of the electron velocity distribution function.

These expressions require knowledge of both the velocity

distribution function, and the variation of Q_m with v. If a Maxwellian distribution is assumed

$$\text{i.e.} \quad f(v) = Av^2e^{-Bv^2} \qquad (I.24)$$

Q_m and λ may be calculated provided Q_m is assumed to vary slowly with v. This will be a reasonable approximation where the swarm has near-thermal energy (low E/P), but at higher energies the error introduced cannot be estimated.

Much of the early analysis of swarm experiments assumed a Maxwellian velocity distribution. Massey[3] tabulated λ values calculated from early data, and observed that these were frequently several orders of magnitude greater than the elastic value ($\sim 10^{-4}$). It was thus recognised that inelastic collisions were important in swarms where the mean energy was so low that the energy loss could only be attributed to rotational and vibrational excitation close to threshold.

Cottrell and Walker[43,49] studied a number of hydrocarbons and hydrides and plotted λ as a function of the mean swarm energy, derived from D/μ. The most striking feature of their results was the large peak observed in many of the λ plots at energies around 0.1 eV. The highest values of λ observed were those for CH_4 and SiH_4 and their deuterium analogues which reached around 30% and 45% respectively at energies corresponding closely to the excitation quanta of the lowest vibrational modes, namely the C-H and Si-H bending modes. This was tentatively suggested to be excitation occurring through an intermediate resonant state.

Phelps and co-workers[20,21] attempted to overcome the velocity distribution problem by measuring the temperature variation of the drift velocity at low E/P where the swarm is virtually in thermal equilibrium with the gas, this condition being assumed when W varies linearly with E/P. At thermal equilibrium,

$$f_o(v) = (m/2\pi kT)^{3/2} \exp(-mv^2/2kT) \qquad (I.25)$$

If this is substituted into (I.22) together with a suitably parameterised analytical form for $Q_m(v)$, an expression relating W to T is obtained, whence $Q_m(v)$ can be calculated from the experimental results. This method was adopted by Christophorou et al.[22], and by Bowman and Gordon[23], the accumulated results covering some twenty gases. The energy range over which Q_m can be determined is limited by the practicable temperature range to $.01 \lesssim \epsilon \lesssim .1$ eV.

The most sophisticated approach to swarm analysis was introduced by Frost and Phelps[24] and subsequently applied to several simple molecular gases[25-27]. The velocity distribution function at any particular E/P is here obtained by solving the Boltzmann equation. The solution requires knowledge of the cross-sections for all processes involved, so a trial set of cross-sections must be assumed to begin with. From the resulting velocity distribution the transport coefficients are readily calculated, and comparison with experimental values indicates the likely changes required in the trial cross-sections. The process is repeated until a set of cross-sections is found which reproduces the

experimental results. A full account of the method, the assumptions and approximations involved, and a discussion of the uniqueness and accuracy of the resulting cross-sections is given in chapter IV. Although the energy resolution of swarm experiments remains inherently limited by the breadth of the distribution, this approach is a considerable improvement on the analysis previously described: partly because the cross-sections at any specific energy are involved in calculations of transport coefficients at a wide range of E/P values; and partly because the distribution function is particularly sensitive to rapid variations in cross-sections, increasing the effective resolution where these occur.

I.2.6. Other types of swarm experiment

By sampling one electron per pulse in a time-of-flight drift tube Hurst et al.[15] constructed the distribution of arrival times, and hence by comparing the longitudinal pulse width at beginning and end of the drift period they calculated the longitudinal diffusion coefficient (D_L) for several gases. The ratio (D_L/μ) turned out to be vastly different from that obtained from transverse diffusion experiments (i.e. D_T/μ). This discrepancy was subsequently explained by Parker and Lowke[34] and Skullerud[28], who showed in rigorous analyses that longitudinal diffusion cannot be conveniently separated from drift as can transverse diffusion, due to the action of the electric field on the diffusion currents. According to the semi-quantitative model given

by Parker and Lowke for elastic collisions, the current density $\underline{J}$ is given by

$$\underline{J} = \mu_o E n \hat{k} - D_o \left[\frac{dn}{dx}\hat{i} + \frac{dn}{dy}\hat{j} \right] - D_o \left[1 - \frac{\gamma}{1 + 2\gamma} \right] \frac{dn}{dz}\hat{k} \qquad (I.26)$$

where the subscript o refers to values at zero density gradient (i.e. at the pulse centre), and γ is given by

$$\gamma = \left(\frac{d\nu}{d\epsilon} \right)_o \frac{\epsilon_o}{\nu_o} \qquad (I.27)$$

ν being the collision frequency. D_o is evidently equal to the transverse diffusion coefficient D_T, while the longitudinal coefficient D_L is given by

$$D_L = D_o \left[1 - \frac{\gamma}{1 + 2\gamma} \right] \qquad (I.28)$$

Thus D_L may be greater or smaller than D_T according to whether $(d\nu/d\epsilon)_o$ is negative or positive respectively. The physical interpretation of this is that in the leading edge of the pulse the mean energy is raised above ϵ_o by the field working on the diffusion current, and in the case of a constant cross-section ($\nu \propto \epsilon^{\frac{1}{2}}$) the mobility is therefore reduced below μ_o. The reverse applies in the trailing edge, so the overall effect is a reduction in the rate of pulse broadening, giving $D_L < D_T$.

The accurate description of pulse broadening, including the effect of inelastic collisions, necessitates the solution of the Boltzmann equation for a spatially dependent velocity distribution[34].

The treatment is very complex and so although D_L can probably be measured with high accuracy it is doubtful whether this quantity can be of much use in the determination of cross-sections.

In the case of zero applied field, the swarm velocity distribution becomes perfectly spherically symmetric and the distinction between longitudinal and transverse diffusion disappears. This is the basis of the "drift-dwell-drift" adaptation of the time-of-flight technique by Nelson and Davis[29]. A swarm pulse was drifted into the centre of the diffusion region, whereupon the field was cut off for a measured interval before being re-applied to accelerate the electrons to the detection apparatus where the arrival-time distribution was determined as before. During the "dwell" period the swarm relaxed to thermal distribution and diffused isotropically, so by varying the relative periods of "drift" and "dwell" the extent of diffusion during the zero-field interval was determined enabling the thermal diffusion coefficient (D_t) to be calculated. This value is of interest since the thermal mobility μ_t may be calculated from

$$D_t/\mu_t = kT/e \qquad (I.29)$$

μ_t is the limiting slope at E/P = 0 of the curve of W vs E/P at the appropriate temperature.

I.3. BASIC PRINCIPLES OF SCATTERING THEORY[1]

Collisions between electrons, ions, atoms and molecules are the subject of much of present research in theoretical physics, so the field is vast and the theories prolific. This section presents a brief outline of fundamental concepts and approaches.

Classical mechanics is not generally applicable to collisions involving slow electrons. This is seen from Heisenberg's uncertainty principle:

$$\Delta z.\ \Delta p_z \gtrsim h \qquad (I.30)$$

If the uncertainty Δz in the position of the colliding electron is to be no greater than the target dimensions ($\sim 10^{-8}$ cm), equation (I.30) gives a resultant uncertainty in momentum Δp_z corresponding to a velocity uncertainty Δv_z of $\sim 10^{8} \text{cms}^{-1}$, which is roughly the velocity of a 3 eV electron. The scattering problem must therefore be treated by quantum mechanics.

I.3.1. Solution of the Schrödinger equation

An exact description of a scattering process involves solution of the Schrödinger equation

$$H\Psi = E\Psi \qquad (I.31)$$

for the complete system of projectile and target. For the case of an electron scattered by a potential $V(\underline{r})$ the electron

wavefunction ψ must obey the wave equation

$$\nabla^2\psi + \left[k^2 - U(\underline{r})\right]\psi = 0 \qquad (I.32)$$

where the incident electron wavenumber k is given in terms of its velocity v by

$$k = mv/\hbar \qquad (I.33)$$

and

$$U(\underline{r}) = 2mV(\underline{r})/\hbar^2$$

At distances far from the scattering centre ψ must represent the incident and scattered wave, having the asymptotic form

$$\psi(r) \xrightarrow[(r \to \infty)]{} e^{ikz} + r^{-1}e^{ikr} f(\theta) \qquad (I.35)$$

The scattered amplitude $f(\theta)$ is related to the differential cross-section $\sigma(\theta)$ by

$$\sigma(\theta) = \left|f(\theta)\right|^2 \qquad (I.36)$$

Thus if solutions for ψ can be obtained the cross-sections may be calculated. In practice, even the simplest electron-atom collision (e + H) is a three-body problem and cannot be solved exactly. Resort must be made to approximations, the validities of which are not always easy to predict. Some of these approximate approaches are outlined in the next section (I.3.2.)

The complexity of quantum-mechanical formulations may be seen in the e + H system[1]. For direct scattering, the total electronic wavefunction for the two electrons is given by

$$\Psi(\underline{r}_1,\underline{r}_2) = \exp(ik_o n_o \underline{r}_1)\,\psi_o(\underline{r}_2) + \sum_j F_j(\underline{r}_1)\,\psi_j(\underline{r}_2) \qquad (I.37)$$

The first term on the right hand side represents the incident wave and the ground state of the atom, the term in the summation with $j = o$ represents elastic scattering, and those with $j > o$ represent the jth inelastic processes, the sum including all possible discrete and continuum states of the atom.

The wavefunction must satisfy the Schrödinger equation (I.31), thus

$$\left[\frac{\hbar^2}{2m}\nabla_1^2 + (E - E_n)\right]F_n(\underline{r}_1) = \int\left[\frac{e^2}{r_{12}} - \frac{e^2}{r_1}\right]\Psi(\underline{r}_1,\underline{r}_2)\psi_n^*(\underline{r}_2)\,d\underline{r}_2 \qquad (I.38)$$

In principle, if the hydrogen atom wavefunctions $\psi_n(\underline{r}_2)$ are known, solutions for the scattered wavefunctions $F_n(\underline{r}_1)$ can be found. The problem is further complicated by the possibility of exchange occurring between projectile and target electrons, which introduces a further set of scattering coefficients $G_n(\underline{r}_2)$ obtained in an analagous way to the $F_n(\underline{r}_1)$ by interchanging the subscripts in the summation term of (I.37); and the total wavefunction must also obey the Pauli exclusion principle, which introduces the spin quantum numbers.

I.3.2. Approximate solutions of the scattering problem

One of the most widely used approaches is the Born approximation.

This assumes that, for cases where the incident electron energy greatly exceeds the interaction energy, the effect of scattering is small and may be treated as a first-order perturbation. Expanding $\psi(r)$ for the projectile by the method of Green's function yields

$$\psi(r) = \psi_o(r) - \frac{1}{4\pi}\int U(r')\psi(r')\frac{\exp(ik|r-r'|)}{|r-r'|}\,dr' \qquad (I.39)$$

The Born approximation assumes $\psi(r') \simeq \psi_o(r) = e^{ikz}$ which results in the following expression for the scattered amplitude:

$$f(\theta) = -\frac{1}{4\pi}\int \exp\left[ik(\underline{n}_o - \underline{n})r'\right] U(r')dr' \qquad (I.40)$$

$\underline{n}_o$ and $\underline{n}$ being unit vectors in the incident and scattered directions respectively.

In the case of direct scattering by the hydrogen atom (I.3.1.) the following substitution is made in equation (I.38):

$$\Psi(\underline{r}_1,\underline{r}_2) \simeq \exp(ik_o\underline{n}_o\underline{r}_1)\,\psi_o(\underline{r}_2) \qquad (I.41)$$

The equation can now be solved for $F_n(\underline{r}_1)$, and the resulting expression for the differential cross-section is

$$\sigma_n(\theta) = \frac{k_n}{k_o}\cdot\frac{4\pi^2m^2}{h^4}\left|\iint\exp\left[i(k_o\underline{n}_o - k_n\underline{n})\underline{r}_1\right]\left[\frac{e^2}{r_1} - \frac{e^2}{r_{12}}\right]\psi_o(\underline{r}_2)\psi_n^*(\underline{r}_2)d\underline{r}_1\,d\underline{r}_2\right|^2 \qquad (I.42)$$

The Born approximation has been widely applied to both elastic and inelastic scattering by atoms and molecules. Its success largely depends on the accuracy of the interaction potentials used. For impact energies of 100 eV or more it has yielded accurate cross-section values,

and many general features of cross-sections at much lower energies have been predicted at least qualitatively. One important result[2] is the prediction that, at energies far above threshold, inelastic processes are governed by the same selection rules as are optical transitions.

At low energies, where the Born approximation is poor, the method of <u>partial waves</u> has proved useful, particularly in the case of elastic scattering by spherically symmetrical potentials. The electron wavefunction is expanded in a series of Legendre polynomials

$$\psi = r^{-1} \sum_{l=0}^{\infty} \phi_l(r)\, P_l(\cos\theta) \qquad \text{(I.43)}$$

which on substitution into the Schrödinger equation gives

$$\frac{d^2\phi_l}{dr^2} - \frac{l(l-1)}{r^2}\phi_l + \left[k^2 - U(r)\right]\phi_l = 0 \qquad \text{(I.44)}$$

for $l = 0, 1, 2 \ldots\ldots\infty$

The asymptotic solution for this may be written

$$\phi_l \underset{r\to\infty}{\longrightarrow} A_l \sin\left(kr - \tfrac{1}{2}l\pi + \eta_l\right) \qquad \text{(I.45)}$$

η_l is physically interpretated as being the phase shift caused by scattering of the lth partial wave, l being the quantum number associated with the angular momentum of the incident electron. By analogy with optical spectroscopy, waves with l = 0, 1, 2....etc. are termed **s, p, d ... respectively.**

The resulting expressions for the scattered amplitude and total cross-sections are respectively

$$f(\theta) = \frac{1}{2ik} \sum_{l=0}^{\infty} (2l + 1)\exp(2i\eta_l - 1)\, P_l(\cos\theta) \qquad \text{(I.46)}$$

and

$$Q = \frac{4\pi}{k^2} \sum_{l=0} (2l + 1) \sin^2 \eta_l \qquad (I.47)$$

The phase shifts can only be obtained analytically for some simple potentials. In other cases, variational methods may be used at low energies, or the Born approximation at higher energies. A further method, useful at lower energy than the Born approximation, is Jeffrey's (WKB) approximation, which is semi-classical and relies on a slowly varying $V(r)$.

An improvement on the Born approximation at low energies is the distorted wave approximation. As in the former case scattering through intermediate states is ignored, but account is taken of the distortion of incident and scattered waves by the field of the target. This approximation has proved to be particularly useful in the description of inelastic collisions at energies not far above threshold. The close-coupling and related approximations go a stage further by including the wavefunctions for a limited number of higher target states in the calculation.

I.3.3. Electron-molecule scattering

When the principle used in calculations of electron-atom scattering are applied to molecules even more formidable complexity results[3,30]. The adiabatic approximation in molecular wave mechanics allows separation of the total molecular wavefunction into electronic, vibrational and rotational components:

$$\Psi_{n,v,J} = \psi_n(\underline{r}_i, R_\nu) \cdot \chi_v(R_\nu) \cdot \rho_J(\theta_B) \qquad (I.48)$$

where r_i, R_ν, and θ_B represent respectively the sets of electronic, vibrational, and rotational co-ordinates and n, v, and J the corresponding sets of quantum numbers.

As the collision duration for even a thermal electron at room temperature is short compared to a vibrational or rotational period, it is necessary to consider the orientation-dependent interaction of the electron with a molecule of fixed nuclei. The cross-section obtained may then be averaged over the rotational and vibrational wavefunctions.

The only molecule which is sufficiently simple to allow calculations based directly on the theoretical electronic structure is H_2[51]. In other cases it is necessary to assume some form of interaction potential, which may include both direct and exchange terms, and proceed to determine phase shifts as for electron-atom scattering. A further difficulty is that to permit separation of co-ordinates in the wave equation either a spherically or axially symmetric potential must be used, the latter being described in terms of spheroid co-ordinates. This restricts accurate calculations to simple molecules.

Where long range forces are dominant it may be sufficient to use the asymptotic form of the interaction at large distance r[30]:

$$V(r,\theta) \underset{r\to\infty}{\sim} -\frac{qe}{r} - \frac{\mu e}{r^2} P_1(\cos\theta) - \frac{Qe}{r^3} P_2(\cos\theta) - \ldots\ldots$$

$$- \frac{\alpha e^2}{2r^4} - \frac{\alpha' e^2}{2r^4} P_2(\cos\theta) - \ldots\ldots \qquad (I.49)$$

Here q is the net charge, μ the electric dipole moment, Q the quadrupole moment, α and α' respectively the spherical and non-spherical parts of the polarisability, and P_n is the Legendre polynomial.

Inelastic collision processes include electronic, vibrational, and rotational excitation. If $\Psi_{n\nu J}$ represents the molecular wavefunction as in (I.48), the differential cross-section for excitation from a state nvJ to one n'v'J' by impact of an electron with initial and final wave vectors $\underline{k}_o, \underline{k}_1$ is given by Born's approximation to be

$$\sigma_{n\nu J}^{n'v'J'} d\omega = \frac{4\pi^2 m^2}{h^4} \cdot \frac{k_1}{k_o} \times \left| \int\int\int\int\int \sum_i e^2 (|\underline{r}_i - \underline{r}|)^2 \exp\left[i(\underline{k}_o - \underline{k}_1)\underline{r}\right] \right.$$

$$\left. \times \Psi_{n\nu J} \cdot \Psi^*_{n'v'J'} d\underline{r} \prod_i d\underline{r}_i \prod_\nu dR_\nu \prod_B d\theta_B \right|^2 d\omega \qquad (I.50)$$

(This is a generalisation of the form given by Craggs and Massey[51] for the diatomic case.)

Using (I.48), the squared term in (I.50) becomes

$$\int\int\int V(\underline{r}, R_\nu, \theta_B) \exp\left[i(\underline{k}_o - \underline{k}_1)\underline{r}\right] \chi_\nu(R_\nu) \chi^*_\nu(R_\nu) \rho_J(\theta_B) \rho^*_{J'}(\theta_B) d\underline{r} \prod_\nu dR_\nu \prod_B d\theta_B \qquad (I.51)$$

where $V(\underline{r}, R_\nu, \theta_B)$ is the mean interaction energy of the incident electron with the molecule in its ground state at fixed nuclear co-ordinates R_ν, θ_B and is given by

$$V(\underline{r}, R_\nu, \theta_B) = e^2 \int \sum_i (|\underline{r}_i - \underline{r}|)^{-1} \left|\psi_n(\underline{r}_i, R_\nu)\right|^2 \prod_i d\underline{r}_i \qquad (I.52)$$

It should be noted that the condition for validity of the Born approximation in the above approach is that $\underline{k}_1 \simeq \underline{k}_0$, and therefore good results near threshold are not to be expected.

I.3.4. Resonances

A considerable body of theory[2,52,53] has accumulated over the last decade to explain experimental observations of resonances. A resonance in electron-molecule scattering may be defined as a temporary negative ion state which is unstable towards auto-detachment. The lifetime of such a state may be anywhere between about 10^{-5} and 10^{-16}s. If the lifetime is long compared with the time the electron takes to traverse the target, severe distortion of the projectile wavefunction occurs resulting in the observation of marked structure in the scattering cross-sections. The nuclear motion of the target molecule will also be severely distorted and greatly enhanced inelastic cross-sections will be likely.

The classification of resonances is based on the mechanism whereby the electron is trapped, but as the models have been developed independently on the basis of experimental results the classification and nomenclature differs somewhat between authors. The most fundamental division is used by Massey and Burhop[2] who refer to Type I (Feshbach or compound state) and Type II (one-body or shape) resonances. The former is said to occur when a molecule is excited

by an electron of kinetic energy slightly lower than the threshold energy of the excited state. The electron potential energy thus becomes negative relative to infinite separation due to trapping in the field of the excited state. The resultant negative ion approximates to a bound state, the wavefunction being dominated by closed-channel components, which usually leads to a relatively longlived state of narrowly defined resonance energy.

A Type II resonance on the other hand occurs at an energy above but close to a target state (ground or excited), the electron being temporarily trapped by a potential barrier which is usually regarded as being a centrifugal barrier set up by the combination of the projectile angular momentum and the potential well caused by the short-range attractive forces. The phenomenon is thus not observed in s-wave scattering. The resonance is a virtual state which can decay by tunnelling through the potential barrier, and the wavefunction is dominated by open-channel components. As such barriers are usually small, the states tend to be short-lived and thus broad in energy.

Bardsley and Mandl[52] consider Type I resonances under the two headings of electron-excited and nuclear-excited Feshbach resonances respectively, according as to whether the compound state is associated respectively with an electronically, or vibrationally and/or rotationally excited state of the target. On the other hand, Taylor[53] classes both together as core-excited Type I resonances, and subdivides the Type II (shape resonances) into core-excited Type II and

single particle resonances, the former occurring with target excitation and the latter where the electronic ground state only is involved, the potential well being attributed to polarisation of the target. Nazaroff[54] has recently described all the above types by a single theoretical model, emphasising the phenomenological nature of the classification.

Quantum mechanically a resonant state Ψ_n can be treated as having formally the same time dependence as a bound state

$$\Psi_n \propto \exp(-iW_n t/\hbar) \tag{I.53}$$

but differing in having a complex energy

$$W_n = E_n - \tfrac{1}{2}i\Gamma_n \tag{I.54}$$

which leads to the exponential decay of the state

$$|\Psi_n|^2 \propto \exp(-\Gamma_n t/\hbar) \tag{I.55}$$

Γ_n is thus the width of the resonant state, and $\tau = \hbar/\Gamma_n$ is the lifetime.

Provided the Born-Oppenheimer separation of nuclear motion can be applied (this is not true for nuclear-excited Feshbach resonances), the wavefunction may be expressed as a close-coupling expansion

$$\Psi_n(\underline{r},q,\underline{R}) = \sum_\nu \psi_\nu(q,\underline{R}).\chi_\nu(\underline{R}).f_{n\nu}(\underline{r}) \tag{I.56}$$

where ψ, χ, and f are respectively the electronic, nuclear and projectile

wavefunctions and ν denotes collectively the relevant system quantum numbers. The object of the analysis is to calculate the scattered amplitude and hence the cross-section for decay into the various exit channels. Many approaches depend upon neglect of terms in the above expansion, based on such knowledge as whether a particular electronic state is dominant, and whether the open-channel components are small or large (i.e. whether the resonance is narrow or broad).

The theory of vibrational excitation through resonance has been developed with a considerable degree of success, by Herzenberg and Mandl[55] and Chen[56] amongst others. Chen considers the v to v' vibrational transition through an intermediate resonant electronic state n in a vibrational state u

i.e. $\quad Ov \rightarrow nu \rightarrow Ov'$

and gives the amplitude for the transition as

$$f^{u}_{vv'} = \frac{\gamma^{Ov}_{nu}\ \gamma^{Ov'}_{nu}}{E-E_{nu} + \frac{1}{2}i\Gamma_{nu}} \qquad (I.57)$$

where $\left|\gamma^{Ov}_{nu}\right|^2 = \Gamma^{Ov}_{nu}$, $\left|\gamma^{Ov'}_{nu}\right|^2 = \Gamma^{Ov'}_{nu}$

the Γ's here being the partial widths of the state nu due to break up into states Ov and Ov'; and Γ_{nu} the total width with respect to all modes of decay. The partial widths are given by

$$\Gamma^{Ov}_{nu} = 2\pi \left\{ \left\langle \Psi_{nu} \middle| H \middle| \Psi^{Ov}_{c} \right\rangle \right\}^2 \qquad (I.58)$$

Here H is the total system Hamiltonian and Ψ_{nu}, Ψ^{Ov}_{c}

respectively the wavefunctions for the resonant state and the initial state Ov, the latter including the wavefunction of the projectile electron.

The cross-section for the excitation process depends strongly on the width of the state Γ_{nu}. The extreme cases[55] of the compound molecule limit and the impulse limit occur respectively when

$$\Gamma_{nu} \ll \hbar\omega \quad \text{and} \quad \Gamma_{nu} \gg \hbar\omega \qquad (1/2\pi\omega = \text{vibrational period})$$

In the former case, the resonant state will possess definite vibrational levels, and the cross-section will consist of a series of peaks separated approximately by $\hbar\omega$, the peaks occurring at the same energy for all exit channels. In the impulse limit, no definite levels exist and the peaks will occur at different energies for different exit channels.

I.4. COMPARISON OF THEORY AND EXPERIMENT

In this section a brief outline will be given of the successes and failures of theoretical calculations on elastic scattering and vibrational and rotational excitation. Not surprisingly, almost all the theoretical work to date has related to diatomic molecules; because of the importance of vibrational excitation to the present research, this will be considered separately for diatomic and polyatomic molecules.

I.4.1. Elastic scattering

Some of the earliest calculations on elastic scattering by molecules were performed by Fisk[57] who considered such homonuclear diatomics as H_2, N_2, and O_2. His method was semi-empirical, using adjustable parameters to describe the scattering potential from which phase shifts were calculated. In this way he achieved reasonable qualitative agreement with experimental results for both the energetic and angular variations of the cross-sections[51]. Later, calculations were done for H_2 based on the actual electronic structure[58]. It was found essential to include the effects of electron exchange in order to give reasonable agreement with experiment at around 1 - 2 eV. More recent calculations[59] have stressed the importance of including the molecular quadrupole and dipole polarisation in the effective scattering potential, even at relatively high energies.

Methane has been shown by both beam[60] and swarm[61] experiments to posses a deep minimum in the total cross-section at around .2 -.5 eV, resembling argon strongly in this respect. This so-called Ramsauer-Townsend effect in the inert gases is interpreted as occurring where the s-wave phase shift passes through an integral multiple of π, higher order waves being little affected by the very short-range forces of these highly symmetrical atoms. Buckingham, Massey, and Tibbs[62] took advantage of the high symmetry of CH_4 in calculating a self-consistent field by averaging the charge of the protons over a sphere. Calculations using this field showed a marked similarity to those for argon and the authors concluded that methane occupied the place of neon in the

Ramsauer-Townsend series. Their calculations of the elastic cross-sections did however give poor correspondence with experiment below about 10 eV in both gases. Swarm experiments in SiH_4 indicate that this molecule exhibits a similar effect[61].

Another class of molecules which are amenable to theoretical study is those having a permanent dipole moment. Altshuler[63] derived the momentum-transfer cross-section of a stationary point dipole by the Born approximation. His result was

$$Q_m = \frac{8\pi}{3k^2}\left[\frac{e\mu m}{\hbar^2}\right]^2 \qquad (I.59)$$

where μ is the dipole moment. Mittleman and von Holdt[64] made an exact calculation for a point dipole but found that no solution existed for $\mu \geq 1.625$ D due to the scattering potential being too attractive and giving rise to an infinity of bound states. By assuming the form of the cross-section variation

$$Q_m = A/v^2 \qquad (I.60)$$

given by (I.59), several authors[50,65] have obtained values of A from drift velocity data. Most molecules show an approximate agreement with Altshuler's theory, although the experimental cross-sections are mostly higher than the theoretical values. Crawford et al.[50] have shown that Q_m is dominated by inelastic scattering (i.e. rotational excitation and de-excitation) in polar molecules at thermal energies, and have qualitatively accounted for the discrepancies

in the Altshuler theory as being due to neglect of higher-order terms in the assumed interaction potential. However substantial discrepancies seem to exist for certain molecules, notably H_2O, H_2S, NH_3, PH_3, and AsH_3, all of which possess anomalously high cross-sections. The minimum dipole moment above which bound states exist for a finite stationary dipole has been calculated to be 1.625 D, which appeared to correlate to a certain extent with the observed anomalies[66,67]. More recently, Garrett[68] has taken account of the dipole rotation and found that in real cases the critical moment will always be greater than the above value and will depend on the masses and separation of the dipole charges. Bottcher[69] has confirmed this and also predicted the existence of shape resonances for dipole moments less than the critical value.

A different approach was taken by Takayanagi and Itikawa[70] who performed a partial wave analysis and found the appearance of a potential resonance in the momentum-transfer cross-section plotted as a function of the dipole moment when the magnitudes of the charges were varied at fixed separation. Christophorou and Christodoulides[67] interpreted their swarm results as bearing out the general prediction of this theory.

The only polar molecule for which a Phelps-type analysis of swarm data has been attempted is CO[27]. Here the Q_m obtained appears to merge with Altshuler's value at low energies where the dipole dominates, at higher energies taking values similar to N_2 with which CO is isoelectronic.

I.4.2. Rotational excitation of diatomic molecules

The first theory of rotational excitation in homonuclear diatomics to meet with any degree of success was that of Gerjuoy and Stein[71,72] who used the molecular quadrupole as the scattering potential in a Born approximation calculation. Their expression for the $J \rightarrow J' = J+2$ rotational excitation cross-section was

$$\sigma_{J\rightarrow J'} = \frac{8\pi}{15}\left[\frac{Q}{ea_o}\right]^2 \cdot \frac{k'}{k} \cdot \frac{(J+1)(J+2)}{(2J+1)(2J+3)} \qquad (I.61)$$

Although a limited amount of information on rotational excitation has been deduced from microwave interaction studies[3], the main test of theory has been in the interpretation of swarm data by the method of Phelps. In H_2, sufficiently few rotational levels are involved, particularly at low temperature, to allow unique determination of cross-sections in a limited region above the excitation threshold[73]. Successive improvements on the above theory have been made, such as the inclusion of polarisation[25], distorted wave[74] and close-coupling[75] calculations, and agreement within 2% of the experimental values has been achieved by Henry and Lane[76] who included polarisation and exchange in a close-coupling calculation. Abram and Herzenberg[77] have also calculated the cross-sections for excitation of the individual levels accompanying the $v = 0 \rightarrow 1$ vibrational excitation of H_2 through a resonance process, and obtained fair agreement with the results of Ehrhardt and Linder[7].

For molecules other than H_2, too many rotational levels are

involved to allow unique determination of cross-sections from swarm data, but Frost and Phelps[24] obtained agreement with Gerjuoy and Stein's theory for N_2 by adjusting the value of the quadrupole moment used in the theory. As the latter is not known to any high degree of accuracy from other sources, it is not yet possible to say which theoretical approach gives the best agreement with experiment.

The validity of the Born approximation at these energies might at first sight appear to be extremely dubious, but a strong case has been argued by Gerjuoy and Stein and supported by a partial wave analysis[30]. The argument is that, in order to cause a rotational transition, the incident electron must have non-zero angular momentum and therefore at low incident velocity a large impact parameter. At such a distance the dominant quadrupole potential will be relatively weak and the p-wave will be only slightly distorted, so the Born approximation is an acceptable approach.

In the case of heteronuclear diatomics, similar arguments apply, the dominant interaction now being due to the permanent dipole. Takayanagi[30] applied the Born approximation to scattering by a point dipole and obtained

$$\sigma_{J\to J+1} = \frac{8\pi}{3k^2}\left[\frac{\mu}{ea_o}\right]^2 \frac{J+1}{2J+1} \ln\frac{k+k'}{k-k'} \qquad (I.62)$$

Hake and Phelps[27] used a well-established value for the CO dipole moment and found good agreement with swarm transport coefficients. However, for high values of μ the interaction will be strong enough to

cause significant distortion of the incident p-wave, and Massey[3] has shown the Born approximation to be valid only for $8\pi^2\mu em/h^2 \ll 1$.

I.4.3. Vibrational excitation of diatomic molecules

The first attempts to calculate vibrational excitation cross-sections for homonuclear diatomics were based on the first Born approximation (I.50), using a simple 2-centre electrostatic potential dependent on the internuclear distance R -

$$V(\underline{r},\underline{R}) = U(|\underline{r} + \tfrac{1}{2}\underline{R}|) + U(|\underline{r} - \tfrac{1}{2}\underline{R}|) \qquad (I.63)$$

The resulting cross-sections were considerably smaller than the results of swarm experiments suggested, even when the R-dependence of U was taken into account. In the early days this was taken as a strong argument against "direct" vibrational excitation. However Takayanagi[30] has found that the magnitude of the observed $v = 0 \rightarrow 1$ cross-section in H_2 can be explained by the R-dependence of the polarisation interaction, making use of the distorted wave approximation. The possibility of excitation occurring through a resonant state was first experimentally indicated by Schulz[78] who observed cross-sections for excitation to v = 1 and 2 peaking broadly around 2 - 3 eV. Bardsley et al.[79] explained the magnitude of the cross-sections by calculating excitation through a resonant state $H_2^-(1s\sigma_g)^2(2p\sigma_u)^2\Sigma_u^+$, for which they estimated the potential energy curve. The latter was later confirmed by Taylor[53] using the stabilisation method. The resonance was thus

interpreted as a ground state shape resonance with a lifetime of around 10^{-16}s. Until recently, analysis of swarm experiments[25,37] in H_2 and also Takayanagi's theory indicated a $v = 0 \rightarrow 1$ cross-section rising sharply from threshold, whereas Schulz's beam experiment[78] and the theory of Bardsley et al. (which was partly parameterised to fit Schulz's data) indicated a very low cross-section between 0.5 and 1 eV. This discrepancy has recently been resolved by experiments of Ehrhardt et al.[80] and Burrow and Schulz[81] who confirm that the cross-section rises from threshold, although the initial slope is in dispute. The two apparent theoretical explanations for the excitation are not incompatible as both Takayanagi and Bardsley and Mandl[52] have pointed out that the ground state H_2^- shape resonance is so short-lived that little difference here exists between "direct" and resonance scattering.

A similar situation exists in N_2, which has been examined in great detail by electron beam experiments[78,82]. Cross-sections for excitation of the first eight vibrational modes have been measured, all with maxima in the vicinity of 2 - 3 eV, and each consisting of a series of evenly spaced peaks. This is consistent with the analysis of transport coefficients[26]. Theoretical calculations by Chen[83] and by Herzenberg and Mandl[55] on the basis of a resonant $^2\Pi_g$ state of N_2^- have reproduced the observed data well, albeit using adjustable parameters. In contrast with H_2, the resonant N_2^- state must be relatively long-lived to show the observed structure. The resonance was in fact first thought to be a core-excited type I, but this was later rejected in favour of a type II in view of the unreasonably high

electron affinity a type I model would imply for the excited state. This conclusion has been supported in recent improved calculations by Soshnikov[84].

For heteronuclear diatomics, the largest "direct" contribution comes from the dipole interaction. Takayanagi[30] gives the cross-section in the Born approximation to be

$$\sigma_{v \to v' = v+1} = \frac{8\pi}{3k^2} \left|(v'|\mu|v)\right|^2 \ln\left|\frac{k + k'}{k - k'}\right| \qquad (I.64)$$

From this he calculated the excitation cross-section for CO from the infrared transition probability. In the region from threshold to ~1 eV this value, and to a lesser extent that of Breig and Lin[85] who included polarisation, gave good agreement with the swarm analysis of Hake and Phelps[27]. Above this energy the cross-section appears to be dominated by a resonant process very similar to that in N_2, which has been the subject of extensive experimental and theoretical investigation.[53]

I.4.4. Vibrational excitation of polyatomic molecules

It has long been known[3,43] that high electron swarm energy losses occur in polyatomic gases, but in spite of a considerable body of data little theoretical work has been done in this field presumably because of the complexity introduced by the additional degrees of freedom. A case in point is that of CO_2, one of the simplest species in this category, the vibrational excitation of which has only recently begun to be understood.

Hake and Phelps[27] based their CO_2 swarm analysis on Schulz's observation of energy losses of ~0.3, 0.6, and 0.9 eV, tentatively associating these with v = 0 → 1, 2 and 3 excitations of the ν_3 antisymmetric stretch mode, and postulated large resonant-like cross-section peaks to explain the swarm energy losses. They were however unable to reconcile this with experiment without including a further large peak at 0.08 eV loss (corresponding to the v = 0 → 1 excitation of the bending mode). Furthermore, it was necessary to place these "resonances" very close to threshold, in contrast to the situations observed in H_2, N_2, and CO where the resonance peaks occur well above the vibrational threshold.

A later publication by Boness and Schulz[86] showed unresolved energy losses around 0.1 eV but ruled out any strong excitation of the ν_1 symmetrical stretch mode at 0.17 eV. However they did observe apparent excitation of up to six levels of this mode at incident energies of 3 - 4.5 eV.

A digression at this point is worthwhile. Most theoretical descriptions of direct scattering assume an interaction potential based on the equilibrium positions of the nuclei. However the transit time for a thermal electron ($\sim 10^{-15}$s) is considerably shorter than a vibrational period (10^{-12} - 10^{-13}s) so the nuclei can be considered as fixed during a collision. For diatomic molecules, averaging the cross-sections for individual values of the intermolecular distance R over the probability distribution of R should give much the same result

as a single calculation based on the equilibrium value of R. However for molecules with three or more atoms this will not generally be the case, since the interaction potential for any particular nuclear configuration may contain lower-order terms than are present in the "equilibrium" interaction potential. Thus in CO_2 the two degenerate bending modes and the asymmetric stretch give rise to temporary dipoles which appear in the infrared transition moment, and should therefore according to (I.64) influence the vibrational excitation. Furthermore, since the Born approximations for momentum-transfer (I.59) and rotational (I.62) cross-sections involve the square of the dipole moment which does not average to zero over the vibration, these cross-sections will be similarly affected. Hake and Phelps[27] appeared to overlook this in calculating rotational excitation from the permanent quadrupole of CO_2, so it is not surprising that the cross-sections they obtained were too low to explain the swarm data. Recently Singh[87] found the energy dependence of experimental Q_m values for CO_2 differed from that expected for a quadrupole-dominated interaction, and stated that this was "probably due to the small dipole moment embedded in the CO_2 molecule."

It is interesting to consider the magnitude of the CO_2 temporary dipoles. For the ν_2 bending modes, the dipole moment is given in terms of the deformation angle θ by

$$\mu \simeq \mu'\theta$$

where μ is the C=O bond moment. At the classical limit, θ is

given by

$$h\nu_2 = F_\theta . \theta^2 \qquad (I.65)$$

F_θ being the force constant. Putting in spectroscopically determined values[88] gives $\mu \simeq 0.18$ D, which may be compared with the permanent moments of CO (0.12D) and N_2O (0.17D).

For any one vibration ν_k, the mean square dipole moment is obtained by averaging over the quantum-mechanical probability distribution of the normal co-ordinate Q_k:

$$\overline{\mu_k^2} = \int_{-\infty}^{\infty} \psi_o^*(Q_k)\,\psi_o(Q_k)\,|\mu(Q_k)|^2\, dQ_k \qquad (I.66)$$

ψ_o is the ground-state vibrational wavefunction -

$$\psi_o(Q_k) = (1/\alpha_k \pi)^{\frac{1}{4}} \exp(-\tfrac{1}{2}Q_k^2/\alpha_k) \qquad (I.67)$$

where $\alpha_k = h/4\pi^2\nu_k$. For small deformations, $\mu(Q_k)$ is given by

$$\mu = Q_k (d\mu/dQ_k)_o \qquad (I.68)$$

Substituting in (I.66) and integrating gives

$$\overline{\mu_k^2} = \tfrac{1}{2}\alpha (d\mu/dQ_k)_o^2 \qquad (I.69)$$

$(d\mu/dQ_k)_o$ is obtainable from measurements of infrared absorption intensities[88]. From (I.69) we find that $\mu_{rms}\left[= (\overline{\mu^2})^{\frac{1}{2}}\right]$ for the ν_2 modes of CO_2 is approximately 0.12 D, and for the ν_3 mode 0.26 D. The total $\overline{\mu^2}$ for the molecule will be roughly the sum of the

individual $\overline{\mu^2_k}$ which gives a total $\mu_{rms} \simeq 0.3$ D. This is the effective value which should appear in Altshuler's Born approximation expression (I.59). It is worth noting that at low energies Pack et al.[21] found Q_m for CO_2 was 2.69 times that for N_2O. Taking the N_2O dipole moment as 0.166 D[87], this suggests an effective CO_2 dipole moment of $\sim$0.27 D, which agrees roughly with the calculation above.

For vibrational excitation, however, the cross-section depends on the transition moment in (I.64), which involves $(d\mu/dQ_k)_o$ and is independent of the permanent dipole. This is consistent with observations in several molecules at medium and high energies, e.g. by Lassettre[89] at 48 eV, and by Geiger and Wittmaack[90] at 33 keV. In the latter case excitation of the infrared-active modes of CO_2, N_2O and C_2H_4 was found to be consistent with calculations based on the infrared absorption intensities[91].

At low energies, Takayanagi's Born approximation calculations could not explain the magnitude of the threshold processes in CO_2[27], but more recent calculations by Claydon, Segal, and Taylor[92] have supported the idea of direct excitation of the optically active modes. They calculated approximate potential curves for CO_2^- using a self-consistent field variational approach and attributed the observed ν_1 excitation in the 3.0 - 4.5 eV region to the formation of a $^2\Pi_u$ compound state with a lifetime of around 10^{-15} s. However they concluded that no compound state was formed below 3 eV and advanced an alternative theory of direct excitation for the lower energy processes. They made semi-quantitative estimates of the cross-sections based on the electric

dipole and higher order transition moments, concluding that cross-sections of the order of 10^{-16} cm^2 were to be expected for the ν_2 and ν_3 excitations but a much lower value for the ν_1 mode due to $(d\mu/dQ_1)_o$ being zero. They stated that Takayanagi's approach failed not because of additional resonant processes but the shortcomings of the straightforward Born calculation at these energies. Furthermore, they firmly stated that direct vibrational cross-sections of this order are likely to be encountered in non-dipolar polyatomic molecules wherever the vibrational modes concerned give rise to a transient dipole (i.e. are infrared-active).

Since this publication fresh evidence has appeared in the work of Stamatovic and Schulz[104], who used a trochoidal monochromator to produce a high-resolution low-energy beam, and obtained threshold energy-loss spectra by SF_6 scavenging of the scattered electrons. Their results indicated that, for all vibrational modes of CO_2 including ν_1, the excitation cross-sections are of similar magnitude within < .05 eV above threshold. Itikawa[105] has attempted to explain the ν_1 excitation by a Born approximation calculation based on the polarisation interaction, but found that the magnitude of the cross-section, whilst always much greater than that derived from the quadrupole interaction, depends strongly on the value of the short-range cutoff parameter used to describe the polarisation potential. This would seem to demonstrate the inadequacy of such long-range potentials in a system where the short-range forces are important.

I.5. BACKGROUND TO THE PRESENT STUDY

Following observations of large mean fractional energy loss (λ) values in swarms by Cottrell and Walker[17], Pollock[65] obtained improved drift velocity data in a large number of polar, quadrupolar, and non-polar gases. He then applied Phelps' method of analysis[24] to CH_4, CD_4, SiH_4, and SiD_4 and obtained rough values for the momentum-transfer cross-section and a total inelastic cross-section based in each case on an energy loss corresponding to the lowest vibrational mode (ν_4)[61]. He encountered difficulties however, largely owing to the lack of reliable low-energy D/μ measurements in these gases. In methane he was unable to reproduce transport coefficients for $E/P < 0.5$ V $cm^{-1}torr^{-1}$, and attempts to fit the cross-sections to Walker's D/μ measurements[43] tended to produce a sharp peak in the inelastic cross-section at threshold[45]. The D/μ values of Cochran and Forester[44] were not compatible with the drift velocity data, and Pollock concluded that reasonable cross-sections could only be derived if D/μ lay somewhere between the two sets of results. Because of this it was impossible to judge whether or not rotational excitation was having a significant effect.

In view of the apparent importance of vibrational excitation in polyatomic gases, it seemed worthwhile to pursue this method of analysis, if possible to give some clue as to which vibrational modes might be involved, and whether rotational excitation occurs. However there appeared to be a lack of reliable D/μ data for most gases of

interest at E/P below about 0.5 V $cm^{-1}torr^{-1}$, as the published data in this range has been almost exclusively for diatomic molecules. As the separation of elastic and inelastic processes in the Phelps analysis is extremely sensitive to variation in D/μ at low values, it was decided to proceed with an experiment primarily to measure D/μ at near-thermal values ($\lesssim 0.2$ V), and to improve the accuracy and versatility of the computer analysis to make best use of the experimental results.

FIG. II.1

Simplified Diffusion Tube Geometry.

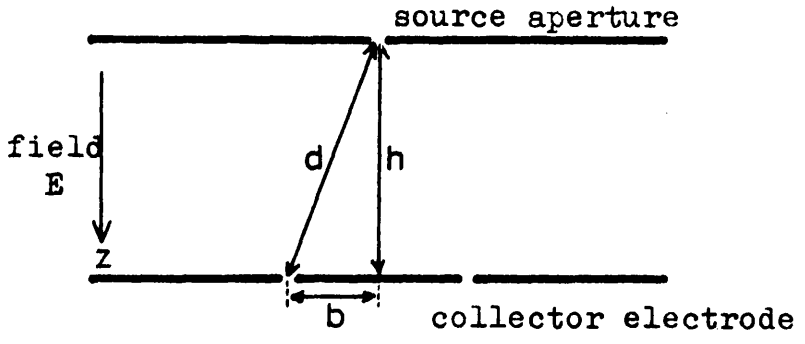

Diffusion Equation.

$$D.\nabla n^2 - W.\frac{\delta n}{\delta z} = 0$$

where n = electron density
D = diffusion coefficient
W = drift velocity

Huxley's Solution.

$$R = \frac{\text{current to inner collector}}{\text{total current}}$$

$$= 1 - \frac{h}{d}.e^{-W.(d-h)/2D}$$

CHAPTER II

APPARATUS DESIGN & CONSTRUCTION

II.1. BASIC REQUIREMENTS OF THE APPARATUS

The object of the experimental project was to measure electron diffusion coefficients transverse to an applied field in a variety of gases. For the reasons discussed in chapter I, accuracy of measurement at low values of E/P was considered to be of prime importance, and the facility to vary temperature was desired.

The conventional Townsend-Huxley diffusion tube method[31] was chosen, no other technique of comparable accuracy being known, and the design of an apparatus was undertaken with the following basic requirements.

(a) The principal parameters h and b of the diffusion tube (Fig. II.1) must be chosen to allow accurate measurement of the full range of W/D values likely to be encountered. These values correspond to swarms of characteristic energy eD/μ ranging from thermal to several eV, in gas pressures varying from a few torr to greater than atmospheric.

(b) The precision of the measurements must be maintained throughout the working range by close adherence to the idealised geometry, uniformity of the electrostatic field and accuracy of collected current measurements.

(c) As the low-energy limit of the swarm is determined by the gas temperature, it may be found desirable to reduce the latter below room temperature to extend the range of investigation. The accuracy of the apparatus must therefore be sustained over a wide range of operating temperatures.

The level of accuracy required in determinations of D/μ is decreed by the cross-section analysis used (Ch. IV). Although the effective momentum-transfer cross-section is only dependent on $(D/\mu)^{\frac{1}{2}}$, the effective inelastic cross-section involves the difference term $(D/\mu - kT/e)$ which approaches zero as E/P approaches zero. Small errors in D/μ therefore become extremely serious in the analysis of near-thermal swarm data - the very region where measurements become increasingly difficult. With present techniques it is unrealistic to hope for an overall accuracy of better than a few percent, and in attempts to eliminate individual sources of error in this work the level of precision usually aimed at is of the order of 0.5% or better.

II.2. DESIGN CONSIDERATIONS

II.2.1. Choice of Principal Parameters

Precise measurement of the current ratio R requires the currents I_1 and I_2 to be of similar magnitude. Also, the gradient $dR/d(W/D)$ given by the Huxley formula (Fig. II.1) becomes very small as R tends to 0 or 1, so that the useful range of R for precise measurement of D/μ is at

most $0.2 < R < 0.9$. An apparatus of fixed dimensions h and b can measure a very restricted range of D/W, and hence a restricted range of D/μ since the useful range of field strength E is also limited. It is therefore necessary to choose the parameters b and h to suit the range of D/μ values under investigation.

At near-thermal D/μ, the lower limit of a few volts per centimeter which must be placed on E means that a very small ratio b/h ($\sim 10^{-2}$) must be employed if the fraction (1-R) of the electron current to the outer collector is to be significant. Due to the finite size of the gap between collectors, which limits the precision of the effective inner collector diameter, the smallest practical radius was determined to be 0.25 cm. Practical considerations also led to a choice of 10 cm for the drift distance h, since as the divergence of the swarm increases with the square of the drift distance, a significant further increase in divergence could only be achieved by making the apparatus unduly cumbersome.

The choice of such a low b/h ratio also restricted the upper limit of D/μ measurable at the maximum available field strength E (approx. 150 V cm^{-1}). To provide for measurement of larger D/W values, the anode was further divided at radii of 1 cm and 2 cm respectively, thereby giving three values of b to cover the full desired range of the apparatus.

II.2.2. Choice of other dimensions

The sources of systematic error and factors influencing the accuracy of the Townsend-Huxley diffusion experiment have been thoroughly investigated by Crompton and co-workers[32,33], and the magnitudes of the errors arising assessed both by numerical calculation and by experiment. Their results were used as a basis for reducing inaccuracy in the present experiment, as described below.

(a) Diameter of source hole: The finite size of the source hole is a departure from the ideal point-source diffusion geometry, but in practice the source must be sufficiently large to transmit the required current. By making the hole diameter 1 mm, the maximum error was kept below 0.5%[32].

(b) Width of annular gaps in anode: The uncertainty in b is of the order of the gap width. The inner two gaps were designed to be .005 cm wide, the smallest possible in practice. When location tolerances were allowed for, the maximum error from this source would not exceed 1%.

(c) Diameter of the diffusion region: To approach the ideal boundary condition of no walls, the diffusion region diameter must be large enough to give negligible electron density at the walls, and to ensure uniform field over the region where electron density is significant. The diameter depends on the guard electrode system employed, and is discussed in II.2.3.

(d) Preliminary field region: Before reaching the source hole

the swarm must have relaxed to the equilibrium velocity distribution. When elastic collisions only are considered, the energy relaxation distance is given by[34]

$$d_\epsilon \simeq \frac{MeE}{2m^2\nu^2} \qquad \text{(II.1)}$$

where ν is the collision frequency. Except at pressures < 1 torr this distance is extremely short and the chosen distance of 1.67 cm was more than adaquate.

(e) Alignment of source: The tolerance on the axial alignment of the source hole to the collector was placed at ±.02 cm. According to Crompton and Jory, this should limit the error in D/μ to 0.1%.

II.2.3. Guard electrode structure

Slight variations in field strength along the tube axis have little effect on the measured value of D/W, as the resulting slight variations in velocity distribution largely average out over the diffusion length. Any radial field component arising from geometrical inaccuracies will however seriously affect the transverse diffusion. Departure of the collector surface from true planarity will have the most serious effect as radial fields will then exist in the vicinity of the annular gaps, causing a spurious current distribution.

Any distortion or misalignment of the guard electrodes which produce the field will likewise introduce radial field components.

Crompton, Elford and Gascoigne[33] replaced the conventional thin knife-edged guard rings with deep closely-spaced cylindrical electrodes. It was decided to employ these in the present apparatus since besides conferring geometrical accuracy and mechanical stability on the system they provide a high degree of shielding from external fields, and eliminate large insulating spacers within the diffusion region which may cause field distortion through dielectric soakage and surface charging. Although the field is highly distorted close to the electrodes, the degree of distortion is accurately known and can be arranged to be negligible within the region of significant electron density.

Fig. II.2. shows a module of the field and the equation giving the form of the equipotentials, which is the solution to the Laplace equation with the appropriate boundary conditions. Calculations were carried out to determine suitable electrode dimensions. The criterion used was that, for current ratio $R > 0.25$ referred to the outermost annular gap, 99.9% of the electron flux at the anode should fall within a radius at which the field deviation is less than 0.05%. This radius was calculated to be just under 5 cm. Further calculations to determine the best compromise between number of electrodes and electrode diameter led to a choice of 6 full electrodes per 10 cm drift distance, of inner diameter 6 cm, and separated by 0.5 cm gaps.

II.2.4. Effect of contact potentials

Contact potential differences between electrodes also cause

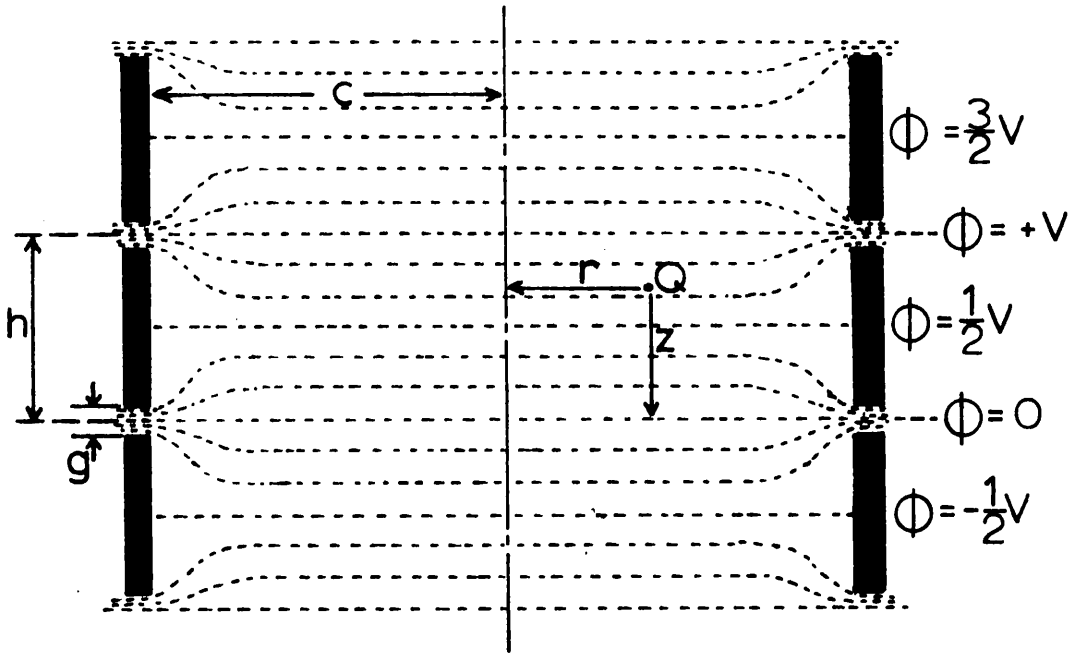

Potential at point Q -

$$\Phi_Q = \frac{Vz}{h} + \sum_{n=1}^{\infty} \frac{V}{n\pi} \cdot \frac{I_o(2n\pi r/h)}{I_o(2n\pi c/h)} \cdot \sin(2n\pi z/h) \cdot \frac{\sin(n\pi g/h)}{n\pi g/h}$$

(I_o = zero-order modified Bessel function)

FIG. II.2. Electric field geometry.

The dotted lines indicate the shapes of the equipotentials.

field distortion, particularly at low field strengths. Most serious is any variation in contact potential across the collector surface where a few millivolts can produce noticeable errors[33]. Parker and Warren[35] investigated the variation in contact potential across various surfaces and found that even electroplated gold gave differences of the order of 100 mV in a centimeter. Crompton et al. succeeded in reducing the differences to a few mV by carefully developed gold evaporation techniques, but since Parker and Warren found colloidal graphite gave variations of less than 10 mV the latter simpler surface treatment was chosen in this case.

II.2.5. Magnetic effects

An electron swarm in an electric field of strength E is deflected through an angle θ by a transverse magnetic field B according to the relationship[31]

$$\tan\theta = C.\frac{BW}{E} \qquad (II.2)$$

C being a constant of the order of unity. Under certain conditions even the earth's field can cause a significant deflection: for instance in methane at 5 torr pressure, $E/P = 1\ V\ cm^{-1}torr^{-1}$, a field of 0.5 gauss would cause an error equivalent to a source displacement of 1 mm. To preserve the required accuracy fields of greater than 0.1 gauss have to be eliminated, and to do this the apparatus was surrounded with three mutually prependicular pairs of Helmholtz coils. Square coils were used, each pair being separated by a distance equal to

0.544 times the length of one side (approx. 1m), giving a highly uniform field over a volume of approximately 15 cm diameter centred on the diffusion region.[36] The currents through each pair of coils (~80 turns each) necessary to produce near-zero field at the centre were found experimentally using a Hall-effect gaussmeter.

Highly localised magnetic fields arising from magnetised tube components could have an even more serious effect, particularly at the collector surface, so nonmagnetic metals were used throughout the electrode assembly.

II.2.6. Collector insulation

The insulation between collectors and from collectors to earth must be of the order of 10^3 times the input resistance ($10^{12}\Omega$) of the vibrating reed electrometers used to measure the currents. This criterion was adhered to when designing the collector supports in both the original and modified versions of the anode (II.3).

II.2.7. Cathode design

It is usual in swarm experiments to produce electrons by ultraviolet illumination of a gold-surfaced cathode. A disadvantage of this technique is that light scattered through the source aperture may give rise to spurious electron currents, and excessive irradiation may initiate chemical reactions in some gases as well as heating the sample gas. In an attempt to reduce these effects, a photocathode of the type described by Moruzzi[37] was chosen, where the gold surface is

evaporated onto a silica window and illuminated from the rear. To minimise the light transmitted to the source aperture, the direction of illumination was fixed at 35° to the tube axis. The electrodes in the vicinity of the cathode (Fig. II.3) were designed to orientate the swarm leaving the cathode towards the source aperture for maximum current. This was achieved by field-plotting with the aid of a resistance paper model.

II.2.8. Stability to temperature variation

To permit low operating and high bakeout temperatures, geometrical accuracy had to be preserved over a 600° range. This presented problems owing to the high differential expansion between suitable metals and insulators. The solution was to allow all electrodes to move concentrically with respect to the tube axis by employing a system of radial location (II.3).

II.3. CONSTRUCTION OF THE DIFFUSION TUBE

Figs. II.4 and II.3 show respectively a cutaway view and a diagrammatic section of the electrode assembly. Electrodes, support tube and vacuum tank were fabricated from Firth-Vickers "Immaculate 5" stainless steel.

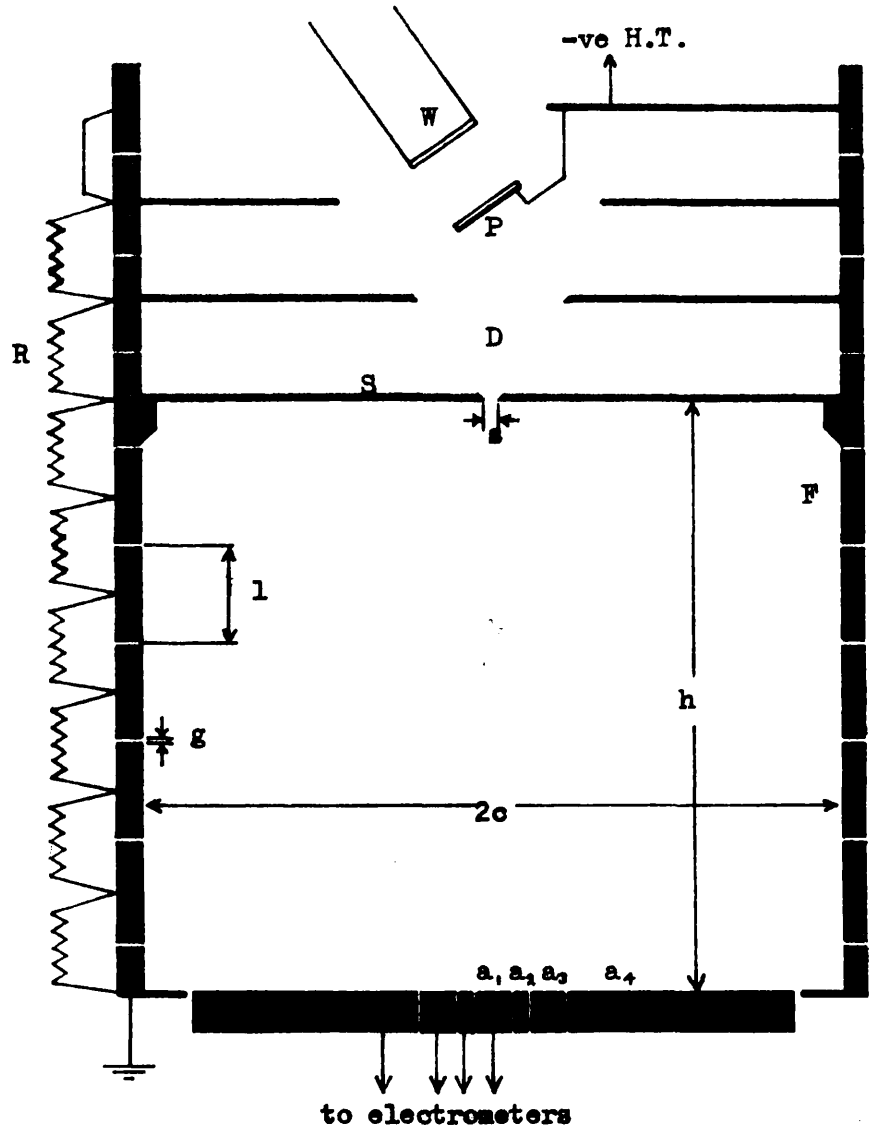

KEY

a_1, a_2, a_3, a_4 - collector electrodes

D - preliminary drift region
F - field electrode
P - photocathode surface
R - 200 K resistor
S - source electrode
W - sapphire vacuum window

For dimensions see Table II.1.

FIG. II.3. Schematic section of the electrode assembly.

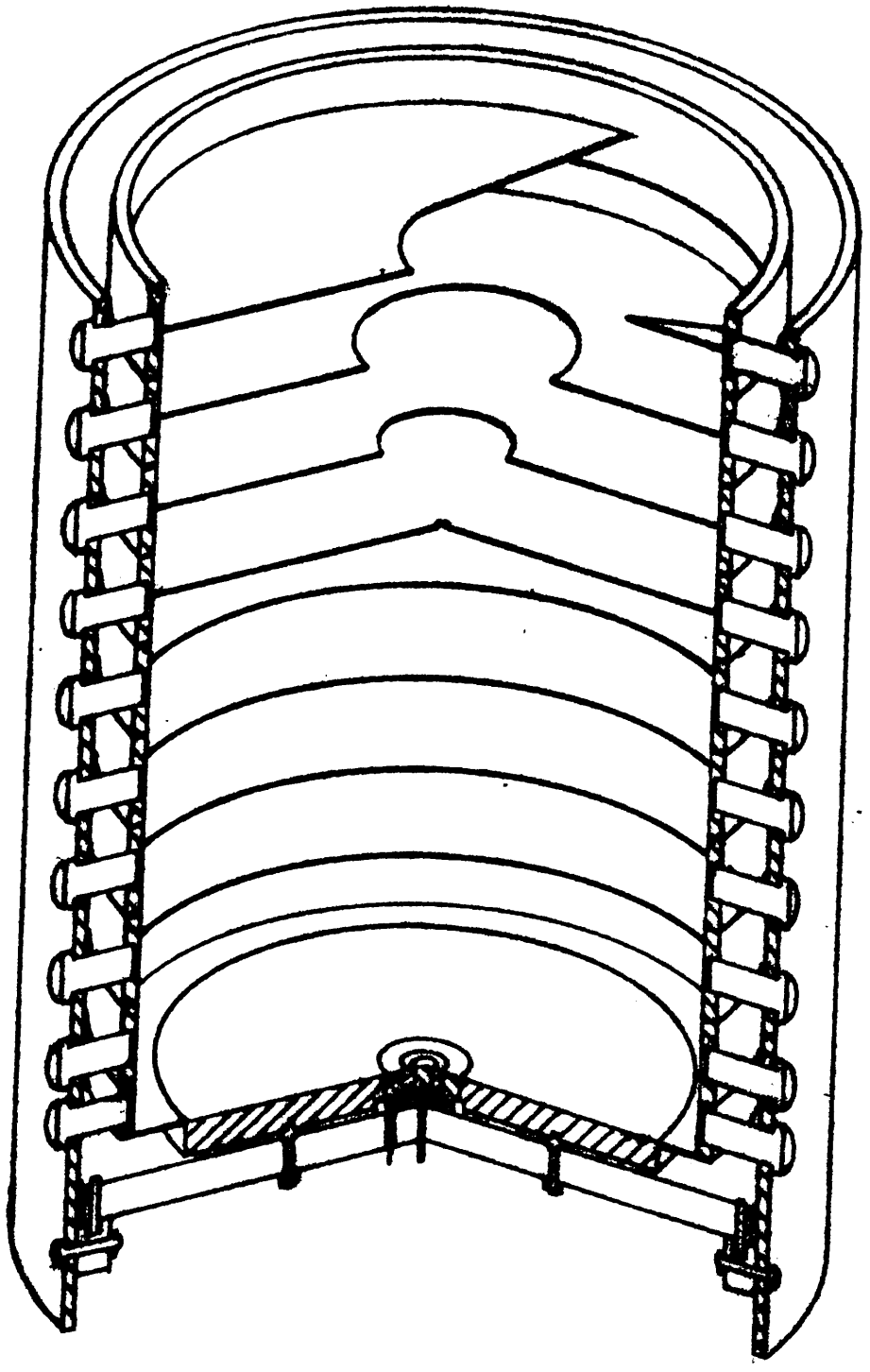

FIG. II.4. Cut-away view of the diffusion tube.

The principal dimensions are summarised below.

Table II.1

h	- measured drift distance	= 10.073 cm
b_1	- radius to centre of 1st anode gap	= 0.251 cm
b_2	- radius to centre of 2nd anode gap	= 0.500 cm
b_3	- radius to centre of 3rd anode gap	= 1.000 cm
l	- height of field module	= 1.676 cm
g	- gap between field electrodes	= 0.051 cm
2c	- inner diameter of field electrodes	= 12.3 cm
s	- diameter of source aperture	= 0.11 cm

II.3.1. Support tube and field electrodes

All electrodes were supported from a 6" diameter stainless steel tube which rested on the baseplate of the vacuum tank. The $\frac{1}{8}$" thick field electrodes were each located and supported radially by three insulating rods mounted at 120° intervals, free to slide in the support tube and thus allowing for differential expansion. These rods were $\frac{1}{4}$" in diameter, precision made in "Ceramtec" machinable ceramic. The disc sections of the upper electrodes were of .025" thick stainless steel.

II.3.2. Anode assembly

The collectors were made $\frac{1}{4}$" thick to ensure mechanical stability,

(a) Boron nitride pin mounting.

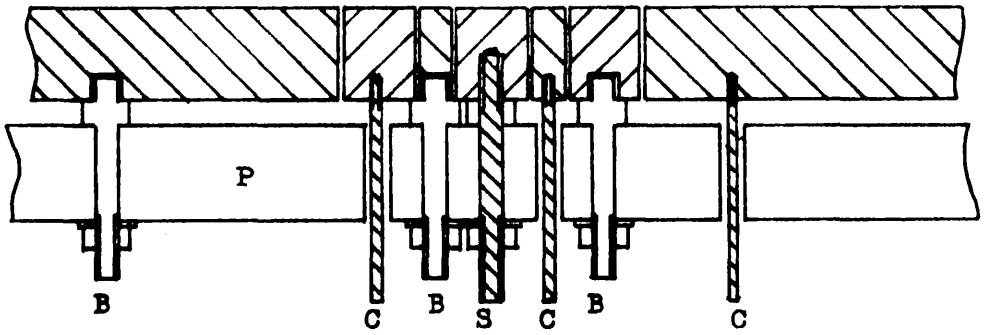

B - boron nitride pin

C - beryllium-copper conductor

P - pyrex base plate

S - locating stud for central collector

(b) Quartz ring mounting.

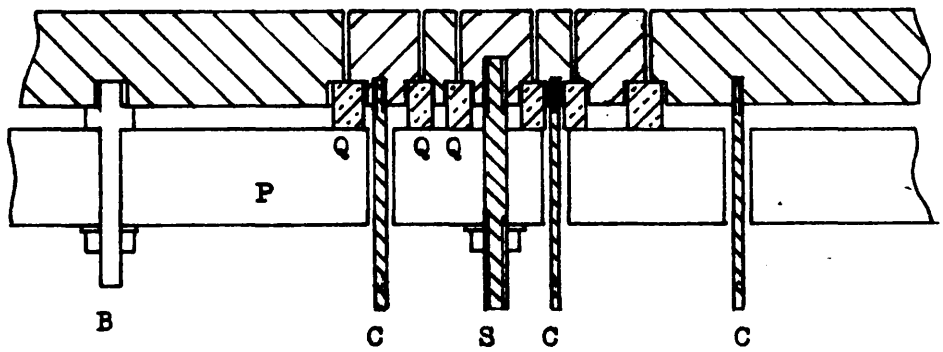

Q - quartz spacing ring

FIG. II.5 Detail of collector assembly

and were smooth-machined until their thickness matched to .0001".

The original design for the mounting system is illustrated in Fig. II.5(a). In this version, the collectors were supported clear of the Pyrex baseplate by high-insulation boron nitride pins, located in close-fitting holes drilled in the baseplate. Each annular section was mounted on three pins at 120° intervals, which fitted into radially elongated slots in the underside of the collector, thus allowing expansion and contraction to occur with concentric movement only. The central collector was located on a single beryllium-copper stud and spaced from the baseplate by a boron nitride washer.

It was thought that this arrangement would provide a high degree of electrical insulation and maintain close tolerances on the collector alignment over a wide temperature range. However the system proved unsatisfactory, as owing to the accumulation of small machining errors, particularly in the boron nitride pins, and in drilling the baseplate holes, the alignment of the collectors was poor in so far as the upper surfaces were not coplanar, and there was sufficient movement in the system to allow adjacent collectors to touch.

To rectify this with the minimum of reconstruction the assembly illustrated in Fig. II.5(b) was adopted. The boron nitride pin mounting was abandoned on the inner two annular collectors (a_2 and a_3), and instead all collectors were supported on precision ground quartz rings which located into machined recesses on the undersides of the collectors as illustrated. The clearances between the rings and the recesses were calculated to allow for differential expansion. These clearances did

allow slight lateral movement, but as the boron nitride pins were retained on the outer annulus (a_4) the maximum possible movement at room temperature was .005 cm on a_3.

The Pyrex baseplate supporting the anode was similarly located by three pins resting in radial slots in ceramic mounting blocks secured to the outer support tube.

II.3.3. Assembly and checking

Prior to assembly all components were thoroughly cleaned by ultrasonic agitation, then finally heated to 1000° C in a high-vacuum furnace to ensure surface cleanliness. The latter treatment also hardened the "Ceramtec" components and was known to reduce their outgassing rate. All metal surfaces within the diffusion region were then coated with colloidal graphite by applying an alcoholic suspension (DAG 580) and burnished when dry. During and after assembly alignments were checked by precision travelling microscope, and accurate values for the parameters h and b were recorded (Table II.1).

II.4. THE PHOTOCATHODE

The complete photocathode assembly (Fig. II.6) was flange-mounted and could be independently withdrawn from the apparatus. Ultraviolet light was admitted through a 1" diameter sapphire vacuum window. To insulate the cathode from earth and facilitate replacement, the gold

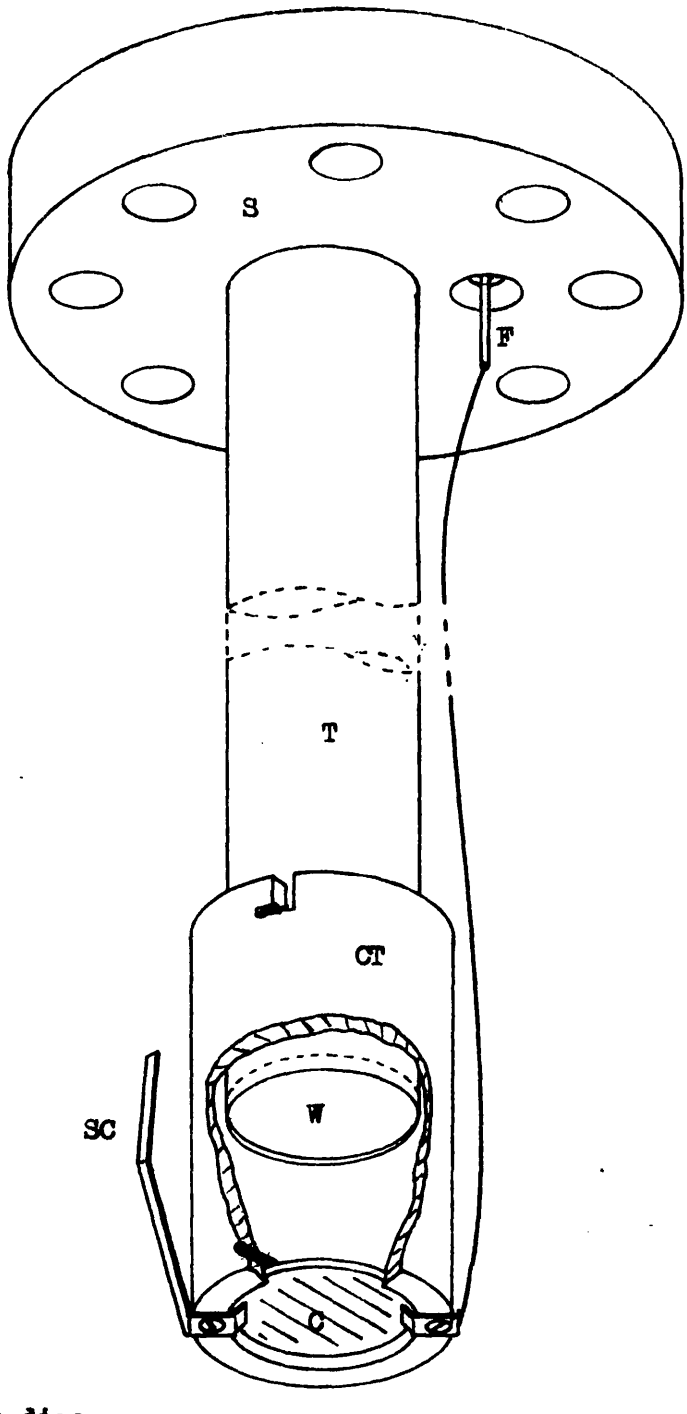

C - cathode disc
CT - ceramic tube
F - high voltage feedthrough
S - flange sealing surface
SC - spring contact
T - steel tube
W - sapphire window

FIG. II.6 Photocathode assembly.

surface was evaporated onto a thin silica disc which was supported 1" inside the window by a ceramic tube. Connection to the cathode was made through two tantalum contacts. One of these served as a spring contact to the topmost field electrode, and a lead connected the other to a feedthrough on the cathode flange, thereby giving two independent connections.

The first cathodes were obtained from E.M.I. Ltd. and gave rather low emission which rapidly deteriorated on prolonged exposure to atmosphere. To minimise the amount of handling in atmosphere, and to enable optimisation of film thickness for maximum emission, a small evaporation unit was built. This consisted of a glass vacuum tank pumped by the reference pressure gas-line (Fig. II.7) which accepted the entire cathode assembly through the upper end-plate. A 1 mm thick tungsten filament placed about 1" below the cathode disc served as an evaporation source, heated by a 30 A Variac-controlled power supply. During evaporation the cathode was held 200 V negative with respect to the earthed baseplate and filament, and irradiated with u.v. light through the sapphire window. The photoelectric emission current was monitored and evaporation continued until peak emission was just passed. The cathode assembly could then be transferred directly to the main vacuum tank with only a brief exposure to atmosphere.

Two ultraviolet sources were used: a 5.5 W "Pen-Ray" lamp, and a 100 W Hanovia UV 100 system. The former was a very compact U-shaped source which fitted into the steel tube immediately behind the vacuum window, and was used whenever the resulting currents were completely

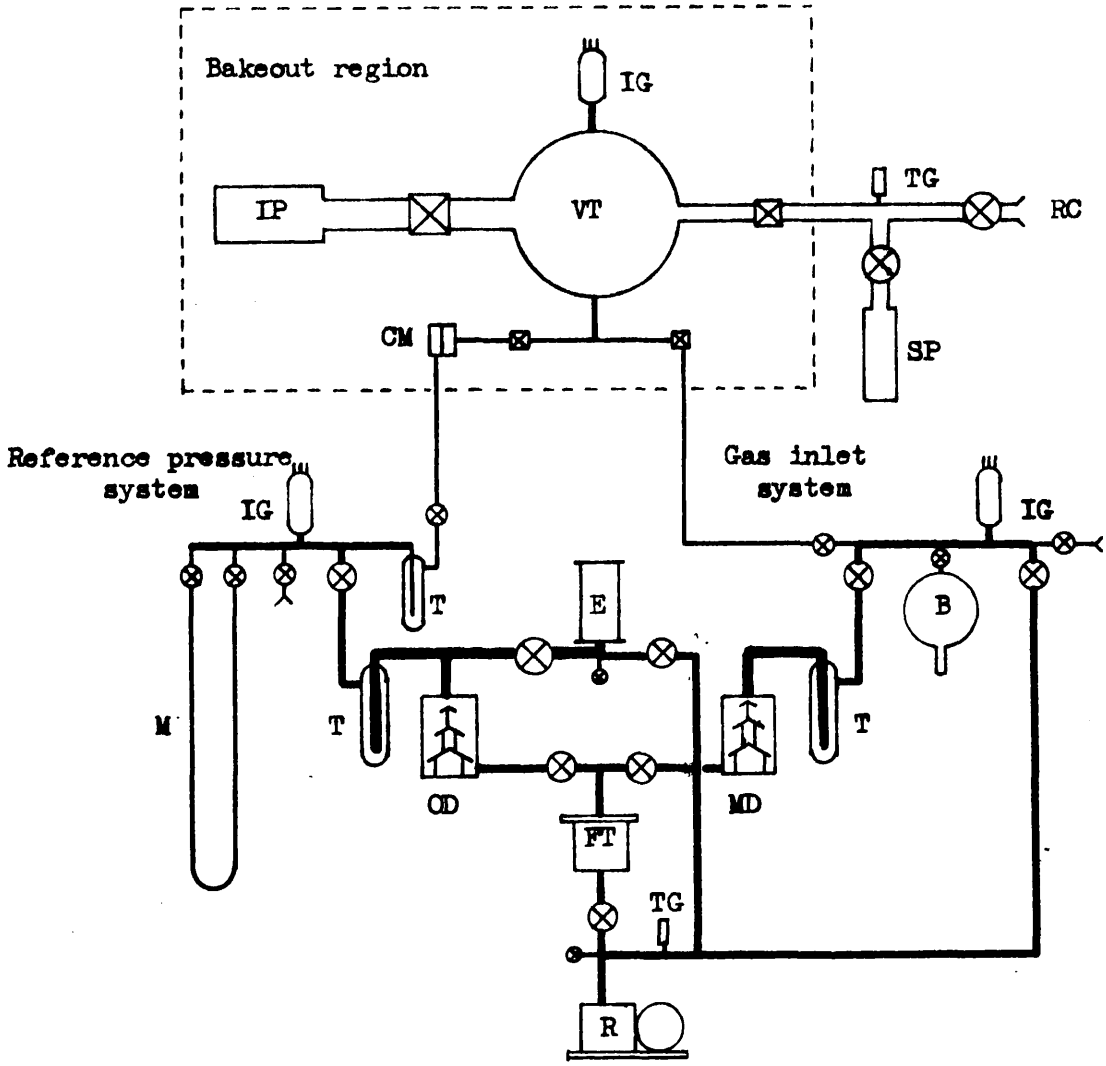

KEY

- bakeable all-metal valve
- diaphragm valve

B - storage bulb
CM - capacitance manometer
E - cathode evaporation tank
FT - foreline trap
IG - ionisation gauge
IP - ion pump
M - mercury manometer
MD - mercury diffusion pump
OD - oil diffusion pump
R - rotary pump
RC - rotary pump connection
SP - sorption pump
T - liquid nitrogen trap
TG - thermocouple gauge
VT - main vacuum tank

FIG. II.7. Vacuum and gas-handling systems.

adequate ($> 10^{-13}$A). At other times it was necessary to use the Hanovia system, which was an optically focussed source projecting a 1 cm diameter spot at a distance of 30 cm.

No detailed investigations of cathode behaviour were made, but total collected currents appeared to obey roughly a relationship of the form

$$I \propto E^a/P^b \qquad (a > b > 0)$$

The magnitudes of the currents varied between sample gases by several factors of ten.

II.5. VACUUM AND GAS-HANDLING SYSTEMS

The vacuum system layout is illustrated in Fig. II.7. The electrode assembly was contained in an 8" diameter welded stainless steel tank. The removable end-plates sealed on gold wire gaskets and carried high-insulation Leybold CM-12/1 feedthroughs. The cathode port and all vacuum connections were situated on the upper end-plate. This allowed easy access to the electrode assembly which rested on the lower plate. The tank was designed to be immersed in a low-temperature bath when required.

Ultra-high vacuum pumping was provided by a 50 l s^{-1} Mullard magnetron sputter-ion pump. Two stages of preliminary pumping were used: a trapped rotary pump down to 10^{-1} torr, and a molecular sieve sorption pump to further reduce the pressure to below 10^{-3} torr prior to ion pumping.

Within the bakeable region (Fig. II.7) all-metal seals and valves were employed. The vacuum tank and ion pump could be surrounded by ovens carrying radiant heaters capable of raising the temperature to over 300° C.

Sample gases were handled in a simple glass-blown system, pumped by a small mercury diffusion pump.

To avoid mercury vapour contamination, sample pressures were measured indirectly via a diaphragm type capacitance manometer (Granville-Phillips 212) with a 100 torr sensing head. The reference pressure for this was measured by a mercury manometer constructed from 10 mm bore thin-walled tubing and viewed with a cathetometer reading to .05 mm. Although the capacitance manometer could be calibrated for direct reading it was normally used as a null-reading instrument for the sake of accuracy, the pressure being read directly on the mercury manometer. The reference side could be pumped by a 25 l s^{-1} oil diffusion pump which also served to evacuate the cathode evaporation chamber.

II.6. ELECTRICAL DETAILS

Voltages to the field electrodes were provided by a potential dividing network, consisting of a chain of 200 kΩ resistors connected between adjacent electrodes. The lowest electrode was earthed and the uppermost connected to a Fluke 412B 0-2200 V stabilised supply, connection being made via a spring contact attached to a feedthrough in the tank

top plate. The cathode was held at the same potential by the dual connection system described.

The resistors (Pyrofilm PT60) were glass-encapsulated carbon film type, of ± 1% tolerance and closely matched temperature coefficients. Due to slight inaccuracies in the vertical positioning of the holes for the field electrode support rods, the electrode positions deviated slightly from equidistant spacing. These deviations were measured after assembly and resistors chosen to match the spacings, thereby improving the vertical field uniformity to better than 0.3% in the diffusion region.

Collected currents were measured by two Keithley 640 vibrating capacitor electrometers, capable of reading 10^{-15} A full scale with a $10^{12}\Omega$ input resistor. Each collector was connected to a three-way high-insulation switch which made connection to either electrometer or earth as desired. These switches were enclosed in a fully shielded box placed directly between the tank baseplate and the input sockets of the electrometer remote heads.

CHAPTER III

EXPERIMENTAL PROCEDURE AND RESULTS

III.1. OPERATING PROCEDURE

The normal sequence of operation was as follows:

(1) Admit gas sample to selected pressure.

(2) Select applied voltage V to give desired field strength E.

(3) Select operating mode 1, 2, or 3 by switching collectors to the two electrometers to give an effective inner collector radius of b_1, b_2, or b_3 respectively (Table II.1).

(4) Measure background currents (i.e. with u.v. light off) then currents with cathode illuminated and obtain true collected currents by subtraction.

III.1.1. Sample pressures

Gas samples were admitted to the tank only when the background pressure had fallen to below 10^{-7} torr, the system being baked if necessary to achieve this. To reduce contamination the tank was first flushed with a high pressure of the sample gas. The gas temperature was monitored with a copper-Eureka thermocouple and kept steady to within $\pm 1^{\circ}$ C.

Sample pressures varied between 3 and 1000 torr and were checked

at intervals throughout the run. Although the reference pressure could be read to ± 0.1 torr the limiting factor was the zero drift of the capacitance manometer which reduced the accuracy to about ± 0.2 torr.

III.1.2. Voltage setting

The range over which the field strength E could be varied was limited by two factors.

(1) At high E/P values ($\gtrsim$ 3-5 V $cm^{-1}torr^{-1}$) electrical breakdown ocurred with sparking between electrodes. To extend this range would require larger gaps between the field electrodes, which would render such an apparatus unsuitable for low field strengths due to field penetration.

(2) At low E/P the collected currents diminished and a poor signal to noise ratio caused rapid loss of accuracy. At the lower pressures used, high currents could be obtained even with very low field strengths, but with fields below about 3 V cm^{-1} irregular results were observed, probably due to the relative importance of contact potentials.

III.1.3. Current measurement

To avoid introducing space charge effects in the swarm[38], currents were not allowed to exceed 10^{-12} A. It was possible to measure currents using either of two electrometer input resistors, of value $10^{10}\Omega$ and $10^{12}\Omega$ respectively. The smaller resistor had the disadvantage of giving a higher noise level and greater zero drift,

whereas when the $10^{12}\Omega$ resistor was used the system required several minutes to come to equilibrium. Another consideration was that the input resistor introduces a potential difference between the collectors and earth, thereby distorting the field at the anode surface. Thus it is desirable to use a low resistor when measuring high currents. In practice, the collected current varied roughly proportionately to the applied field, so the potential difference at the anode was a fairly constant small fraction of the applied field, and at the lower values of E was probably smaller than the contact potentials. In addition, accurate measurements were made with the currents to the two collectors as equal as possible, so the potential difference between collectors was minimised. It was found best to use the $10^{10}\Omega$ resistor for currents greater than 10^{-13} A.

In the absence of cathode illumination, fairly constant total background currents of around + 10^{-15} A were recorded, probably arising from insulation leakage. Any increase in background above this level could usually be remedied by baking the apparatus. Slow fluctuations in the measured background reduced the accuracy with which true currents could be obtained by subtraction, so poor results were obtained when the total collected current was less than 10^{-14} A. With higher currents, however, the fluctuation was unimportant and it was only necessary to measure background currents occasionally during a run.

Currents arising from light penetration through the source aperture were investigated by biassing the cathode positive with respect to the

source electrode. No measurable currents were collected, indicating that such currents would certainly not exceed 0.1% of the total current.

III.1.4. Data logging

To improve accuracy in current measurement a Solartron series 2 data logging system was used to collect most of the data presented in this chapter. The electrometer feedback voltages were fed to the system's digital voltmeter and sampled at 15 s intervals for times varying from 2 to 10 minutes. The applied voltage was also sampled, along with signals indicating the collector mode and the u.v. light on/off position, thus enabling D/μ values to be computed directly from the punched tape output by a simple averaging of sampled current values. The averaging improved the signal to noise ratio somewhat and led to more consistent results than manual reading of the electrometers.

III.1.5. Calculation of results

Values of D/μ were calculated from Huxley's formula[31]:

$$R = \frac{I_1}{I_1 + I_2} = 1 - \frac{h}{d} \exp\left[-\frac{W}{2D}(d-h)\right] \qquad \text{(III.1)}$$

where I_1 and I_2 are the currents to inner and outer collectors respectively. The use of this formula was justified by the determination of empirical current ratio curves (III.2.2).

Preference was given to results where $0.3 < R < 0.8$. Where it was possible to compare results from the use of different collector modes, these agreed within the general experimental scatter. Occasionally a

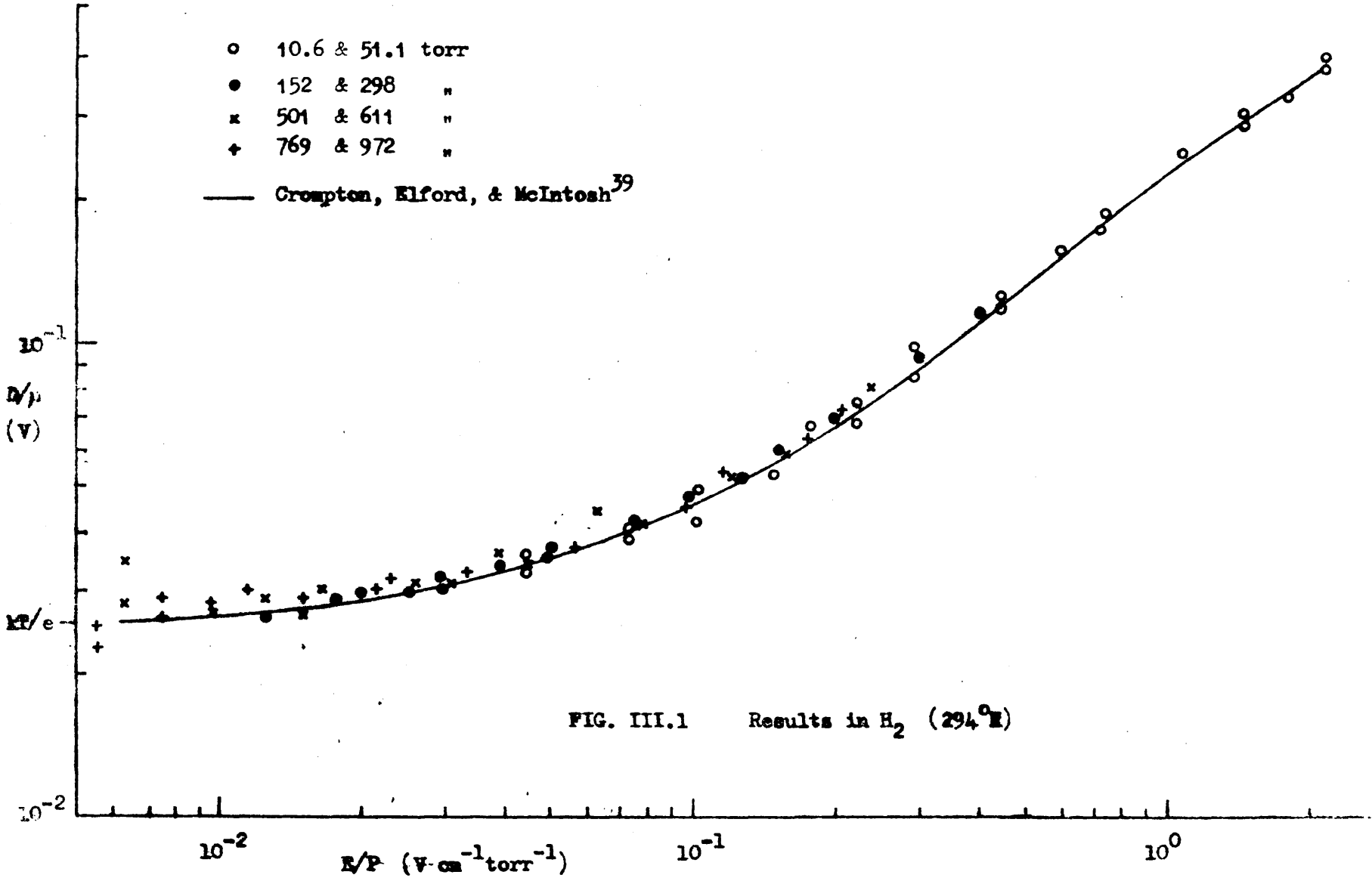

FIG. III.1 Results in H_2 (294°K)

slight but consistent difference was noticed between results obtained in modes 1 and 2; the difference varied in magnitude and sense between different runs, and was put down to variation in collector contact potentials with different gas samples and pressures.

III.2. CALIBRATION AND ESTIMATION OF ERRORS

III.2.1. Results in H_2

Measurements were made in hydrogen at 294°K, at eight pressures ranging from 10 to 970 torr. The gas was obtained from a B.O.C. cylinder (stated purity 99.9%). The results are plotted in Fig. III.1 and compared with the results of Crompton, Elford, and McIntosh[39], who claim an accuracy of ± 1%. The present results are seen to exhibit a scatter which is around ± 5% over most of the E/P range, becoming large below ~0.02 V $cm^{-1} torr^{-1}$. However a smooth curve drawn through the experimental points would not deviate from the results of Crompton et al. by more than 2-3% for $E/P > 10^{-2}$ V $cm^{-1} torr^{-1}$. This procedure was therefore adopted with all results to obtain the D/u values used in the cross section calculations.

III.2.2. Empirical current ratio curves

Huxley's formula for the current ratio R was obtained by solution of the diffusion equation using boundary conditions of a point source, no walls, and ignoring the effect of the collector. It has been found to give the best agreement with experiment for diffusion geometries where

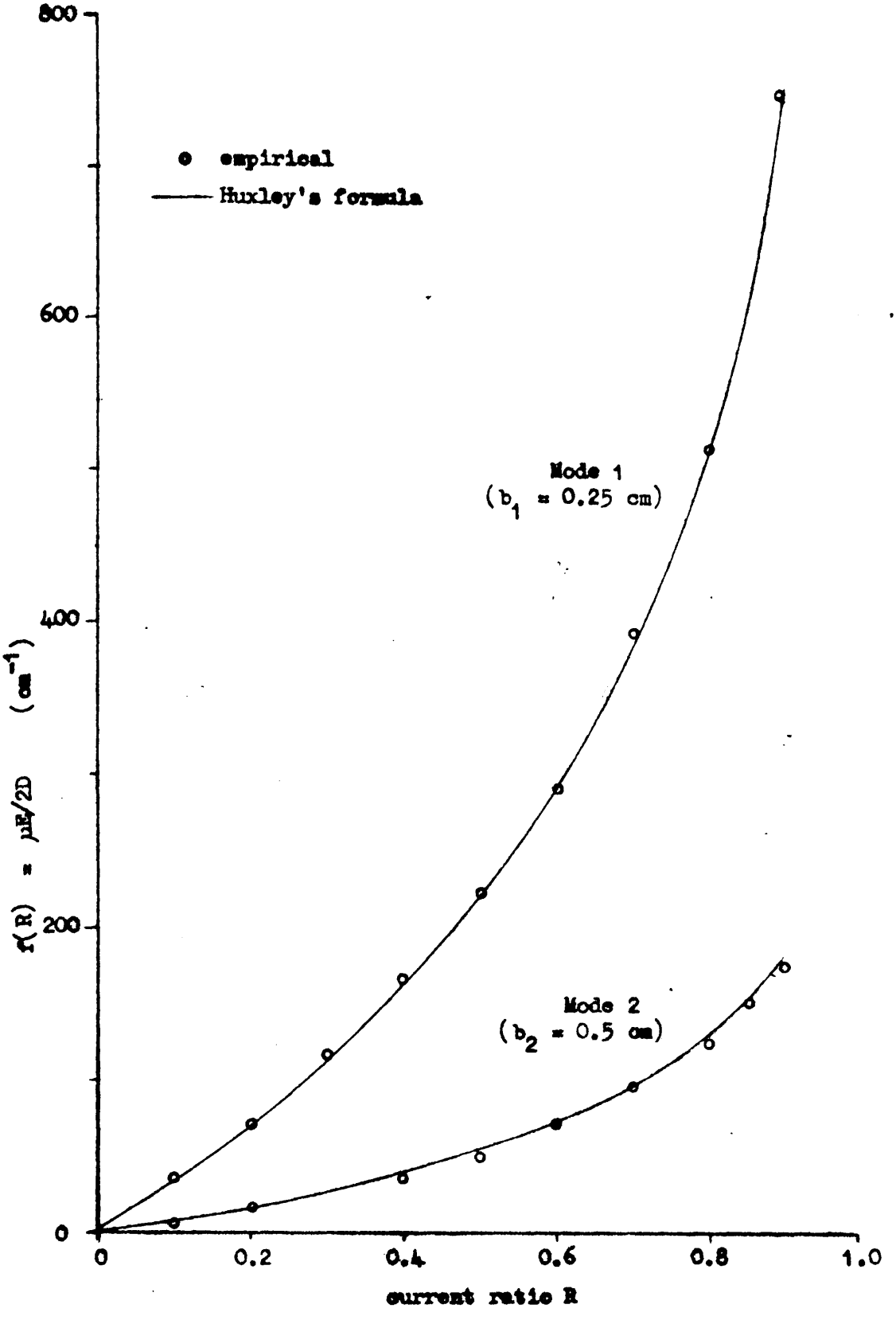

FIG. III.2. Empirical current ratio functions from CH_4 data.

$h \gg b$[41]. This conclusion was supported by Francey[42] using an alternative theoretical approach, namely the solution of the Boltzmann equation for certain forms of the elastic cross-section. Warren and Parker[40] ascribed apparent deviations from this formula in their experiments to systematic errors, particularly in apparatus geometry, and calculated their results from expirical ratio curves obtained as follows:

It is assumed that

$$D/\mu = g(E/P) \qquad \text{(III.2)}$$

$$\text{and } \mu E/2D = f(R) \qquad \text{(III.3)}$$

This gives

$$\log (E/2) = \log \left[g(E/P)\right] + \log \left[f(R)\right] \qquad \text{(III.4)}$$

The experimental data is plotted on a graph of R vs E, and smooth curves are drawn through the points corresponding to each pressure. For R values at suitable intervals from 0 to 1, E values are taken from the intersections of the curves with each R value and plotted on a new graph of $\log(E/2)$ vs $\log(E/P)$. Smooth curves are drawn for each R value and $f(R)$ is estimated from the displacement of each curve given by equation (III.4), using the requirement that $\log \left[f(R)\right] = 0$ for $D/\mu = E/2$ and $D/\mu \to kT/e$ as $E \to 0$. A graph of $f(R)$ vs R is thus obtained for the apparatus.

This procedure was carried out with the present results in methane, for the current ratios corresponding to collector modes 1 and 2. Fig. III.2 compares the resulting $f(R)$ curves with those obtained from

Huxley's formula. The agreement is good for mode 1, and although slight deviations occur for mode 2 these are apparently random and probably arise from a shortage of experimental points. For mode 3, insufficient data was available to make the process meaningful. To calibrate the apparatus fully for all three modes in this way would require a very large number of data points, preferably in a gas with high D/μ (e.g. the inert gases). However in view of the close correspondence of the empirical curves derived for methane, and the agreement of the hydrogen results with previous data, the use of Huxley's formula was considered justified.

III.2.3. Sources of error

(a) Error in E/P: The uncertainty in E/P is almost wholly due to the random error of $\pm$ 0.2 torr in pressure measurement. This became important at pressures below 10 torr and limited the accuracy of high E/P data. At low E/P the variation of D/μ with E/P is small and errors in E/P were consequently insignificant.

(b) Error in current ratio R: Random errors in current measurement were large when currents were $\lesssim 10^{-14}$ A. The data logging procedure gave a slight improvement, but over much of the E/P range systematic errors were probably dominant, and could not be quantitatively assessed as contact potentials and collector variations probably played a major role. The overall accuracy may be roughly assessed from the scatter in experimental points and the deviation of the hydrogen results from those of Crompton et al. A safe estimate of accuracy in the averaged values would be $\pm$ 5% for

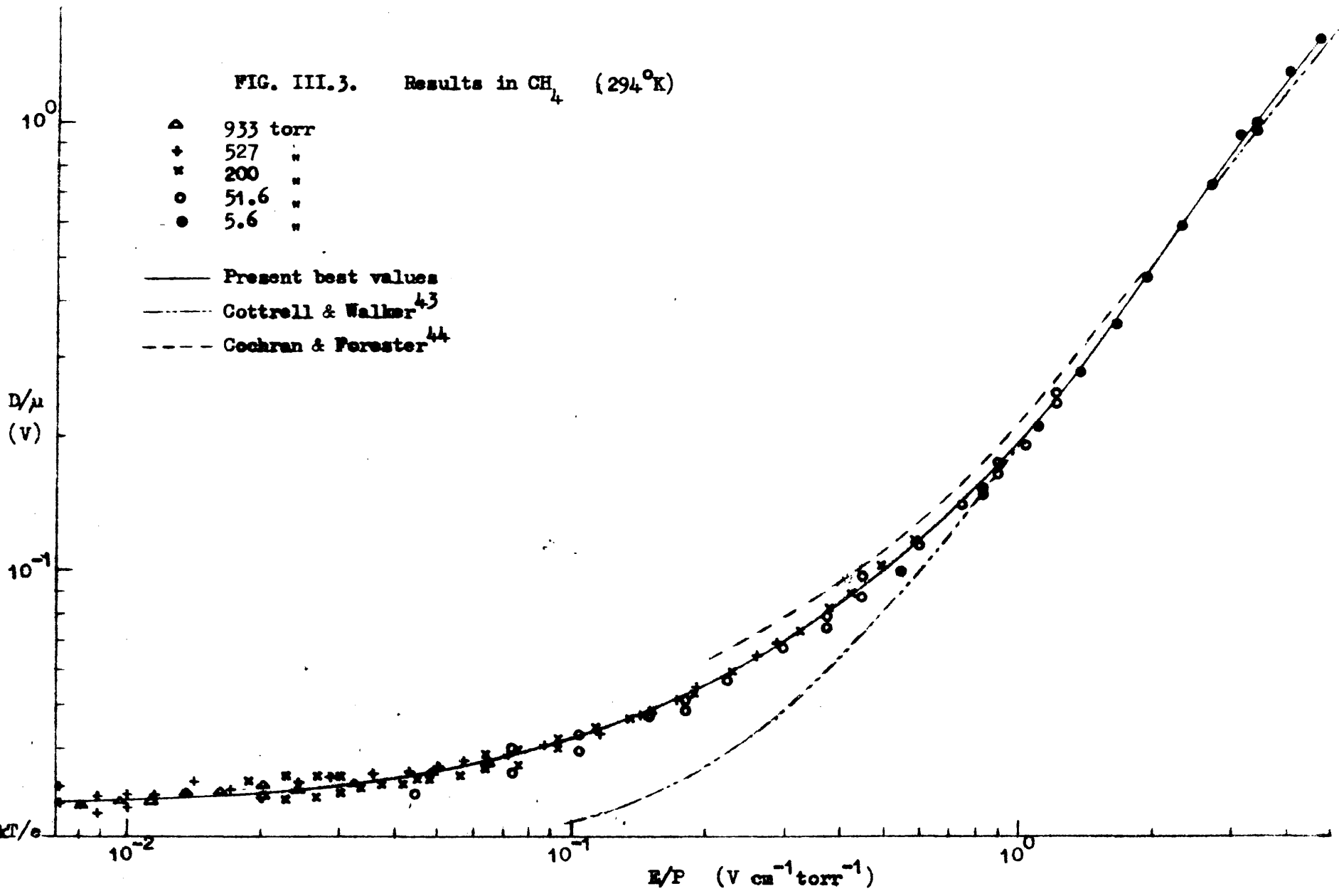
FIG. III.3. Results in CH_4 (294°K)
933 torr
527 "
200 "
51.6 "
5.6 "
Present best values
Cottrell & Walker[43]
Cochran & Forester[44]
10^0
10^{-1}
D/μ (V)
kT/e
10^{-2}
10^{-1}
10^0
E/P (V cm^{-1} $torr^{-1}$)

D/μ values above ~ 0.04 V, rising to nearer $\pm$ 10% close to thermal values.

III.3. EXPERIMENTAL RESULTS

III.3.1. Methane CH_4

B.O.C. purified grade methane with a stated minimum purity of 99% was pumped briefly at 77°K and distilled from an ethanol slush bath (161°K). Fig. III.3 shows D/μ results at 294°K and Table III.1 gives the best average values. The results of Cottrell and Walker[43] and Cochran and Forester[44] are also shown in Fig. III.3 for comparison

Pollock[45] discounted the results of Cochran and Forester, as when plotted on a small scale linear graph the D/μ values did not appear to extrapolate to kT/e at $E/P = 0$. However, as is seen from a logarithmic plot, D/μ approaches kT/e asymptotically as $E/P \to 0$, and little distinction can be drawn between any of the existing results on this basis. The logarithmic plot is the better method of presentation for all transport coefficients as they generally vary most rapidly at low E/P.

III.3.2. Tetradenteromethane CD_4

A sample of CD_4 was obtained from Merck, Sharp and Dohme Ltd., who stated 97% purity, and treated as was methane.

The results obtained (Fig, III.4) were completely anomalous. From Cottrell and Walker's values[43], close similarity to methane was

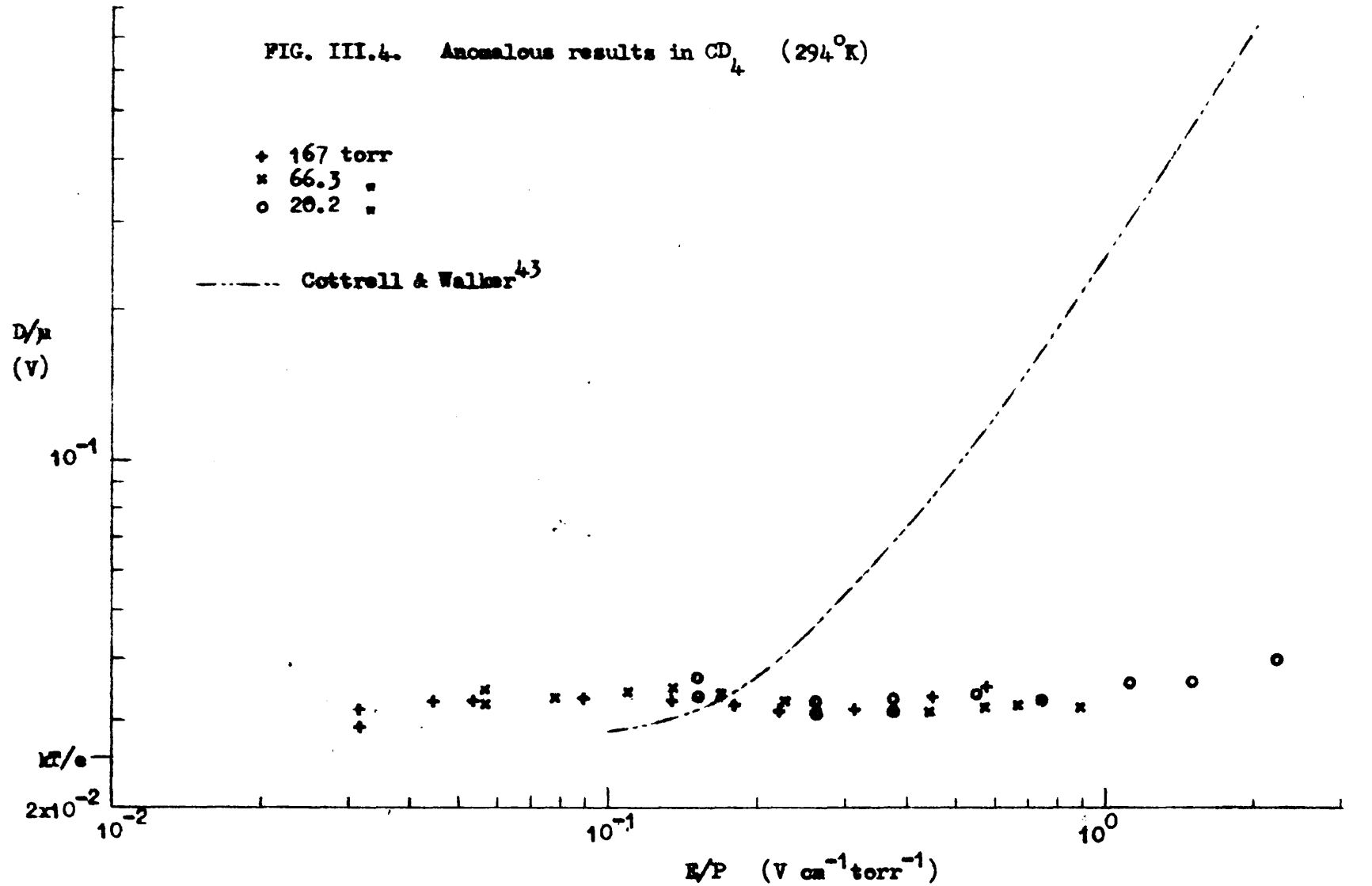
FIG. III.4. Anomalous results in CD_4 (294°K)
+ 167 torr
× 66.3 "
o 20.2 "
Cottrell & Walker[43]
D/μ (V)
10^{-1}
kT/e
2×10^{-2}
10^{-2}
10^{-1}
10^{0}
E/P (V $cm^{-1}torr^{-1}$)

expected but in fact near-thermal values of D/μ were obtained for E/P up to 2 V $cm^{-1}torr^{-1}$. The results showed no pressure effect between 20 and 160 torr and were reproducible after evacuating the tank and admitting CH_4 samples to check for apparatus malfunction. An electronegative contaminant was therefore suspected, which would give a negative ion current with a low D/W value, but as successive distillations from ethanol slush and liquid argon baths had no effect on the results, it seemed that air could be the only major impurity, as the manufacturers analysis indicated. High-resolution mass-spectrometry failed to detect any contaminants other than N_2, O_2, and H_2O - the latter at instrument background level. Addition of 10% air to methane gave less than 20% reduction in D/μ at $E/P \simeq 0.3$ V $cm^{-1}torr^{-1}$. Results in H_2 are known to be sensitive to very small concentrations of oxygen[39], but in this case the CD_4 values were a factor of ten lower than results for pure O_2[46]. Negative ion formation would appear to be a possible explanation but further experiments would be required to determine the nature of the species and the dependence on the gases present.

III.3.3. Ethylene C_2H_4

Ethylene (Air Products Ltd.) of stated purity 99.8% was pumped at 77°K to an ultimate pressure of 5×10^{-3} torr, and distilled from an ethanol slush bath. (A similar purification procedure was used for the remaining gases in this chapter.) The collected currents were less than

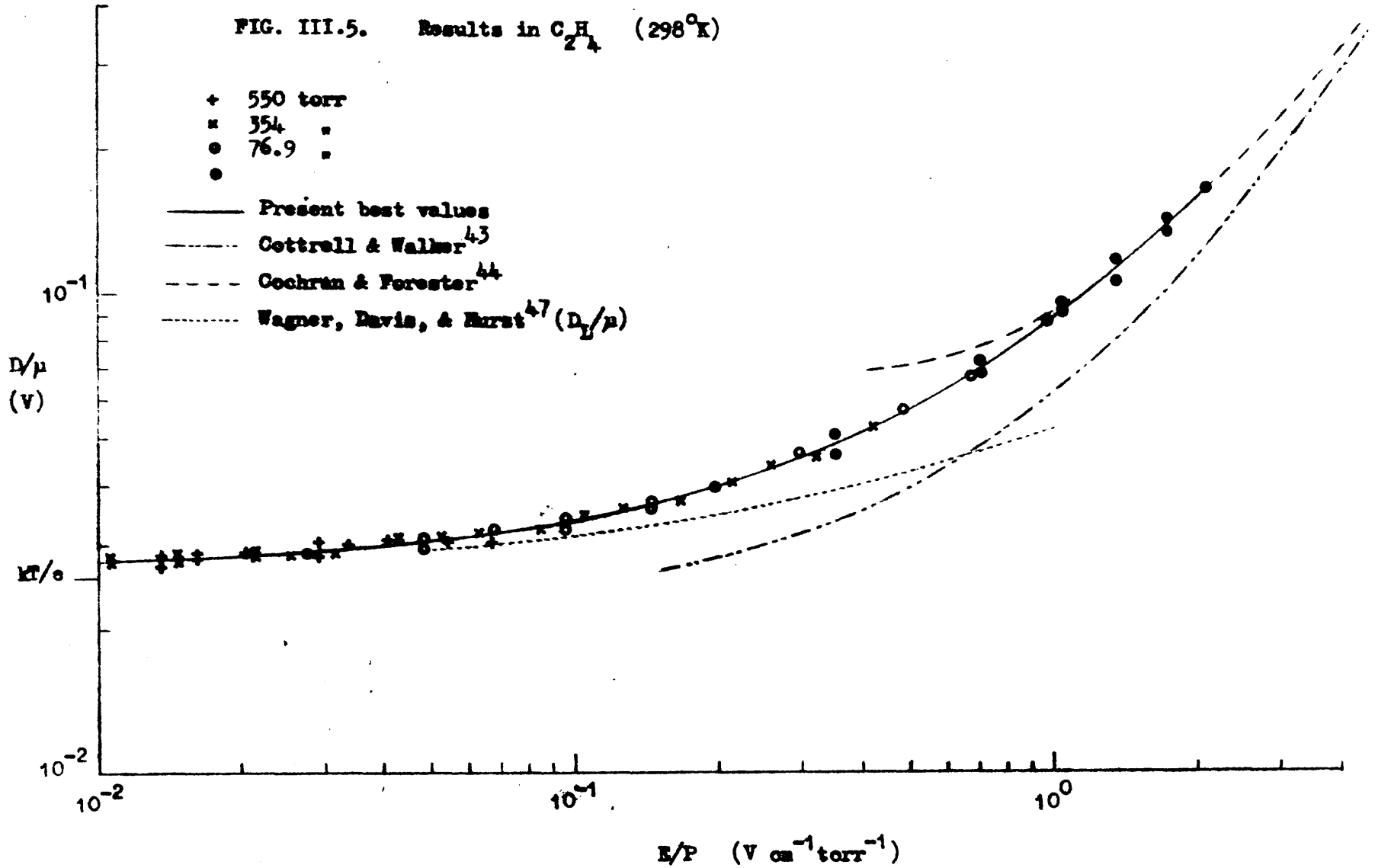
FIG. III.5. Results in C_2H_4 (298°K)
+ 550 torr
× 354 "
● 76.9 "
●
Present best values
Cottrell & Walker[43]
Cochran & Forester[44]
Wagner, Davis, & Hurst[47] (D_L/μ)
10^{-1}
D/μ
(V)
kT/e
10^{-2}
10^{-2}
10^{-1}
10^{0}
E/P (V cm^{-1} $torr^{-1}$)

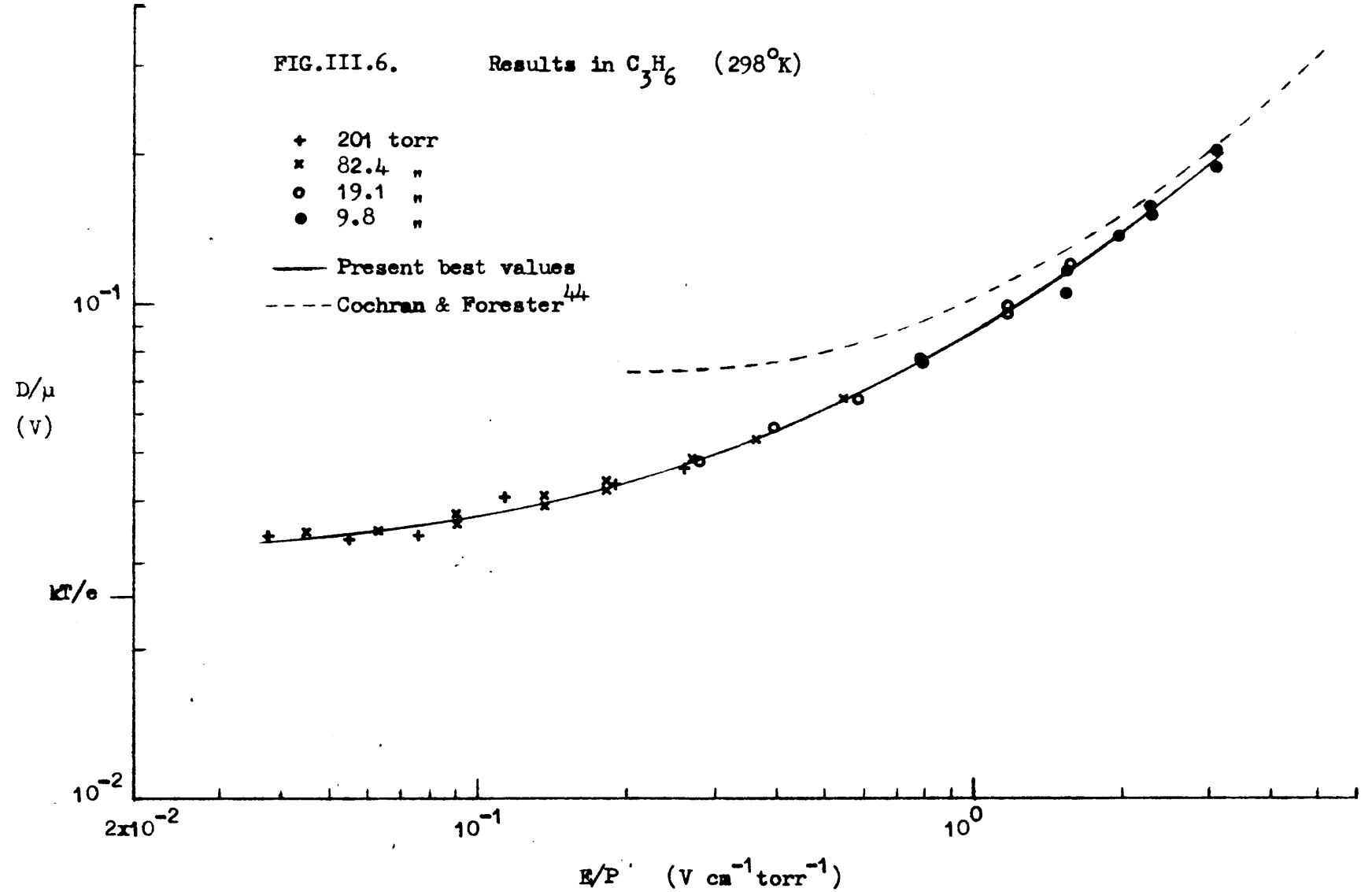
FIG.III.6. Results in C_3H_6 (298°K)
201 torr
82.4 "
19.1 "
9.8 "
Present best values
Cochran & Forester[44]
10^{-1}
D/μ
(V)
kT/e
10^{-2}
$2x10^{-2}$
10^{-1}
10^{0}
E/P (V $cm^{-1}torr^{-1}$)

a tenth of those obtained in methane, which were exceptionally high.

D/μ results are shown in Fig. III.5 and best values are given in Table III.1. At intermediate E/P the results again fall between those of Cochran and Forester[44] and Cottrell and Walker[43]. Also shown in Fig. III.5 are the time-of-flight results of Wagner, Davis and Hurst[47] for longitudinal diffusion which have been used to estimate mean swarm energies[48].

III.3.4 Cyclopropane C_3H_6

Cyclopropane was obtained from a Matheson cylinder, stated purity 99.9%, and purified by low temperature distillation. The collected currents in this gas were low, rarely exceeding 5×10^{-14} A, and measurements were not possible at $E/P < 4 \times 10^{-2}$ V cm^{-1}torr^{-1}. Fig. III.6 shows D/μ results and Table III.1 gives best average values. The only other data for cyclopropane is that of Cochran and Forester[44], and as with the other gases studied their D/μ values are significantly higher than the present results for $E/P < 2$ V cm^{-1}torr^{-1}. Both sets of results show a close similarity in the bahaviour of cyclopropane and ethylene, in keeping with many of their chemical properties.

III.3.5. Acetylene C_2H_2

The sample was from a Matheson cylinder, stated purity 99.8%, and the currents obtained were of the same order as those in ethylene. D/μ results are given in Fig. III.7 and best values in Table III.1.

No other data is available for comparison, the only known

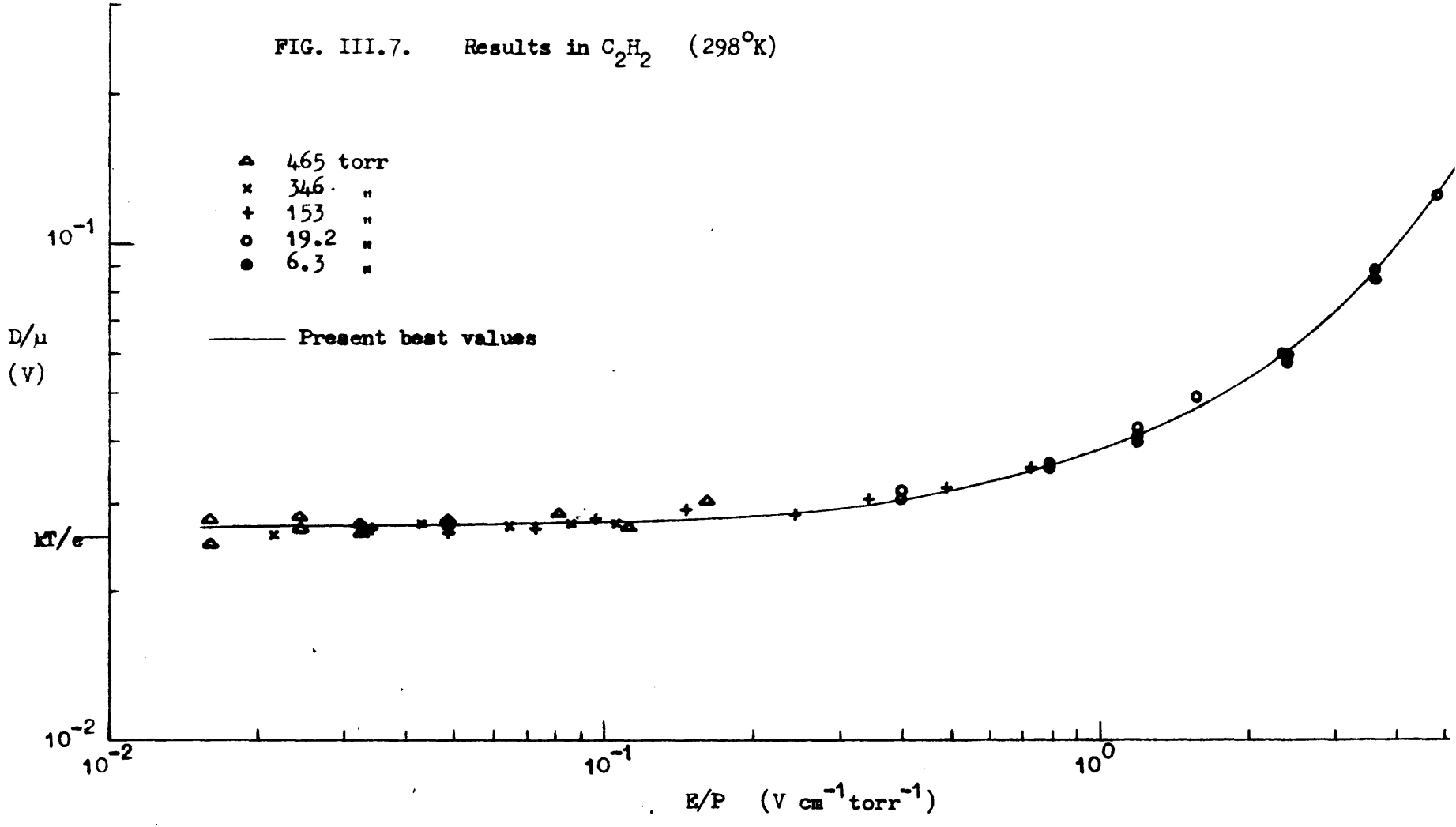
FIG. III.7. Results in C_2H_2 (298°K)
465 torr
346 "
153 "
19.2 "
6.3 "
Present best values
D/μ (V)
kT/e
10^{-1}
10^{-2}
10^{-2}
10^{-1}
10^{0}
E/P (V cm^{-1} $torr^{-1}$)

FIG. III.8. Results in H_2S (298°K)

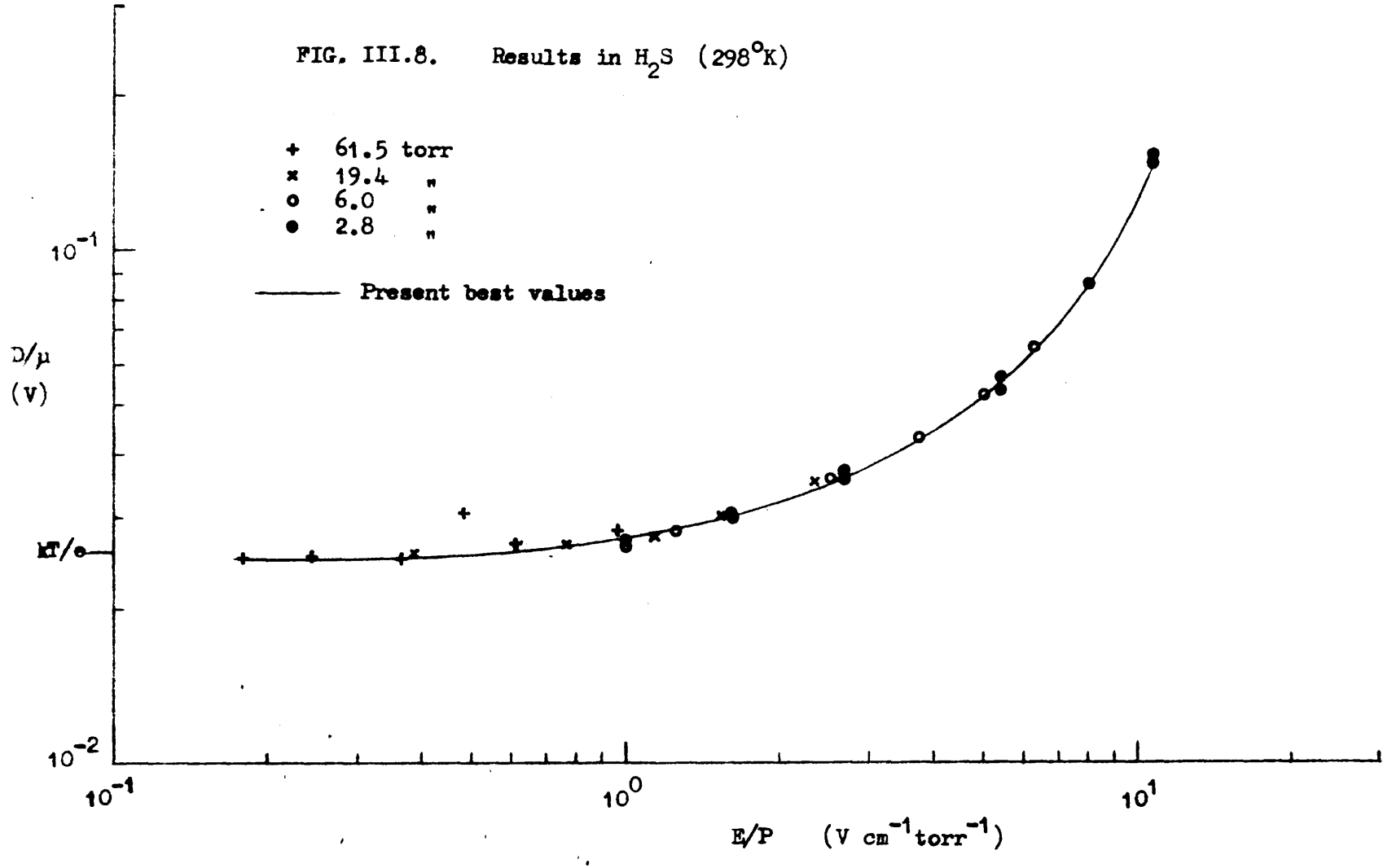

previous measurements in acetylene being those by Maydan[49] which exhibit a wide scatter and do not extend below E/P = 10 V $cm^{-1}torr^{-1}$. The two sets of results do however appear to join up smoothly.

III.3.6. Hydrogen sulphide H_2S

The sample was Matheson C.P. grade, stated purity 99.5%. The gas appeared to have a very adverse effect on the photocathode and it was only possible to obtain measurable currents at low gas pressures ($\lesssim 50$ torr). Although the cathode recovered almost fully after evacuation and filling with CH_4, this treatment did not improve the subsequent emission in H_2S. It was not possible to make measurements at $E/P < 0.1$ V $cm^{-1}torr^{-1}$, but as the D/μ value appears to be nearly thermal for $E/P < 1$ this was of little importance.

No other measurements appear to have been made in H_2S, but it was noticed that the results resembled published data[49] for NH_3, which is believed to have a total cross-section close to that of H_2S at low energies[50].

Table III.1. Best experimental values of D/μ (V)

E/P ($V\ cm^{-1}\ torr^{-1}$)	CH_4 (294°K)	C_2H_4 (298°K)	C_3H_6 (298°K)	C_2H_2 (298°K)	H_2S (298°K)
8.0×10^{-3}	3.05×10^{-2}				
1.0×10^{-2}	3.10	2.75×10^{-2}			
1.5	3.15	2.80			
2.0	3.20	2.85		2.70×10^{-2}	
2.5	3.25	2.90		2.70	
3.0	3.35	2.95	3.25×10^{-2}	2.70	
4.0	3.45	3.00	3.30	2.70	
5.0	3.55	3.05	3.40	2.70	
6.0	3.65	3.10	3.50	2.70	
8.0	3.90	3.20	3.65	2.70	
1.0×10^{-1}	4.15	3.35	3.80	2.70	
1.5	4.85	3.60	4.10	2.75	
2.0	5.6	3.95	4.40	2.85	2.50×10^{-2}
2.5	6.3	4.25	4.70	2.90	2.50
3.0	7.1	4.55	5.0	2.95	2.50
4.0	8.7	5.2	5.6	3.05	2.55
5.0	1.05×10^{-1}	5.7	6.2	3.20	2.55
6.0	1.24	6.2	6.7	3.35	2.60
8.0	1.62	7.4	7.8	3.60	2.70
1.0×10^{0}	2.05	8.5	8.9	3.90	2.80
1.5	3.35	1.19×10^{-1}	1.14×10^{-1}	4.55	3.05
2.0	5.0	1.57	1.40	5.3	3.30
2.5	6.8		1.67	6.2	3.55
3.0	8.6		1.97	7.2	3.85
4.0	1.26×10^{0}			1.02×10^{-1}	4.50
5.0				1.36	5.3
6.0					6.2
8.0					8.6
1.0×10^{1}					1.30×10^{-1}

CHAPTER IV

ANALYSIS OF SWARM DATA

The method of analysis described in this chapter was introduced by Frost and Phelps[24], and has met with success in the treatment of very simple molecules. Only a brief outline will be given of the mathematical treatment, which has been described in detail elsewhere, and emphasis will be placed on the computational approach used in this research.

IV.1. DERIVATION OF THE BOLTZMANN EQUATION

The central feature of the analysis is the determination of the electron velocity distribution by solution of the Boltzmann equation, which is basically a statement of all forms of energy gain and loss by the swarm. The equation appropriate to a steady-state swarm was derived by Holstein[112]. The velocity distribution function $f(\underline{v},\underline{r},t)d\gamma\, dV$ is defined as the fraction of electrons at time t in an element of velocity-position space $d\gamma\, dV$ with co-ordinates $\underline{v},\underline{r}$. If f is spatially independent (see IV.5.2) and the sole external force is a field E along the z axis, the result of expressing f in terms of partial

derivatives is

$$\frac{\partial f}{\partial t} = -\frac{Ee}{m}\left(\frac{\partial f}{\partial v_z}\right) + \left(\frac{\partial f}{\partial t}\right)_{\text{collisions}} \qquad \text{(IV.1)}$$

which is the appropriate non-explicit form of the Boltzmann equation. Further, the steady state assumption implies $\partial f/\partial t = 0$.

The second term on the right of (IV.1) must be written in terms of the relevant collision cross-sections, which is done by considering the rates of scattering in and out of $d\gamma\, dV$. For example, the probability of elastic scattering through an angle ψ into a solid angle $d\omega'$ is

$$P(v,\psi,d\omega',dt) = Nv\sigma_o(v,\psi)d\omega' dt \qquad \text{(IV.2)}$$

which when multiplied by f and integrated over total solid angle gives the rate of elastic scattering from $d\gamma\, dV$. Considering thus all scattering in and out of $d\gamma\, dV$ by elastic and inelastic collisions, equation (IV.1) becomes (in polar co-ordinates referred to the z-axis)

$$\begin{aligned}\frac{\partial f}{\partial t} = &-\frac{Ee}{m}\cdot\frac{\partial f}{\partial v_z} + Nv\int_{\omega'}\left[f(\theta';v)-f(\theta,v)\right]\sigma_o(\psi,v)d\omega' \\ &+ Nv^{-2}\frac{m}{M}\cdot\frac{\partial}{\partial v}\int_{\omega'}(1-\cos\psi)v^4 f(\theta';v)\,\sigma_o(\psi,v)d\omega' \\ &+ \sum_i Nv\int_{\omega'}\left[f(\theta';v')\,\sigma_i(\psi,v')(v'/v)^2 - f(\theta,v)\,\sigma_i(\psi,v)\right]d\omega' \qquad \text{(IV.3)}\end{aligned}$$

the summation in the last term including superelastic collisions.

The above integro-differential equation has two variables

(θ and v) and is intractable in this form. Holstein's approach was to expand f in spherical harmonics, retaining only the first two terms:

$$f(\theta,v) \simeq f_o(v) + \cos\theta f_1(v) \qquad (IV.4)$$

This is valid provided that (a) the distribution is nearly spherical ($v >> W$), and (b) $Q_m >> \sum Q_i$; these assumptions will be discussed in IV.5.2.

This substitution permits integration of (IV.3). Conversion is made to energy units ($\epsilon = \frac{1}{2}mv^2$), f(v) being replaced by $f(\epsilon)$ such that the normalised probability distribution of ϵ is given by

$$\phi(\epsilon)d\epsilon = \epsilon^{\frac{1}{2}} f(\epsilon)d\epsilon \qquad (IV.5)$$

After inclusion of an additional term to allow for the thermal motion of the gas molecules, the resultant simplified Boltzmann equation is

$$0 = \frac{(eE)^2}{3} \cdot \frac{d}{d\epsilon}\left[\frac{\epsilon}{NQ_m(\epsilon)} \cdot \frac{df_o}{d\epsilon}\right] + \frac{2m}{M} \cdot \frac{d}{d\epsilon}\left[\epsilon^2 NQ_m(\epsilon).(f_o + kT\frac{df_o}{d\epsilon})\right]$$
$$+ \sum_i \left[(\epsilon + \epsilon_i)f_o(\epsilon + \epsilon_i)NQ_i(\epsilon + \epsilon_i) - f_o(\epsilon)NQ_i(\epsilon)\right]$$
$$+ \sum_i \left[(\epsilon - \epsilon_{-i})f_o(\epsilon - \epsilon_{-i})NQ_{-i}(\epsilon - \epsilon_{-i}) - f_o(\epsilon)NQ_{-i}(\epsilon)\right] \qquad (IV.6)$$

Here, the first term is associated with the energy input by the field, the second with the energy exchange through elastic collisions, and the third and fourth with inelastic and superelastic energy exchange respectively. The nonspherical component f_1 is related to f_o by

$$f_1(\epsilon) = -\frac{eE}{N} \cdot \frac{1}{Q_m(\epsilon)} \cdot \frac{df_o(\epsilon)}{d\epsilon} \qquad (IV.7)$$

The object is to solve (IV.6) for a given set of cross-sections and use the resulting $f_o(\epsilon)$ to calculate transport coefficients.

IV.2. SOLUTION OF THE BOLTZMANN EQUATION

The summation terms in (IV.6) complicate the solution considerably and the available numerical methods all involve approximations.

IV.2.1. Solution neglecting superelastic collisions

This is the method upon which the present computer program is based. For convenience, the following normalised variables are used:

$$\begin{aligned} z &= \epsilon/kT \\ \theta &= Q_m/Q_o \text{ where } Q_o \text{ is a unit cross-section e.g. } 10^{-16}\text{cm}^2. \\ \eta_i &= (M/2m)(Q_i/Q_o) \\ \alpha &= (M/6m)(eE/NQ_o kT)^2 \end{aligned} \qquad \text{(IV.8)}$$

These are substituted in (IV.6), omitting the superelastic term, giving upon integration

$$\frac{df_o(z)}{dz}\left[\frac{\alpha z}{\theta} + z^2\theta\right] + z^2\theta f_o(z) + \sum_i \int_z^{z+z_i} x\eta_i(x) f_o(x)\,dx = 0 \qquad \text{(IV.9)}$$

Introducing the functions

$$h(z) = z\alpha/\theta + z^2\theta \qquad \text{(IV.10)}$$

$$g(z) = z^2\theta/h(z) \qquad \text{(IV.11)}$$

and factorising f_o as

$$f_o(z) = v(z)\exp\left[-\int_o^z g(x)dx\right] \qquad (IV.12)$$

where $v(z)$ is a measure of the influence of inelastic collisions on f_o, (IV.9) becomes

$$\frac{dv(z)}{dz} = -\sum_{i=1}^{n}\int_z^{z+z_i}\frac{x n_i(x)v(x)}{h(z)}\exp\left[-\int_z^x g(y)dy\right]dx \qquad (IV.13)$$

A three-point Simpson's rule integration from z_{j-1} to z_{j+1} with step length L yields

$$v(z_{j-1}) = v(z_{j+1}) + \tfrac{1}{3}L\left[s(z_{j-1}) + 4s(z_j) + s(z_{j+1})\right] \qquad (IV.14)$$

where

$$s(z_j) = \sum_{i=1}^{n}\int_{z_j}^{z_j+z_i}\frac{x n_i(x)v(x)}{h(z_j)}\exp\left[-\int_{z_j}^x g(y)dy\right]dx \qquad (IV.15)$$

This permits direct calculation of $v(z_{j-1})$ and hence $f_o(z_{j-1})$ for any j provided that $v(z_{j+1})$ is known. The calculation is therefore carried out by "backward prolongation". At high energy, as $z^{\frac{1}{2}}f_o(z) \to 0$. $v(z)$ is assigned the value 1, and calculation proceeds stepwise down the energy scale.

The foregoing approximation is useful when the power absorbed by rotational transitions is negligible compared to that by vibrational and/or electronic transitions. A very special case also is that of hydrogen at low temperature, where superelastic collisions may be disregarded owing to the low populations of excited levels.

IV.2.2. Exact solution

When the superelastic term is retained in (IV.6), the mathematical treatment is similar, but as $f(\epsilon)$ now depends on both $f_o(\epsilon + \epsilon_i)$ and $f_o(\epsilon - \epsilon_{-i})$ for each inelastic process, the backward prolongation technique is inapplicable. The approach taken by Frost and Phelps was to integrate the equation and approximate the result by a set of linear equations, one equation for each energy grid point involving $f_o(\epsilon)$ at every other grid point. However, as the spacing of the grid points must be rather smaller than the lowest rotational quantum, the number of grid points N required for a typical calculation is large, and solution necessitates inversion of an N x N matrix with calculation of all the N^2 coefficients, so the energy range of the solution is limited by the feasibility of the calculation. In nitrogen, for example, Frost and Phelps were able to use this method only for $D/\mu \lesssim .02$ V at 77^oK. As the rotational spacing of simple polyatomic molecules is similar in magnitude, solution by this method would probably be limited to subthermal energies, so no attempts have been made at an exact solution in the present analysis.

Gibson[113] has modified this approach by combining backward prolongation with a Gauss-Seidel iteration method of calculating $f_o(\epsilon - \epsilon_{-i})$ at each ϵ. This has been found useful for H_2 and D_2, but in polyatomic gases a large energy grid would still be essential, and each solution requires several iterations to produce the desired accuracy.

IV.2.3. Continuous approximation to rotational excitation

At energies well above the rotational thresholds the effects of energy exchange with the many levels can be approximated by a single function. When the selection rule is $\Delta J = \pm 1$, the last two terms of equation (IV.6) become

$$Z = N \sum_J F_J \Big[(\epsilon + \epsilon_J) f_o(\epsilon + \epsilon_J)\, \sigma_{J\to J+1}(\epsilon + \epsilon_J) - f_o(\epsilon)\sigma_{J\to J+1}(\epsilon)\Big) + (\epsilon - \epsilon_{-J}) f_o(\epsilon - \epsilon_{-J})\, \sigma_{J\to J-1}(\epsilon - \epsilon_{-J}) - f_o(\epsilon)\sigma_{J\to J-1}(\epsilon)\Big] \quad (IV.16)$$

where F_J is the fractional population of the J'th level. Provided that for the important J levels $\epsilon_J \ll \epsilon$, the following Taylor series expansions can be made:

$$f_o(\epsilon + \epsilon_J) \simeq f_o(\epsilon) + \epsilon_J f_o'(\epsilon) \quad (IV.17)$$

$$f_o(\epsilon - \epsilon_{-J}) \simeq f_o(\epsilon) - \epsilon_{-J} f_o'(\epsilon) \quad (IV.18)$$

If the cross-sections are assumed independent of ϵ over an interval of the order of ϵ_J, (IV.16) reduces to

$$Z = N \sum_J F_J \Big[(J+1)\sigma_{J\to J+1} - J\sigma_{J\to J-1}\Big] \cdot 2B_o \frac{d}{d\epsilon}\Big[\epsilon f_o(\epsilon)\Big] \quad (IV.19)$$

where B_o is the rotational constant. Phelps et al. used theoretical cross-section forms for the cases of homonuclear[24] and heteronuclear[27] diatomics to derive expressions corresponding to (IV.19). However for the general case it is convenient to define a "net rotational cross-section" Q_r' as

$$Q'_r = \sum_J F_J \left[(J+1)\sigma_{J\to J+1} - J\sigma_{J\to J-1} \right] \qquad \text{(IV.20)}$$

in which case (IV.19) becomes

$$Z = 2NB_o \frac{d}{d\epsilon} \left[\epsilon f(\epsilon) \right] \qquad \text{(IV.21)}$$

This can now be added to (IV.6), and using the normalised parameters

$$\eta'_r = (M/2m)(Q'_r/Q_o)$$
$$z_r = 2B_o/kT \qquad \text{(IV.22)}$$

the new version of (IV.9) is

$$\frac{df_o(z)}{dz} \left(\frac{\alpha z}{\theta} + z^2\theta \right) + (z^2\theta + z z_r \eta_r) f_o(z) + \sum_i \int_z^{z+z_i} x\eta_i(x) f_o(x)\,dx = 0 \qquad \text{(IV.23)}$$

where the summation includes all inelastic processes other than rotation. This equation can be solved in the same way as (IV.19), making use of a new function

$$g'(z) = (z^2\theta + z z_r \eta_r)/h(z) \qquad \text{(IV.24)}$$

The overall effect of rotation in this approximation is to add a contribution to the elastic energy-loss term. However, the condition $\epsilon_J \ll \epsilon$ means the approximation is valued only when $D/\mu \gg kT/e$. At room temperature, it is therefore applicable to polyatomic gases only in the region of E/P where vibrational excitation is important, and thus unique determination of Q'_r highly unlikely.

IV.3. COMPUTATIONAL APPROACH

IV.3.1. Energy distribution calculation

The solution for $f_o(\epsilon)$ by the method of IV.2.1 was obtained by direct calculation of $s(z)$, $v(z)$ and hence $f_o(z)$ through equations (IV.15), (IV.14) and (IV.12). For this a grid of energy points z_j was selected, characterised by a step-length L. To optimise the accuracy of the various integrations, cross-section values were input at half-step intervals. To minimise the computer time usage, recursive calculations were used wherever possible, which eliminated the repetition involved in evaluating long series of overlapping integrals.

The high-energy starting point for the backward prolongation can be tested through the requirement that a further increase in the starting energy should not effect the calculated transport coefficients. A similar test may be applied to check that the step length L is sufficiently small, in addition to the power-balance check (IV.3.5). Preliminary investigations indicated that sufficient accuracy resulted from an energy range of about $5(eD/\mu)$ and a step length around $(eD/\mu)/10$. The adoption of 250-step grids in the program (IV.4.1) was thus considered to allow sufficient margin.

The precise choice of L is governed by the requirement that z_i be an integral multiple of L to permit numerical integration of (IV.15). Where more than one inelastic threshold is involved, a value L_{max} must be fixed as the highest common factor of the various z_i, and the choice of L is then restricted to integral subdivisions of L_{max}.

IV.3.2. Calculation of transport coefficients

This follows directly from $f_o(z)$ through the expressions (I.22) and (I.23), which in normalised variables become

$$W = -\frac{e}{3}\left[\frac{2}{mkT}\right]^{\frac{1}{2}} \frac{E}{NQ_o} \int_o^\infty \frac{Z}{\theta} \cdot \frac{df_o}{dz}\, dz \qquad \text{(IV.25)}$$

$$D = \frac{1}{3}\left[\frac{2kT}{m}\right]^{\frac{1}{2}} \frac{1}{NQ_o} \int_o^\infty \frac{Z}{\theta} f_o\, dz \qquad \text{(IV.26)}$$

IV.3.3. Fitting parameters

Frost and Phelps[24] introduced two combinations of transport coefficients, ν_m/N and ν_u/N, known as the momentum-transfer and energy-exchange collision frequencies respectively, to separate the effects of elastic and inelastic collisions on W and D/μ. By comparing values of these calculated from the observed and calculated transport coefficients, an indication was received of the required changes in the trial cross-sections. The collision frequencies were thus used as "fitting parameters" in the cross-section refinement. Crompton, Gibson and McIntosh[73] later proposed two alternative parameters which they claimed effected a better elastic/inelastic separation. These are the effective momentum-transfer cross-section (q_m^*) and the effective inelastic cross-section (q_i^*), defined as

$$q_m^* = \frac{A(E/N)}{W(D/\mu)^{\frac{1}{2}}} \qquad \text{(IV.27)}$$

$$q_i^* = B.\frac{W(E/N)}{(D/\mu)^{\frac{1}{2}}}\left[1 - 2.47\frac{(eD/\mu - 1.07kT)}{MW^2}\right] \qquad \text{(IV.28)}$$

where A and B are constants. Improved separation is here achieved by considering the power input to elastic collisions when deriving the effective inelastic cross-sections, whereas the formula for ν_u/N assumes this to be negligible. Within a reasonable range, the ratio of observed to calculated values of q_m^* and q_i^* should represent the ratio of actual to assumed Q_m and $\sum Q_i$ respectively, averaged over the energy distribution.

IV.3.4. Adjustments to cross-sections

At each E/P considered, comparison of the observed and calculated fitting parameters yields adjustment factors C_m and C_i applicable to the momentum-transfer and total inelastic cross-sections respectively, viz.

$$C_m = q_m^*(\text{obs})/q_m^*(\text{calc})$$
$$C_i = q_i^*(\text{obs})/q_i^*(\text{calc}) \qquad \text{(IV.29)}$$

These cannot be applied over the entire swarm energy range, as the latter will normally overlap with the energy range of swarms at other E/P values for which different adjustment factors are obtained. Instead, the factors are applied at the points on the energy scale where the cross-sections have greatest influence on the energy distribution. For each process, this is the point of maximum power absorption; in the case of elastic collisions, the power absorbed is proportional to $\epsilon^2 f(\epsilon) Q_m(\epsilon)$, and for an inelastic process is proportional to $\epsilon_i \epsilon f(\epsilon) Q_i(\epsilon)$. The energies at which these functions maximise are

therefore the points where the adjustment factors should be applied to the cross-sections. Where several inelastic processes occur, the adjustment factor applies primarily to that process causing the greatest power absorption, this dominant cross-section being that for which the maximum of $\epsilon_i \epsilon f(\epsilon) Q_i(\epsilon)$ is greatest.

If calculations are made at a large number of E/P values, there is obtained for each cross-section a set of adjustment factors relevant at different energies, which may then be interpolated to give the adjustment as a continuous function of energy. This method was used for refining the cross-sections between successive trials, and was found to be satisfactory, usually leading to a fairly rapid agreement with experiment.

IV.3.5. Power balance

If (IV.6) is multiplied by $(2/m)^{\frac{1}{2}}$ and integrated twice with respect to ϵ, the result (neglecting superelastic collisions) is

$$eEW = \frac{2m}{M}\left[\frac{2}{m}\right]^{\frac{1}{2}} \int_0^\infty \epsilon^2 N Q_m(\epsilon) \left[f_o(\epsilon) + kT \frac{df_o(\epsilon)}{d\epsilon}\right] d\epsilon + \left[\frac{2}{m}\right]^{\frac{1}{2}} \sum_i \epsilon_i \int_0^\infty \epsilon f_o(\epsilon) N Q_i(\epsilon) d\epsilon \qquad \text{(IV.30)}$$

The term on the left is the power per electron input by the field while the first and second terms on the right are respectively the net power losses to elastic and inelastic collisions. The balance provides a check on the accuracy of the computation, as any discrepancy found when the terms are evaluated is likely to have arisen from

cumulative errors in the many numerical integrations and differentiations. At each E/P considered, the percentage error in the power balance was calculated and used as a rough indication of the accuracy. Unacceptably high values were normally remedied by reducing the step-length of the energy grid.

IV.3.6. Energy limit

Practical considerations set an upper limit on the energy range covered, thereby excluding a certain fraction of the swarm from the calculations. For accuracy's sake it was considered unsatisfactory for this remainder R to exceed 1%, so an estimate of R was required in each case. This was inferred from the corresponding Maxwellian distribution (i.e. that producing the same D/μ) which in normalised form is

$$\phi(z) = 2\pi^{-\frac{1}{2}}K^{-3/2}z^{\frac{1}{2}}e^{-z/K} \qquad (IV.31)$$

where $K = (eD/\mu)/kT$. R is obtained by integrating $\phi(z)$ from the upper energy limit z_m to infinity, which is possible if the error function is approximated as

$$2\pi^{-\frac{1}{2}}\int_a^\infty e^{-x^2}dx \simeq \pi^{-\frac{1}{2}}ae^{-a^2} \qquad (IV.32)$$

(valid in the high-energy tail of the distribution). The resulting expression for the remainder is

$$R \simeq 2\pi^{-\frac{1}{2}}\exp(-z_m/K)\left[(z_m/K)^{\frac{1}{2}} + \tfrac{1}{2}(z_m/K)^{-\frac{1}{2}}\right] \qquad (IV.33)$$

FIG. IV.1 Cross-section fitting program

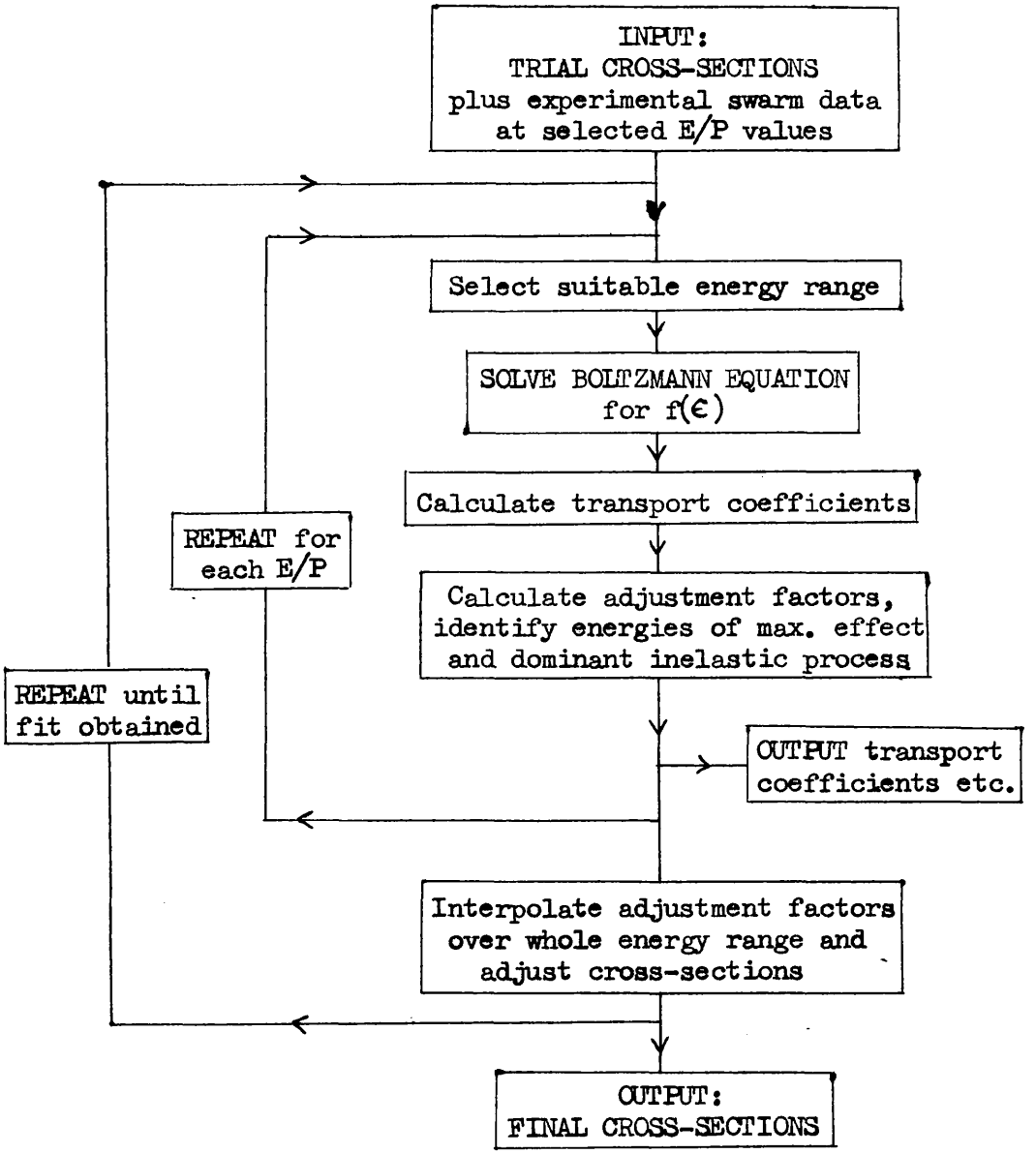

IV.4. CROSS-SECTION REFINEMENT PROGRAM

The labour involved in making successive manual adjustments to the input cross-sections puts a practical limit on the number of fitting attempts. However the establishment of a fairly mechanical adjustment routine as described in IV.3.4 stimulated the development of an automatic cross-section refinement program to carry out the successive calculations and adjustments within the computing routine.

IV.4.1. Outline of program

Fig. IV.1. illustrates the main program steps. The starting cross-sections are input (or generated by suitable functions) at each of the energy grid-points. The latter may cover several energy ranges, each of 250 equal steps from zero energy, the cross-sections being tabulated at half-step intervals. The first 500 cross-section values after the zero-energy value therefore constitute the lowest energy range; each succeeding higher range extends to twice the energy of the preceding range, the first 250 points being provided by alternate points from the latter. Prior to the Boltzmann equation solution procedure the cross-section values corresponding to the appropriate energy range are transferred to an array which holds the working energy grid. The choice of range is controlled by the program: working through the E/P values in ascending order, the next higher range is automatically selected whenever the remainder R exceeds 1% on the lower range.

At each E/P value for which experimental data is input

(typically 15-25 points), $f_o(\epsilon)$ is obtained and the associated calculations described in IV.3 are performed. Parameters of interest are output, these being the calculated transport coefficients and percentage deviation from experiment, fitting parameters, adjustment factors along with the energies of peak sensitivity at which they are applicable, estimates of error and remainder, and the energy range used. The adjustment factors are stored and the calculation repeated for each desired value of E/P. The adjustment factors are interpolated over the whole energy range and used to refine the cross-sections, when required. The entire process may be repeated any number of times to achieve the desired concordance with experiment.

IV.4.2. Program testing

The backward prolongation procedure was tested by the use of two special analytical forms of the elastic cross-section:

$$(1) \quad \theta = \beta z^{-\frac{1}{2}} \text{ giving } f(z) = G \exp\left[-\beta^2 z/(\alpha^2 + \beta^2)\right] \qquad \text{(IV.34)}$$

(Maxwell distribution)

$$(2) \quad \theta = \beta \quad \text{giving for } \bar{\epsilon} >> kT,\ f(z) \to G' \exp\left[-\beta^2 z^2/2\alpha\right] \qquad \text{(IV.35)}$$

(Druyvesteyn distribution)

The computed distributions agreed closely with the above expressions.

The automatic refinement program was tested on the data for para-hydrogen at 77°K, which was the subject of similar calculations

by Crompton, Gibson and McIntosh[73]. In this case the only low-energy processes of importance are $J = 0 \rightarrow 2$ rotational excitation (threshold .0439 eV) and $v = 0 \rightarrow 1$ vibrational excitation (threshold .51 eV). Starting cross-sections were chosen which were linear functions of energy and bore poor resemblance to the real situation. The program was operated with nine E/P values from .015 to 7 V $cm^{-1} torr^{-1}$, using the data of Crompton et al.. Although initially the discrepancies in transport coefficients were 50% or more, after three or four refinements they had been reduced to < 10%. After about 10 refinements agreement was to better than 2% and the derived cross-sections were almost identical to those of Crompton et al. between .01 and 1 eV, except for the rotational cross-section Q_r which is not uniquely determinable above about 0.4 eV due to domination by Q_v.

IV.4.3. Use of the program

The program performed extremely well for p-H_2 at 77°K, but this is a very special case as H_2 is the only molecule which exists almost entirely in the ground rotational state at this temperature. This combined with the large threshold energy difference between Q_r and Q_v means that these cross-sections can be obtained with a high degree of uniqueness at least to within a few times their respective threshold energies.

In the majority of cases, however, quite apart from the complications when many rotational levels are involved, the various

vibrational modes are close in energy. This causes loss of uniqueness, and agreement with experiment may result from varying the cross-sections in many different ways. When the power absorptions by different processes are similar in magnitude, the policy of adjusting only the "dominant" cross-section is no longer justified. This situation was encountered, for example, in methane (V.1), where resort had to be made to a different policy, namely that of using only one inelastic cross-section as a variable and fixing the others relative to it.

Although a version of the program incorporating the continuous approximation to rotational excitation has been used for H_2S (V.5), the lack of uniqueness negates any advantage to be gained by computer refinement of the net rotational cross-section Q'_r.

The program eliminates most of the labour in adjusting cross-sections but does not altogether eliminate the need for human interference. Apart from the uniqueness problem, another situation calling for intervention arises when the shortcomings of the adjustment factor energy scaling and interpolation procedures cause spurious "bumps" in the cross-sections. These generally arise in the initial stages where drastic adjustments occur and tend to remain thereafter throughout many refinement stages.

IV.5. ACCURACY OF THE ANALYSIS

IV.5.1. Uniqueness of derived cross-sections

Only in special cases (e.g. that of p-H_2 above) does the uniqueness of the derived cross-sections ultimately depend on the accuracy of the experimental measurements. This occurs when over a range of energy which is appreciable in terms of swarm width, only one inelastic process is significant. It is fundamentally impossible to determine uniquely several microscopic properties from observation of only two macroscopic ones. On the other hand, by virtue of the separability of inelastic and elastic effects in the fitting parameters, the momentum-transfer cross-section can be determined with a high degree of uniqueness, particularly when calculations are made over a wide range of E/P.

If simple assumptions are made regarding the shapes or interrelations of inelastic cross-sections, the situation may be considerably improved, but usually there is little ground for such assumptions. More particularly, where direct experimental evidence (e.g. from beam studies) is available, this can be combined with swarm analysis to provide good estimates of the absolute magnitudes, and possibly the energy scale calibration, of the cross-sections concerned. As an example of what can be tackled, Myers[114] has analysed swarm data for oxygen in terms of nine inelastic processes, using a combination of beam evidence, attachment coefficients, and simple assumptions about cross-section shapes.

IV.5.2. Approximations involved in the analysis

The accuracy of the Boltzmann equation itself as given by (IV.6) hinges on the approximations made in the derivation. Firstly, the assumption of spatial independence of the velocity distribution is tantamount to ignoring the density gradients which must exist in a real swarm experiment. A position-dependent distribution in turn means that the swarm cannot be characterised by a single diffusion coefficient or mobility. Parker[117] studied the effects of this approximation on the Townsend-Huxley D/μ experiment, by deriving the Boltzmann equation for a spatially dependent distribution and solving for special forms of elastic cross-sections only. He concluded that the effect on the measured D/μ should only be significant when the swarm width is large relative to the drift distance. The geometry of the present apparatus should lead to a negligible effect i.e. the measured D/μ should not differ significantly from that which would result from a spatially uniform distribution. The drift velocity should similarly be unaffected since at the centre of a pulse a pseudo-uniform condition exists (zero density gradient); however, in considering the diffusion of the pulse, the spatial dependence of the velocity distribution is of paramount importance and leads to the observation of a different diffusion coefficient.

The retention of only two terms in the spherical expansion of the distribution function is a central feature of the foregoing

analysis, and depends on two important assumptions. The first, that the velocity variation Δv between collisions is small compared to v (i.e. mean $\cos\theta$ is small), is unlikely to cause great error at low energies; however for high drift velocities it may lead to an underestimate of W, and a corresponding overestimate of D/μ. The second assumption is that the elastic cross-section is much greater than the total inelastic cross-section. This is really an a posteriori condition, deduced by considering higher order terms in the expansion. In the present work, this condition is not strictly met, as in methane for example, where the inelastic cross-sections derived (V.1) are in places $> 50\%$ of the momentum-transfer cross-section. The effect of the approximation is not easy to assess, but probably again results in an underestimate of W, due to neglect of higher order harmonics which reflect the high anisotropy caused by the loss of random motion in inelastic collisions. The effect of this on the present analysis could be to reduce Q_m and increase Q_i over the true values. This might cause poor separation of elastic and inelastic effects, but in fact when the second Q_v was introduced in methane, no change in Q_m around the minimum was required in spite of a 30% reduction in $\sum Q_i$ in this region.

Cavalleri and Sesta[115] derived a form of the Boltzmann equation which obviated the above assumptions, by considering the "initial" distribution function $f_o(v_o)$ representing the immediate post-collision velocities. They obtained a rigorous expression for the drift velocity

W_o of electrons having initial velocity v_o, allowing the overall drift velocity to be obtained in terms of $f_o(v_o)$. However with the exception of the special case of elastic collisions only and constant flight times[116], no general solution of this Boltzmann equation has so far been published.

CHAPTER V

RESULTS OF ANALYSIS AND DISCUSSION

V.1. METHANE

V.1.1. Experimental Data

The available transport coefficient data governs the choice of the effective cross-sections q_m^* and q_i^* used as fitting parameters in the Boltzmann equation analysis. The present D/μ results (Table III.1) cover the range $.008 \leq E/P \leq 1.5$ V $cm^{-1}torr^{-1}$ and merge well at the upper limit with Walker's values[43] which were used for $1.5 \leq E/P \leq 6$. No data exists for higher E/P so the present analysis was restricted to swarms for which $D/\mu < 2$ V. The best drift velocity data in this range was taken to be that of Pollock[45], extrapolated for $E/P < 0.5$ using the results of Bowman and Gordon[23] and Wagner et al.[47] as a guide to merge at $E/P \simeq 0.25$ with the values predicted by the dwell-drift thermal mobility measurements of Nelson and Davies[29] (μ = 9.97 $cm^2V^{-1}\mu s^{-1}$ torr at 300°K). (This might appear to suggest a thermal swarm for $E/P < .025$, in contradiction to the D/μ measurements; however the tendency of μ to decrease as the swarm energy rises is probably being counteracted by the effect of inelastic collisions giving an increasingly asymmetric energy distribution, thus tending to increase μ.)

V.1.2. Preliminary work

Before the present D/μ data became available, calculations were performed to check the results of Pollock[45,61] using a similar set of cross-sections (i.e. one vibrational excitation at 0.162 eV threshold). The results agreed in that the low D/μ values of Cottrell and Walker were inconsistent with cross-sections derived from swarms of mean energy around 0.1 to 0.2 eV. This could have been due to erroneous D/μ data but could also conceivably have been explained by large rotational excitation cross-sections which were not considered in the calculations. However, the latter would have to be extremely large to account for the observed energy exchange collision frequency[24] ($>10^{-9}$ $cm^3 sec^{-1}$) in a near-thermal swarm - about 10 times that in CO[27] and 100 times that in N_2[24].

In contrast, the present D/μ results give ν_u/N values of the order predicted by Pollock for vibrational losses alone. In view of the difficulties involved in accounting for rotational transitions, it was decided to ignore these in the cross-section analysis, and use the Boltzmann equation solution given in chapter IV for the case of negligible superelastic collisions.

V.1.3. Choice of cross-sections

Methane has nine normal vibrational modes, reducing by degeneracy to four fundamental frequencies[103]:

ν_4	1306 cm^{-1}	(0.162 eV)	asymmetric bend
ν_2	1526 cm^{-1}	(0.189 eV)	symmetric bend
ν_1	2914 cm^{-1}	(0.361 eV)	symmetric stretch
ν_3	3020 cm^{-1}	(0.374 eV)	asymmetric stretch

The threshold energy differences between ν_4 and ν_2, and between ν_1 and ν_3 are clearly so small in terms of swarm energy distribution widths that the effects of excitation of these modes will not be separable in the cross-section analysis. This was confirmed by successive calculations using respectively the ν_4 and ν_2 excitations alone, resulting in almost identical sets of cross-sections (vibrational excitation and momentum-transfer) both predicting transport coefficients to within a few percent of the observed over most of the E/P range available. The cross-sections derived for the ν_4 process (set 1) are shown by the broken curve in Fig. V.1., and the predicted transport coefficients in Fig. V.2.

An attempt was made to fit a vibrational cross-section for the ν_1 mode (0.361 eV) alone, but this did not succeed in matching the observed data for $E/P < 2$ V $cm^{-1}torr^{-1}$. Attempts to adjust the cross-sections to improve the fit produced a persistently increasing sharp peak in the vibrational cross-section (Q_v) at threshold. This situation is similar to that encountered by Pollock[45] in trying to fit the ν_4 cross-section to the earlier D/μ data, and is symptomatic of neglect of lower-energy inelastic processes. At best, results of these calculations gave W values 20-30% low and D/μ 60-70% high for $E/P \simeq 0.2$

V cm^{-1} $torr^{-1}$. This is far beyond expected experimental errors so it seems that one or both of the ν_2 and ν_4 modes must be involved to a significant degree.

This is the only separation of the effects of different vibrational modes which can be made without assumption of the cross-section energy dependence for which there are as yet no theoretical predictions or experimental evidence. It is likewise impossible to separate double ($v = 0 \rightarrow 2$) excitation of the ν_2 and ν_4 modes from single excitation of ν_1 and ν_3. Pollock chose to consider only the ν_4 excitation on the basis of the sharp peak in the observed fractional energy loss per collision (λ) at a mean swarm energy of 0.15 eV; but the subsequent fall in λ with energy is almost certainly due to the increasing elastic cross-section (not to a diminishing vibrational contribution) as supported by the derived cross-sections (Fig. V.1.). In fact, as most theories of non-resonant vibrational excitation point to a decreasing cross-section at energies much above threshold, the continuing high magnitude of the cross-section derived for the ν_4 process suggests that higher-energy processes are quite probably contributing.

On the basis of the arguments presented in I.4.4. it appeared reasonable to assume predominant excitation of the two infrared active modes ν_4 and ν_3. This implies domination by the dipole interaction, whereas ν_2 excitation would occur through a quadrupole interaction, and ν_1 (for which the lowest order moment is an octupole) mainly through polarisation. (It should be noted that the ν_1 mode is strongly Raman

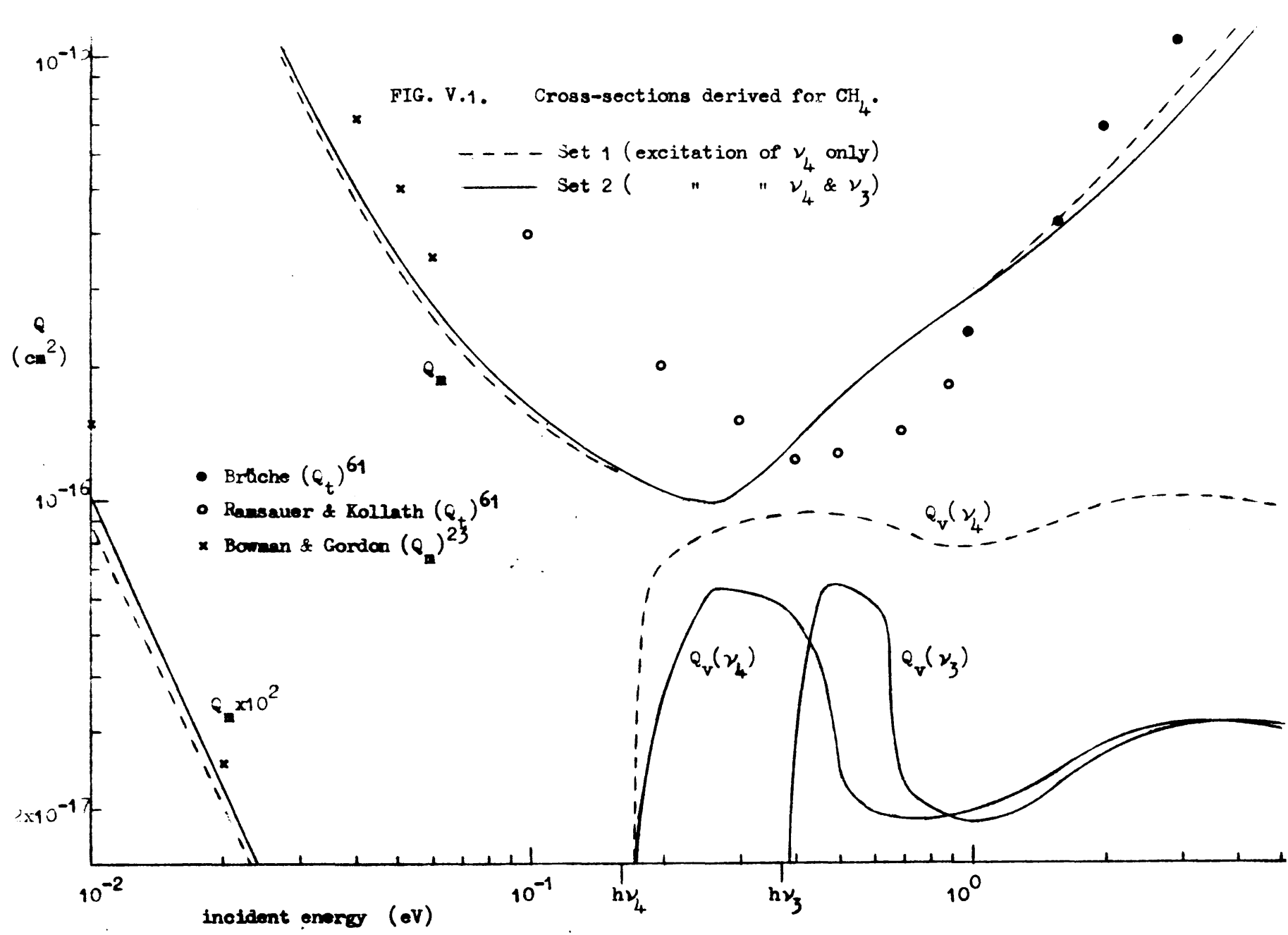
FIG. V.1. Cross-sections derived for CH_4.
Set 1 (excitation of ν_4 only)
Set 2 (" " ν_4 & ν_3)
Q_m
$Q_v(\nu_4)$
$Q_v(\nu_4)$
$Q_v(\nu_3)$
$Q_m \times 10^2$
Brüche $(Q_t)^{61}$
Ramsauer & Kollath $(Q_t)^{61}$
Bowman & Gordon $(Q_m)^{23}$
Q (cm^2)
10^{-16}
10^{-17}
10^{-2}
10^{-1}
$h\nu_4$
$h\nu_3$
10^0
incident energy (eV)

active, indicating a high dependence of the polarisability on the normal co-ordinate, so excitation should occur but through a shorter range force, giving a smaller cross-section than for the dipole-active modes.)

V.1.4. Derived cross-sections

The inelastic thresholds used for the final set of cross-sections were respectively 0.162 and 0.378 eV, the latter being put ~1% above the actual ν_3 threshold for computational convenience. Solution of the Boltzmann equation was carried out over the range $0.04 \leq E/P \leq 6$ V $cm^{-1} torr^{-1}$, which required three energy ranges, the lowest having a step-length of 6.75 meV and the highest extending to 6.75 eV.

It was found possible to vary the relative magnitudes of the two vibrational cross-sections quite considerably, while still obtaining good correspondence with experiment, the only prerequisite being a fairly steep rise in $Q_v(\nu_4)$ from threshold to a maximum of not less than $4 \times 10^{-16} cm^2$. To overcome this absence of uniqueness some assumptions must be made about the shape and/or relative magnitude of the cross-sections. It was therefore decided to make $Q_v(\nu_4)$ and $Q_v(\nu_3)$ identical except for a displacement along the energy scale, viz.

$$Q_3(\epsilon - h\nu_3) = Q_4(\epsilon - h\nu_4) \qquad (V.1)$$

Although Takayanagi's cross-section resulting from an electron-dipole interaction depends rather less simply on $(\epsilon - h\nu)$, in the high-energy limit the present cross-sections become independent

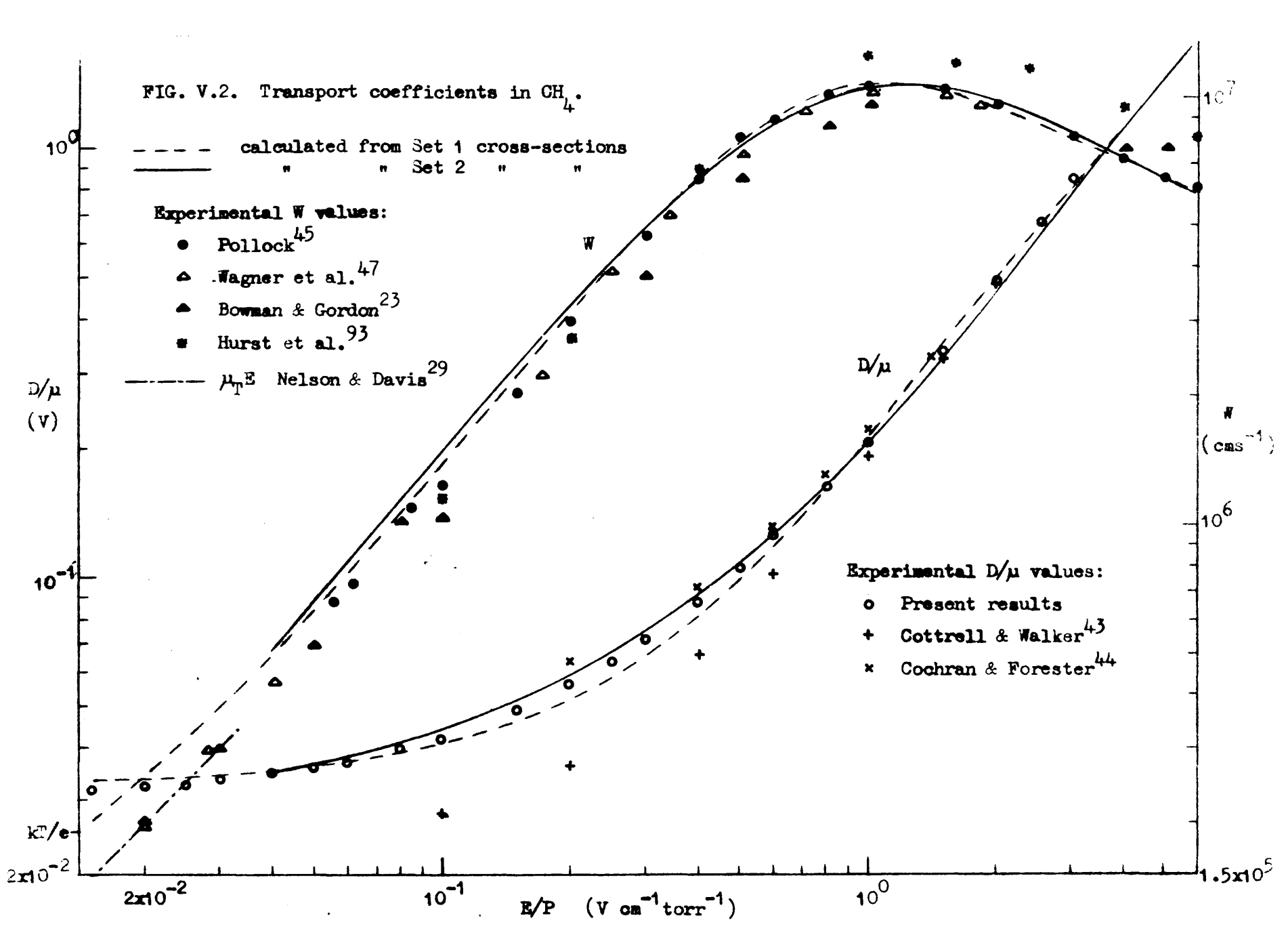
FIG. V.2. Transport coefficients in CH_4.
calculated from Set 1 cross-sections
" " Set 2 " "
Experimental W values:
Pollock[45]
Wagner et al.[47]
Bowman & Gordon[23]
Hurst et al.[93]
$\mu_T E$ Nelson & Davis[29]
W
D/μ
Experimental D/μ values:
Present results
Cottrell & Walker[43]
Cochran & Forester[44]
D/μ (V)
W (cms^{-1})
kT/e
E/P (V cm^{-1} torr^{-1})
10^0
10^{-1}
2×10^{-2}
10^7
10^6
1.5×10^5

of $h\nu$ as does the theoretical expression.

The final derived set of cross-sections (set 2) is shown in Fig. V.1 and values given in Table V.1. The momentum-transfer cross-section (Q_m) can be seen to be virtually independent of whether one or two vibrational processes are included, confirming good separation of elastic and inelastic effects. The Q_v's reach maxima of $\sim 6 \times 10^{-17}$ cm^2 at around 0.1 eV above threshold, diminishing to about half this value at 0.3 eV above threshold. Q_m in this region exhibits a minimum at $\sim$0.25 eV, somewhat deeper and at lower energy than the minimum in the total cross-section (Q_t) measured by Ramsauer experiments (Fig. V.1). As 'direct' excitation leads to forward-peaked scattering[92], Q_m should be less than Q_t at these energies. (A similar situation has been observed in CO_2[27].)

The transport coefficients W and D/μ calculated from these cross-sections are given in Table V.2 and compared with experimental results in Fig. V.2. The computational accuracy as indicated by the power balance (IV.3.5.) is everywhere within $\pm$ 4%, and within $\pm$ 2% for $E/P > 0.3$. The agreement with experiment is expressed by the tabulated ratio of observed to calculated values for the effective momentum-transfer and inelastic cross-sections q_m^* and q_i^*, which are illustrated in Fig. V.3. Correspondence is mostly within $\pm$ 5%, no worse that the experimental uncertainty, except for $E/P < 0.2$ ($D/\mu < .06$ V) where there is a significant discrepancy due to the predicted W values being somewhat higher than experimental (Fig. V.2).

FIG. V.3. Effective cross-sections for CH_4

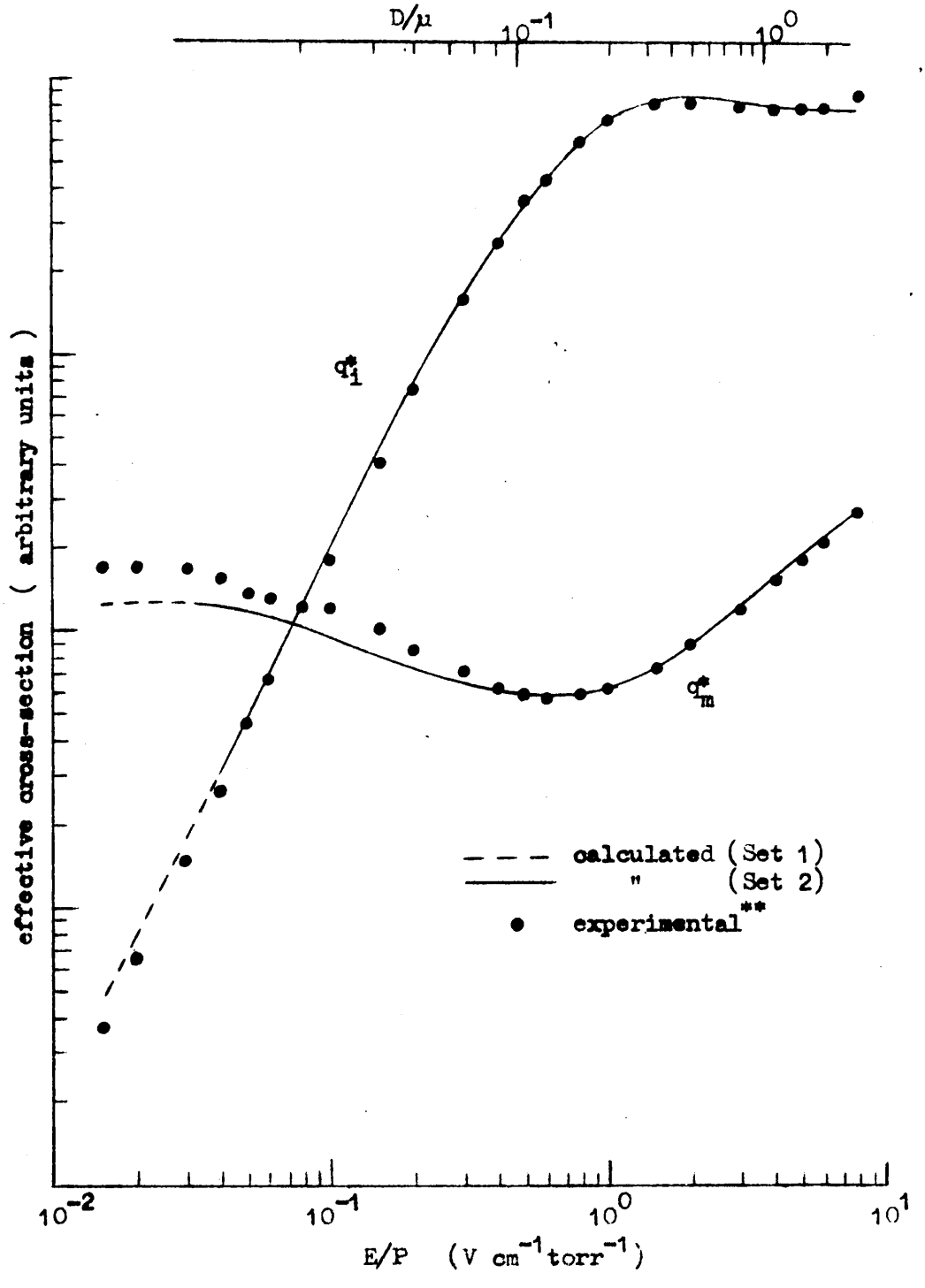

** Experimental values are calculated from transport data used in the cross-section analysis (section V.2)

Fig. V.4 illustrates the calculated electron energy distribution in methane at E/P = 0.4 V $cm^{-1}torr^{-1}$. The unusual 'bump' in Pollock's calculated distribution[45] does not appear here, since this phenomenon resulted from attempting to force agreement with the D/μ values of Cottrell and Walker by giving the ν_4 cross-section a sharp peak at threshold. Compared with a Maxwell distribution, there is a reduction in $f(\epsilon)$ at high energies and an increase at low, representing the effect of inelastic collisions.

V.1.5. Low-energy behaviour

The derived cross-sections give quite good agreement with D/μ results at low energies but the low observed values of W suggest a much higher Q_m is required. The derived Q_m is already rising steeply at low energies and it does not seem possible to increase this sufficiently to give correspondence at low E/P without adversely affecting the agreement at higher E/P. Neglect of rotational excitation could not explain this effect as the discrepancy in q_i^* suggests that inelastic losses are in fact lower than those postulated. Inelastic collisions in this energy region would have little effect on the energy distribution which is close to thermal, and would only influence the drift velocity through the additive contribution to Q_m.

It would be difficult to include rotational transitions in the methane computation. The low rotational constant ($B_o = 6.5 \times 10^{-4}$ eV)[103] causes population of many levels at room temperature, the maximum population occurring at J = 6. Exact solution of the Boltzmann

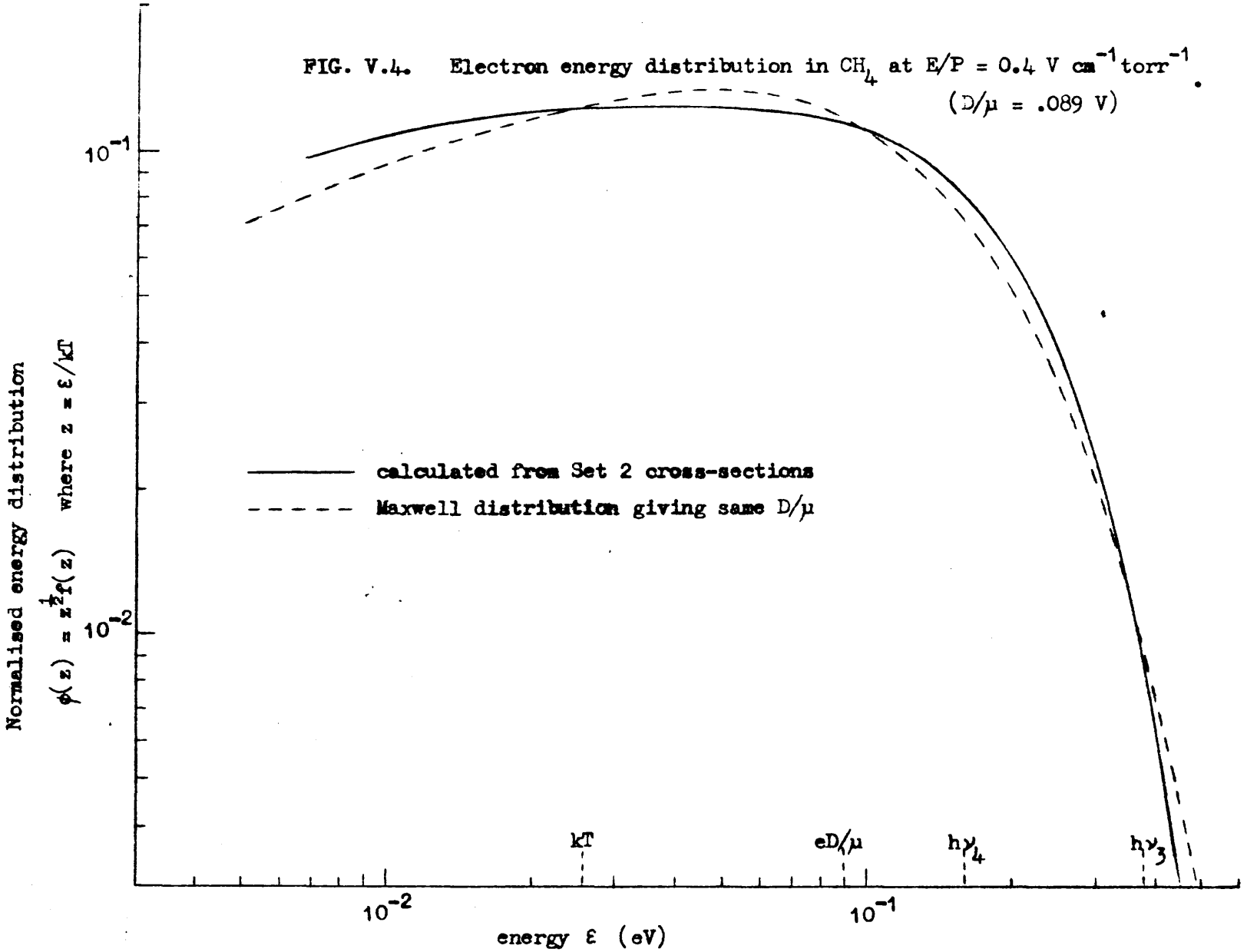
FIG. V.4. Electron energy distribution in CH_4 at E/P = 0.4 V cm^{-1} $torr^{-1}$
(D/μ = .089 V)
Normalised energy distribution
$\phi(z) = z^{\frac{1}{2}} f(z)$ where $z = \varepsilon/kT$
10^{-1}
10^{-2}
calculated from Set 2 cross-sections
Maxwell distribution giving same D/μ
kT
eD/μ
$h\nu_4$
$h\nu_3$
10^{-2}
10^{-1}
energy ε (eV)

equation, taking superelastic collisions into account, will only be practicable for $T < 100^{o}K$, and even then will be limited to energies below about .02 eV[24]. The continuous approximation (IV.2.3.) is only valid for $D/\mu >> kT/e$ and requires some assumptions concerning the cross-section dependence on energy and J if the results are to be meaningful. It would be feasible to apply this approximation for $E/P \gtrsim 0.2$ V $cm^{-1}torr^{-1}$. However, owing to the low vibrational threshold in CH_4, for $D/\mu >> kT/e$ the rotational energy losses are likely to be swamped by vibrational losses as in the case of CO_2[27]. This is evident from the power-balance equation (IV.30). The power loss to an excitation process with threshold ϵ_i is

$$P_i = N(2e/m)^{\frac{1}{2}} \epsilon_i \int_0^\infty \epsilon f(\epsilon) Q_i(\epsilon) d\epsilon \qquad (V.2)$$

For $\epsilon < \epsilon_i$, $Q_i(\epsilon) = 0$, and if $Q_i(\epsilon)$ is approximated by a constant Q_i for $\epsilon > \epsilon_i$, (V.2) becomes

$$P_i = N(2e/m)^{\frac{1}{2}} \epsilon_i Q_i \int_{\epsilon_i}^\infty \epsilon f(\epsilon) d\epsilon \qquad (V.3)$$

Hence the ratio of the power losses for two processes with thresholds ϵ_1 and ϵ_2 is given by

$$\frac{P_1}{P_2} = \frac{\epsilon_1 Q_1}{\epsilon_2 Q_2} + \frac{\int_{\epsilon_1}^\infty \epsilon f(\epsilon) d\epsilon}{\int_{\epsilon_2}^\infty \epsilon f(\epsilon) d\epsilon} \qquad (V.4)$$

Approximating $f(\epsilon)$ by the Maxwell distribution

$$f(\epsilon) = 2\pi^{-\frac{1}{2}} (eD/\mu)^{-3/2} \exp\left[-\epsilon/(eD/\mu)\right] \qquad (V.5)$$

this becomes

$$\frac{P_1}{P_2} = \frac{\epsilon_1 Q_1}{\epsilon_2 Q_2} \cdot \frac{(\epsilon_1 + eD/\mu)}{(\epsilon_2 + eD/\mu)} \exp\left[(\epsilon_2 - \epsilon_1)/(eD/\mu)\right] \qquad (V.6)$$

Taking $\epsilon_2 = 0.162$ eV (ν_4 excitation) and $\epsilon_1 = .009$ eV ($J = 6 \rightarrow 7$ rotational excitation), (V.6) gives at $E/P = 0.2$ (the minimum used to fix Q_v)

$$P_1/P_2 \simeq 1.4\, Q_1/Q_2$$

and at $E/P = 0.5$ (mean energy $\simeq \epsilon_2$)

$$P_1/P_2 \simeq 0.1\, Q_1/Q_2$$

where Q_1 here is equal to $\sigma_{J=6\rightarrow7}$ multiplied by the fractional population F_6. If the rotational and vibrational cross-sections are of similar magnitudes then the contribution of any one rotational process to the power loss might appear from the above to be quite considerable. However for near-thermal D/μ the rotational power loss is largely cancelled by the superelastic power gain. In fact the Klein-Rosseland relation[24] gives

$$\sigma_{J+1\rightarrow J}(\epsilon) \simeq \sigma_{J\rightarrow J+1}(\epsilon) \frac{\epsilon}{\epsilon - \epsilon_J} \exp(-\epsilon_J/kT) \qquad (V.7)$$

which for $J = 6$ gives $\sigma_{7\rightarrow6} \simeq \sigma_{6\rightarrow7}$ x 0.7 in the region of interest. The power loss for this excitation will therefore be reduced by ~70% due to superelastic power gain. It thus seems that unless the rotational cross-sections are unusually large the effect of their neglect will be to increase the derived Q_v's over their actual values by a relatively small amount.

As far as the drift velocities at low E/P are concerned, the explanation must either lie in an extremely high Q_m at low energy or in the formation of transient negative ions by trapping of low-energy electrons in the molecular field. The present Q_m values cannot be held to be of much significance well below kT/e, but at around .02 to .1 eV appear to have an energy dependence similar to that of other published results (Fig. V.1). The strongest long-range interaction (electron-dipole) leads to an ϵ^{-1} dependence, whereas the present Q_m varies more nearly as ϵ^{-2}, the power of an electron monopole interaction.

Frommhold[96] proposed low-energy rotational resonances in H_2 and N_2 to explain the density-dependent drift velocities reported by Grünberg[18]. Taking the slope α of the linear W^{-1} vs P graphs to be proportional to $\nu\tau$ (collision frequency x resonance lifetime) he deduced that the cross-section for resonance formation in H_2 might be around 2×10^{-15} cm^2. This could be attributed to a Feshbach-type compound state resonance associated with the molecule's rotational levels. Frommhold later[97] suggested an upper limit of $\sim 10^{-9}$ s for τ in H_2 by examining the aftercurrents in the pulsed drift experiments.

High pressures (up to 50 atmospheres) were employed by Grünberg in calculating the pressure dependence in H_2 and N_2. Crompton and Robertson[107] have recently studied H_2 (normal and para-) and D_2 in detail at pressures from 0 to 1 atmosphere (the W variations for this range are only 1-2%). They considered the variation of α with E/P and found peaks at low energies which support the resonance hypothesis.

Using the known energy distributions and postulating a narrow resonance width they were able to place the resonances on the energy scale at a little below the 0 → 2 and 1 → 3 thresholds in H_2 and the 0 → 2 threshold in D_2.

Another explanation for the high-pressure effects has been put forward by Legler[108], who proposed that when the electron mean free path is reduced to the same order of magnitude as the incident wavelength, the gas can be treated as a homogeneous scattering medium where the wave decay time is identified with the relaxation of electron momentum. His theory gives a good prediction of the experimental results in H_2, N_2, He and CH_4. The latter has been observed to give an inverse dependence, i.e. W increases with P, between 8,000 and 32,000 torr[109], this being attributed by Legler to negative scattering length, consistent with the Ramsauer minimum phenomenon.

It is probable that each theory is correct within its appropriate pressure region, hence helium shows no pressure effect below 1 atmosphere (having no rotational resonances) but does at high pressures where the homogeneous theory is applicable. The high pressure methane results do no therefore necessarily exclude a positive value of α at low pressures due to rotational 'trapping'. If such an effect is responsible for the current anomaly it must be quite marked and an investigation of this would be well worth while. Also, conducting swarm experiments at low temperatures would extend the energy range under investigation and produce firmer evidence on the low-energy behaviour of Q_m.

V.1.6. Higher energy processes

The effect of multiple excitation of any mode when considering only single excitation in the present analysis is to give a derived cross-section

$$Q_v \simeq Q_{0\to1} + 2Q_{0\to2} + 3Q_{0\to3} + \ldots\ldots\ldots \qquad (V.8)$$

Thus if $Q_{0\to2}$ is comparable with $Q_{0\to1}$, the derived cross-section Q_v should continue to increase rapidly well above threshold. As the Q_v's in Fig. V.1 drop to a minimum of $\sim 2 \times 10^{-17}$ cm^2 at around twice the threshold energy, it appears that multiple excitation is relatively weak below 1-2 eV incident energy. Cottrell and Walker[43] suggested that the methane vibrational excitation may occur via a resonant state of lifetime comparable to that of the N_2 resonance ($\sim 10^{-14}$ s). The present results however indicate that any resonance involved must be extremely short-lived and broad in energy (cf. H_2) since multiple excitation is weak and the cross-sections peak very close to threshold.

At higher energies (2-3 eV) the Q_v's again rise somewhat. Brongersma and Oosterhoff[98] have failed to observe any inelastic processes in an electron trap experiment between roughly 2 and 7.5 eV incident energy, the latter energy marking the onset of a process ascribed to excitation to a triplet state. On the other hand Boness et al.[99] claim to have observed a 'resonance' in the transmission spectrum of methane in the region of 2.5 eV, with superimposed secondary maxima of $\sim .25$ eV separation suggestive of vibrational levels. This might be due to a relatively long lived negative ion state, which would decay causing the

vibrational excitation suggested by the present results at this energy.

V.2. ETHYLENE

V.2.1. Experimental data

Considerable discrepancies exist between the D/μ values given by different authors for ethylene (Fig. V.6). To calculate the fitting parameters for the analysis, the present results were taken for $.01 \leq E/P \leq 2$ V $cm^{-1}torr^{-1}$ and extrapolated to merge with the values given by Bannon and Brose[95] at higher E/P. The drift velocities used were those given by Cottrell, Pollock, and Walker[65] combined with Nelson's data[29] at low E/P. These W values are below those corresponding to Nelson's thermal mobility ($\mu_t P = 10.86$ $cm^2V^{-1}\mu s^{-1}torr$) for E/P down to $<.01$ V $cm^{-1}torr^{-1}$, in support of the present D/μ values which are significantly above thermal under these conditions.

V.2.2. Cross-section analysis

Appropriate starting values of Q_m were taken from a combination of the results of Christophorou, Hurst, and Hendrick[22] (temperature dependence of drift velocity); Cottrell, Pollock, and Walker[65] (swarm analysis based on Maxwellian distribution); and Brüche[45] (Ramsauer Q_t measurement). For inelastic collisions a similar procedure was adopted as with methane. Pollock inferred excitation of the ν_4 mode from his λ results, this having the lowest threshold at 0.102 eV, but in the present analysis only infrared active modes were considered. Five of

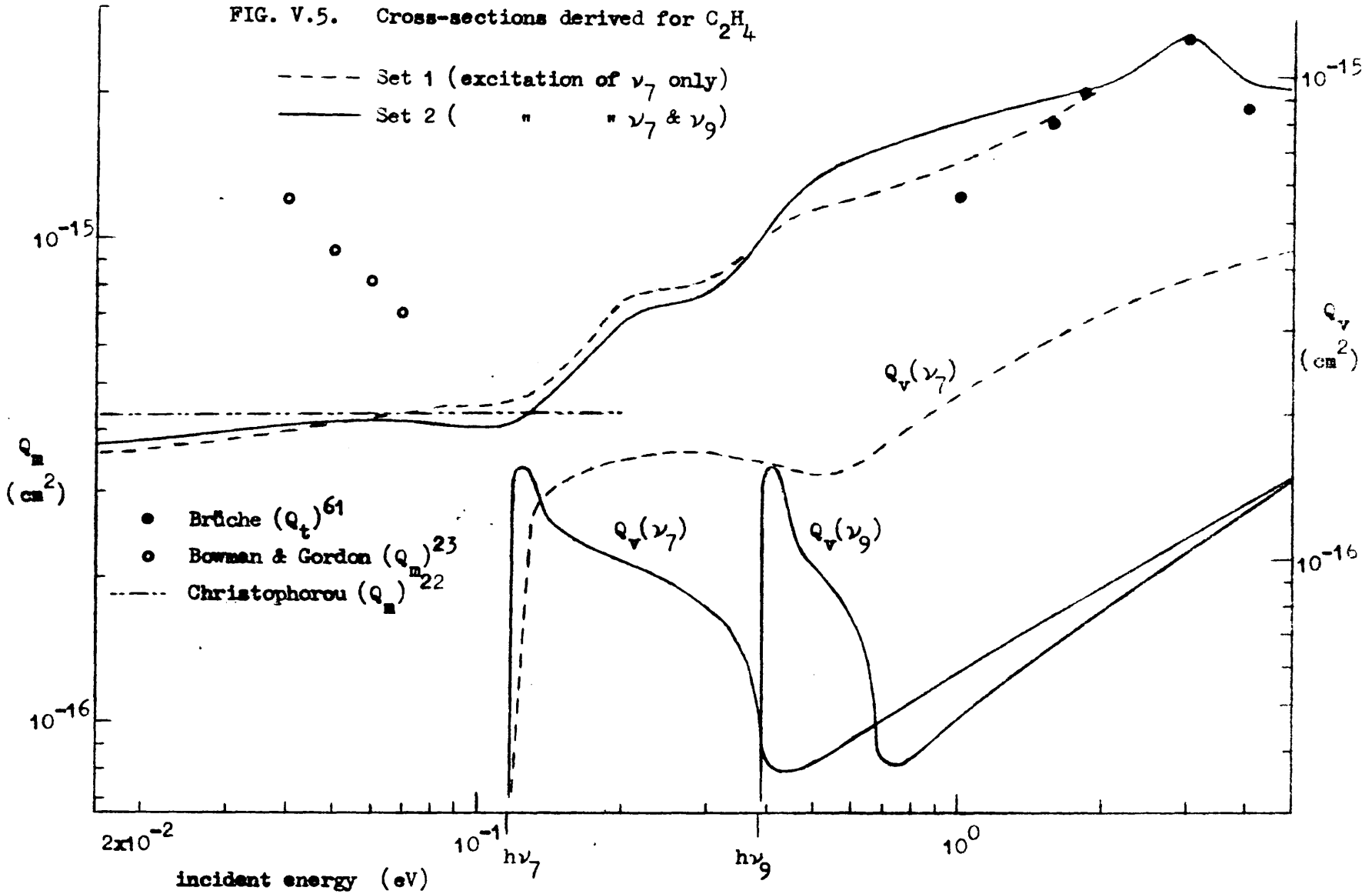
FIG. V.5. Cross-sections derived for C_2H_4
Set 1 (excitation of ν_7 only)
Set 2 (" " ν_7 & ν_9)
10^{-15}
10^{-16}
Q_m (cm^2)
Q_v (cm^2)
$Q_v(\nu_7)$
$Q_v(\nu_7)$
$Q_v(\nu_9)$
Brîche $(Q_t)^{61}$
Bowman & Gordon $(Q_m)^{23}$
Christophorou $(Q_m)^{22}$
$2x10^{-2}$
10^{-1}
$h\nu_7$
$h\nu_9$
10^{0}
incident energy (eV)

ethylene's twelve normal modes are in this category:

ν_7	(vs)	949 cm^{-1}	(0.117 eV)
ν_{10}	(m)	995 cm^{-1}	(0.123 eV)
ν_{12}	(s)	1444 cm^{-1}	(0.179 eV)
ν_{11}	(s)	2990 cm^{-1}	(0.370 eV)
ν_9	(s)	3106 cm^{-1}	(0.385 eV)

In the first analysis, single excitation of the ν_7 mode was taken as the only inelastic cross-section. It was found that the chosen experimental data could be reproduced to within $\pm$ 5% for $E/P < 5$ V $cm^{-1}torr^{-1}$ above which value there is considerable uncertainty in the D/μ data. The cross-sections derived on this basis are shown by the broken curves in Fig. V.5. There is a noticeable second rise in Q_v well above threshold which suggests a contribution from higher energy-loss processes.

The final set of cross-sections (Set 2, Fig. V.5 and Table V.3) were derived assuming single excitation of two vibrational modes (ν_7 and ν_9). Excitation of these modes alone was observed by Geiger and Wittmaack[90] at 33 keV incident energy. The other dipole-active modes fall between these two in energy and their inclusion would have small effect other than to the absolute magnitudes of the individual Q_v's. Calculations were performed for $0.03 \leq E/P \leq 14$ V $cm^{-1}torr^{-1}$, considering incident energies up to 4.87 meV. Four energy ranges were employed, the lowest having a step-length of 2.44 meV. The resulting

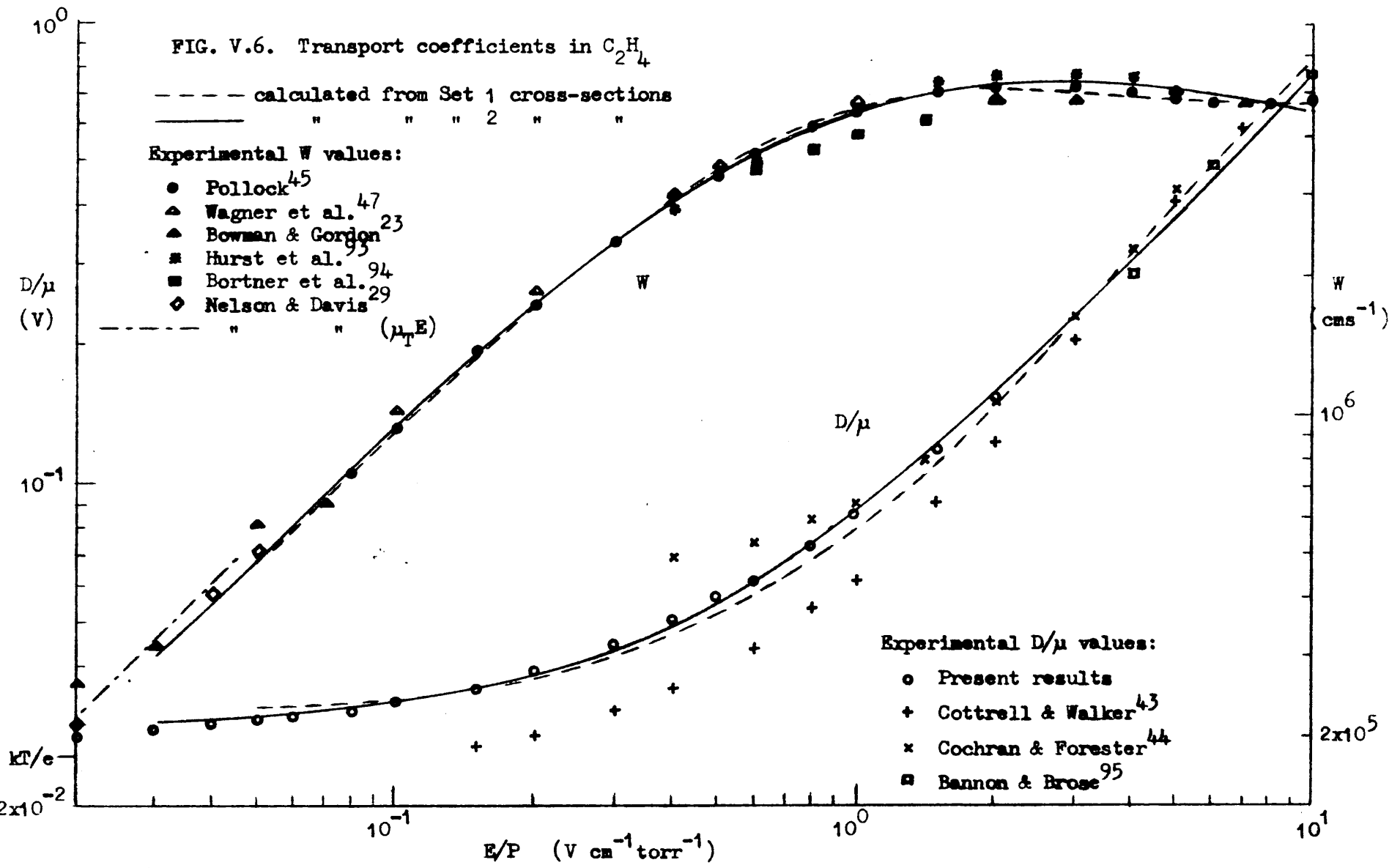
FIG. V.6. Transport coefficients in C_2H_4
calculated from Set 1 cross-sections
" " " 2 " "
Experimental W values:
Pollock[45]
Wagner et al.[47]
Bowman & Gordon[23]
Hurst et al.[93]
Bortner et al.[94]
Nelson & Davis[29]
" " ($\mu_T E$)
W
D/μ
Experimental D/μ values:
Present results
Cottrell & Walker[43]
Cochran & Forester[44]
Bannon & Brose[95]
D/μ (V)
W (cms^{-1})
kT/e
10^0
10^{-1}
$2x10^{-2}$
10^6
$2x10^5$
10^{-1}
10^0
10^1
E/P (V cm^{-1}torr^{-1})

transport coefficients are given in Table V.4 and compared with experimental values in Fig. V.6. Over most of the range, the agreement with the favoured experiments is within 5%, which is about the accuracy of the calculations.

V.2.3. Final cross-sections

At low energies the derived Q_m falls a little below the constant value of Christophorou et al.[22]. This is expected since the latter assumed a thermal (Maxwellian) swarm for $E/P < 0.1$ V cm^{-1}torr^{-1}, whereas the present D/μ results refute this. Such an assumption could lead to an error decreasing with temperature, which qualitatively accounts for the present discrepancy below .05 eV. Calculations using the very different Q_m values of Bowman and Gordon[23] met with no success, predicting excessively low drift velocities. These authors found a temperature dependence of W of the opposite polarity to that reported by Christophorou et al..

There is thus no indication that Q_m rises sharply at low energies as in the case of CH_4. This situation is similar to that found in other quadrupolar molecules[3] suggesting that this interaction dominates in C_2H_4 at low energy. However it should not be concluded that no low-energy rise in Q_m exists as the present analysis is fairly insensitive to Q_m below .01 eV. Low-temperature swarm experiments would provide additional information on this topic.

At 2-3 eV the Q_m values are consistent with Brüche's Q_t

measurements. At intermediate energies, a certain amount of structure is observed. In case this had been artificially produced by the refinement program, attempts were made to smooth out the structure, but it reappeared as agreement was sought in the calculations. It is possible that this structure is associated with the vibrational excitation processes.

The final Q_v's show distinct peaks close to threshold, which arose from trying to match the observed D/μ values at low E/P, and are probably an artificial feature caused by the neglect of rotational excitation. The latter would probably account for the increasing discrepancy between observed and calculated q_i^* values at low E/P.

Above threshold, the Q_v's show the expected fall with energy; but in contrast to the CH_4 results there is a very noticeable steady rise after the minimum, suggestive of higher inelastic processes. Excitation of the first triplet state (4.6 eV) is known to occur at threshold impact energy, showing up in electron trap[12] and SF_6 scavenger[100] experiments, as well as in energy-loss spectra at higher impact energies[6]. At $E/P = 10$ V cm^{-1} $torr^{-1}$, around 1.5% of the present calculated energy distribution exceeds the triplet energy, so it is probable that a threshold cross-section somewhat greater than 10^{-16} cm^2 could explain the experimentally observed q_i^* at this and lower values of E/P. To establish a cross-section for this process would however require swarm data at higher E/P than that currently available.

On the other hand, there is some evidence for other energy-loss

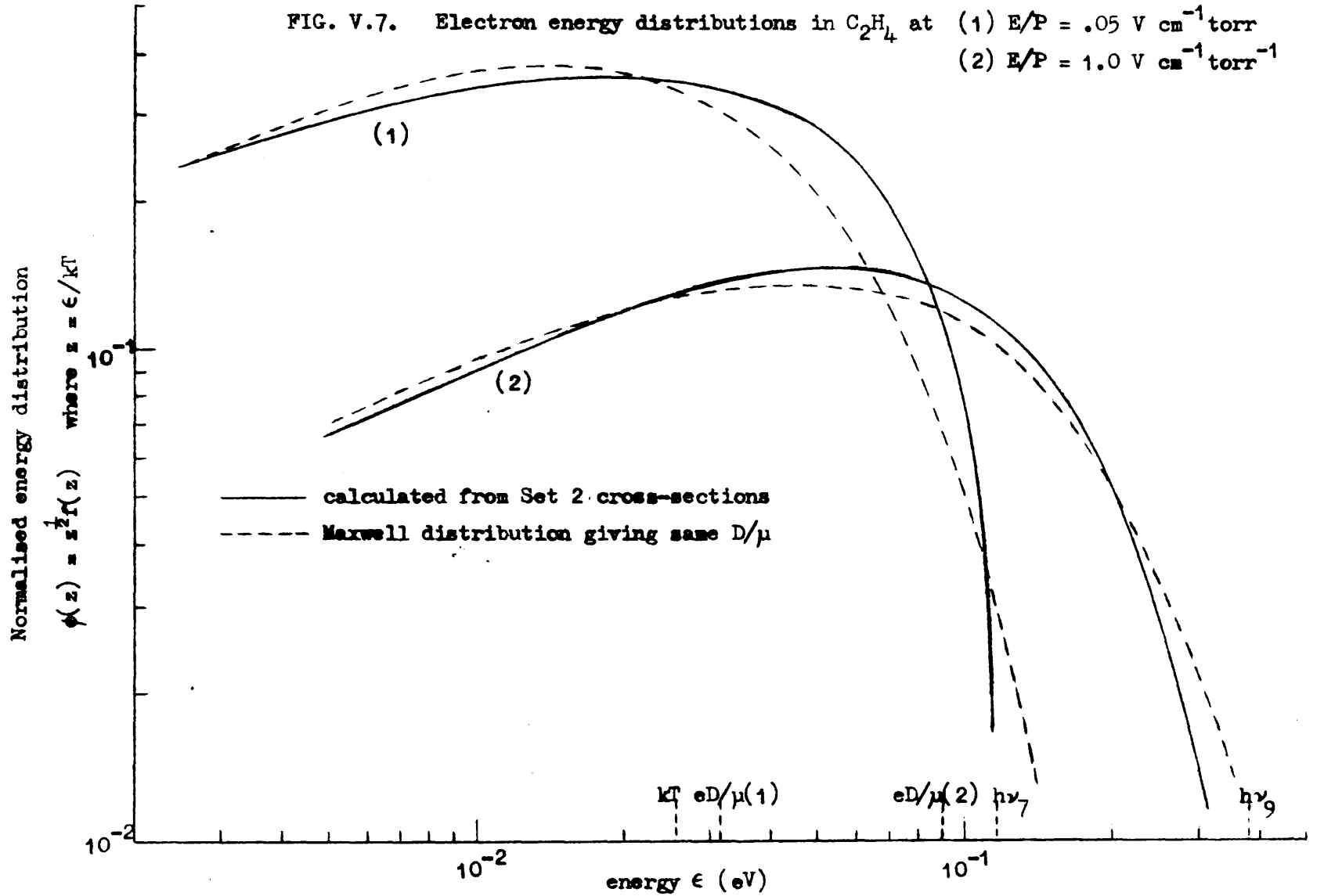
FIG. V.7. Electron energy distributions in C_2H_4 at (1) E/P = .05 V cm^{-1} $torr^{-1}$
(2) E/P = 1.0 V cm^{-1} $torr^{-1}$
(1)
(2)
calculated from Set 2 cross-sections
Maxwell distribution giving same D/μ
Normalised energy distribution
$\phi(z) = z^{\frac{1}{2}} f(z)$ where $z = \epsilon/kT$
10^{-1}
10^{-2}
kT
eD/μ(1)
eD/μ(2)
$h\nu_7$
$h\nu_9$
10^{-2}
10^{-1}
energy ϵ (eV)

processes below 4.6 eV. Hubin-Franskin and Collin[100] observed a weak SF_6^- peak at 2.15 eV which they attributed to a transient $C_2H_4^-$ state; and Bowman and Millar[12] reported energy-loss thresholds at 1.7 eV. It is possible that a resonance could exist in this energy region, which by decaying to excited vibrational levels of the ground state would contribute to the cross-section rise found here. In addition Boness et al.[99] reported transmission "resonances" at 0.2 and 1.3 eV. The former might possibly be due to strongly forward-peaked scattering associated with "direct" vibrational excitation.

V.2.4. Energy distribution in ethylene

Fig. V.7 illustrates the electron energy distributions in ethylene calculated at E/P = .05 and 1 V $cm^{-1}torr^{-1}$, assuming the Set 2 cross-sections of Fig. V.5. The Maxwell distributions corresponding to the same D/μ values are shown for comparison. Both distributions deviate appreciably from the Maxwellian form, the inelastic processes causing a marked reduction in the number of high energy electrons. This distortion is manifested in the ratio $\bar{\epsilon}/(eD/\mu)$, $\bar{\epsilon}$ being the calculated mean energy; the Maxwell distribution gives this ratio to be exactly 1.5, whereas the present calculations give respectively 1.39 and 1.29 at E/P = .05 and 1. Christophorou, Hurst, and Hendrick[22] assumed that swarms in C_2H_4 possessed a thermal Maxwellian distribution for E/P < 0.1, and Bowman and Gordon[23] made a similar assumption. This was based on the linear rise of W with E/P under these conditions (a constant energy distribution giving rise to a constant μP). Later Christophorou et al[48] recognised

that the mean swarm energy was above thermal at E/P = 0.5, but continued to use a Maxwellian distribution to calculate mean energies from the longitudinal diffusion coefficients of Wagner, Davis and Hurst[47] (Fig. III.4) for E/P up to 1 V $cm^{-1}torr^{-1}$.

The present results demonstrate the error in the foregoing assumptions. Although it must be recognised that the energy distributions of Fig. V.7 are not unique, and the inclusion of rotational transitions in particular might serve to reduce the departure from the Maxwellian form slightly, two important points arise. Firstly, it is incorrect to assume that a constant μP implies a swarm in thermal equilibrium with the gas, since this may arise from a combination of circumstances as discussed in V.1.1. This may be a significant source of error in the calculation of Q_m from the temperature variation of W (I.2). Secondly, the departure from Maxwellian may be large even for a swarm with a very nearly thermal D/μ value. This is true because the swarm condition is primarily a steady state one; the distinction between steady state and equilibrium has not been sufficiently stressed by some authors who have tended to assume equilibrium properties as $D/\mu \rightarrow kT/e$. The condition for true equilibrium is $E/P \rightarrow 0$, which is only realised in such cases as the dwell-drift technique[29].

The energy distributions of reference 48 were used principally for establishing a mean-energy scale for measurements of mean electron attachment rates in swarms[101]. The poor energy resolution of results thus expressed will not therefore be sensitive to small variations in

$f(\epsilon)$, but it should be noted that the use of D_L/μ rather than D_T/μ to calculate $\bar{\epsilon}$ does lead to an error in the energy scale of ~40% at 0.1 eV. However, when the energy distribution is used to derive the energy-dependence of the attachment cross-section[102], the use of a Maxwellian distribution may be quite inappropriate.

V.3. ACETYLENE

V.3.1. Experimental data

Fitting parameters were calculated from the present D/μ measurements extrapolated for $5 \leq E/P \leq 19$ V $cm^{-1}torr^{-1}$ by drawing a smooth curve through the scattered results of Maydan[45]. The two published sets of W data[23,65] are at considerable variance; however owing to the general disagreement of all the Bowman and Gordon results with those of other experimenters, the drift velocities reported by Cottrell, Pollock and Walker[65] were considered more reliable and used in this analysis.

V.3.2. Cross-section analysis

Approximate starting values for the momentum-transfer cross-section Q_m were obtained by combining Pollock's mean Q_m results[65] with the total cross-sections measured by Brüche[45].

There is again no direct experimental evidence for excitation of particular vibrational modes. The fundamentals of C_2H_2 are as follows:

FIG. V.8. Cross-sections derived for C_2H_2

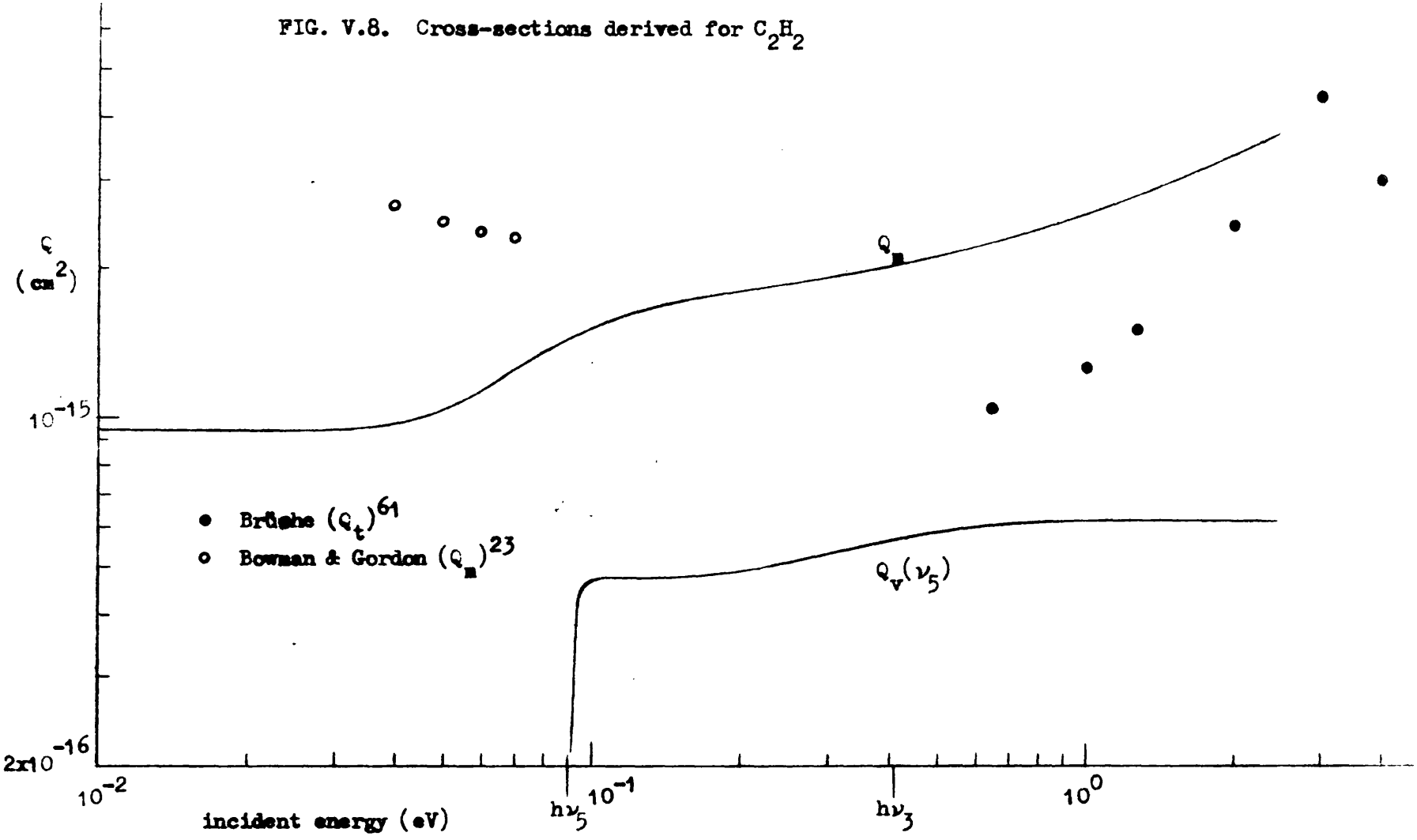

ν_4	612 cm^{-1}	(.076 eV)	centrosymmetric bend
ν_5	729 cm^{-1}	(.090 eV)	anticentrosymmetric bend
ν_2	1974 cm^{-1}	(.224 eV)	C≡C stretch
ν_3	3287 cm^{-1}	(.407 eV)	C-H antisymmetric stretch
ν_1	3374 cm^{-1}	(.418 eV)	C-H symmetric stretch

Of these, ν_5 and ν_3 are strongly infrared active, while the remaining modes have only Raman activity. Furthermore, the ν_4 mode gives a very weak Raman spectrum, and so should not be strongly excited through a simple polarisation interaction. It was therefore decided to represent inelastic collisions by a cross-section for $v = 0 \rightarrow 1$ excitation of the ν_5 fundamental.

Calculations were carried out for $0.15 \leq E/P \leq 19$ V $cm^{-1}torr^{-1}$ using 3 ranges of energy up to 2.81 eV, with a step-length on the lowest range of 2.81 meV. Over most of the range the calculation accuracy was better than ± 3%. Drift velocities were readily obtained which agreed with Pollock's to within 5%, but the final set of cross-sections gave D/μ values deviating from the present experimental results by up to 10%. This discrepancy suggested that Q_v should be increased somewhat at threshold relative to higher energies, but owing to the uncertainty of the D/μ data at $E/P > 5$ V $cm^{-1}torr^{-1}$, and the neglect of rotational transitions in the calculations, it was not considered to be worthwhile attempting a better fit.

V.3.3. Final cross-sections

The final derived cross-sections are given in Table V.5 and

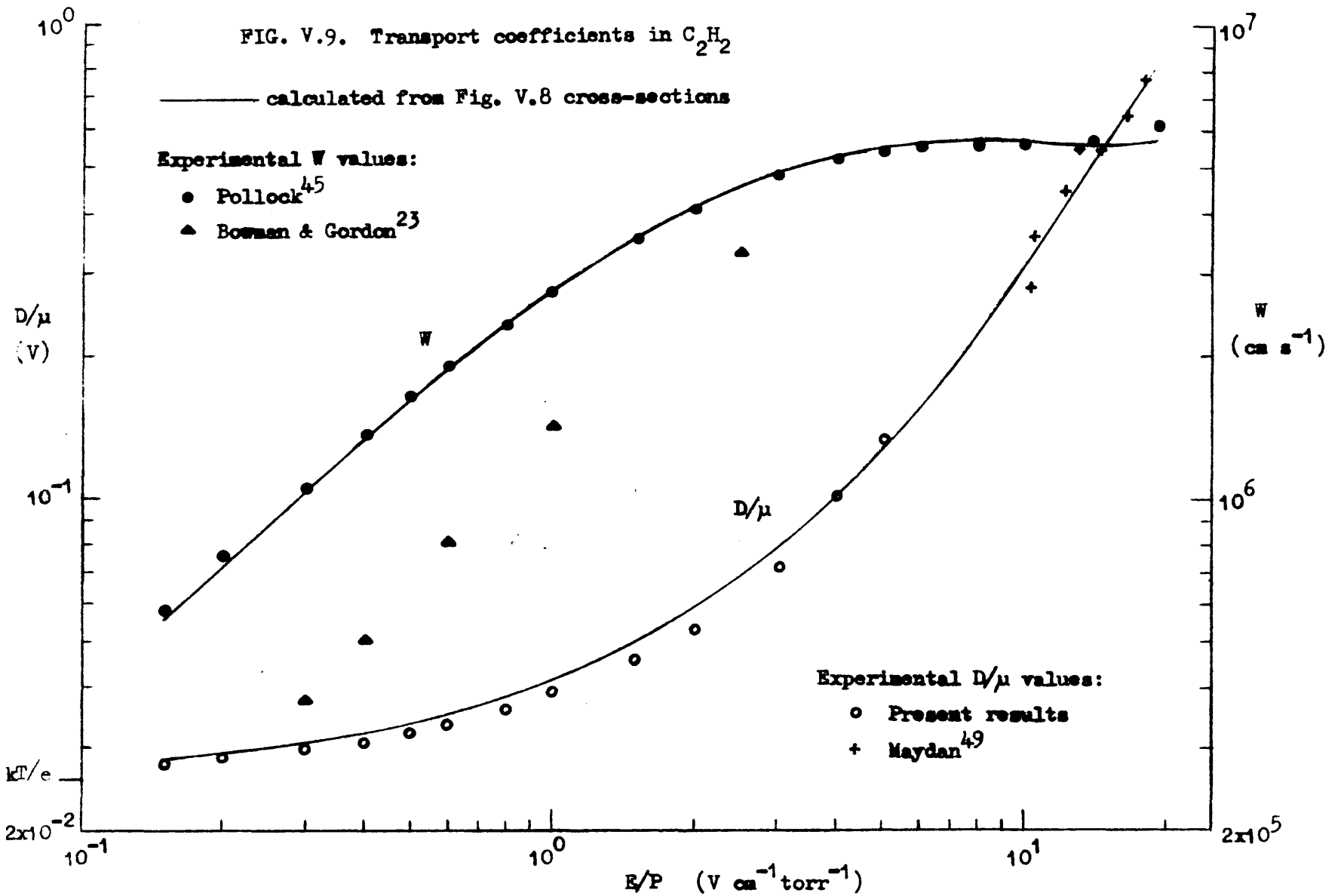
FIG. V.9. Transport coefficients in C_2H_2
——— calculated from Fig. V.8 cross-sections
Experimental W values:
● Pollock[45]
▲ Bowman & Gordon[23]
W
D/μ
Experimental D/μ values:
o Present results
+ Maydan[49]
D/μ (V)
W (cm s^{-1})
kT/e
10^0
10^{-1}
2×10^{-2}
10^7
10^6
2×10^5
10^{-1}
10^0
10^1
E/P (V cm^{-1}torr^{-1})

Fig. V.8, and the calculated transport coefficients in Table V.6 and Fig. V.9.

As with ethylene, the Q_m results plainly disagree with those of Bowman and Gordon[23] in the energy range .04 - .07 eV. At around 1 eV Q_m exceeds Brüche's Q_t by a factor of 2 - a somewhat greater discrepancy than that found in ethylene. Whether this is due to anistropic scattering or experimental errors is a question which must await new measurements of Q_t.

There is no evidence for a rising Q_m at low energy. However Q_m at .01 eV appears to exceed that for ethylene by a factor of 2.5, suggesting that the π - electron structure makes a considerable contribution to the scattering potential at these energies.

The ν_5 excitation cross-section rises sharply at threshold, levelling off thereafter but with a slight rise at around .3 - .5 eV. This is possibly due to excitation of the infrared active ν_3 mode. No attempt has been made at present to fit more than one vibrational cross-section, but it is expected that a situation similar to that in ethylene would result if the ν_3 mode were included: namely, a peaking of the individual Q_v's a little above threshold with a fall-off at higher energy.

The present data does not permit meaningful cross-section fitting for $\epsilon > 2$ eV, so it is as yet impossible to conjecture on higher energy-loss processes. The lowest electronically excited state is probably a triplet at 5.2 eV[6]. Bowman and Millar[12] observed threshold

energy losses at about 2 eV, but Boness et al.[99] failed to find any transmission structure indicative of a resonance at this energy.

V.4. CYCLOPROPANE

V.4.1. Experimental data

The present D/μ results were used in preference to those of Cochran and Forester[44]. The only W results are those of Bortner, Hurst, and Stone for $.05 \leq E/P \leq 1.4$ V $cm^{-1}torr^{-1}$. These were taken to be correct and extrapolated to 3 V $cm^{-1}torr^{-1}$ by analogy with ethylene. It should be noted, however, that the drift velocities reported by Bortner et al. for ethylene are lower than those of most authors, especially for $E/P \gtrsim 0.4$, and their cyclopropane data should therefore be treated with caution.

V.4.2. Cross-section analysis

Starting values for Q_m were obtained from calculations based on a Maxwellian distribution[65]. Calculations of λ on this basis give a peak value of $\sim.055$ at $E/P = 0.8$ V $cm^{-1}torr^{-1}$, corresponding to a mean swarm energy of approximately 0.11 eV. As with all the molecules previously discussed, this corresponds closely to the excitation energy of the lowest vibrational modes.

The vibrational analysis of cyclopropane is exceedingly complex as there are 21 normal modes, but the infrared spectrum shows only six active fundamentals:

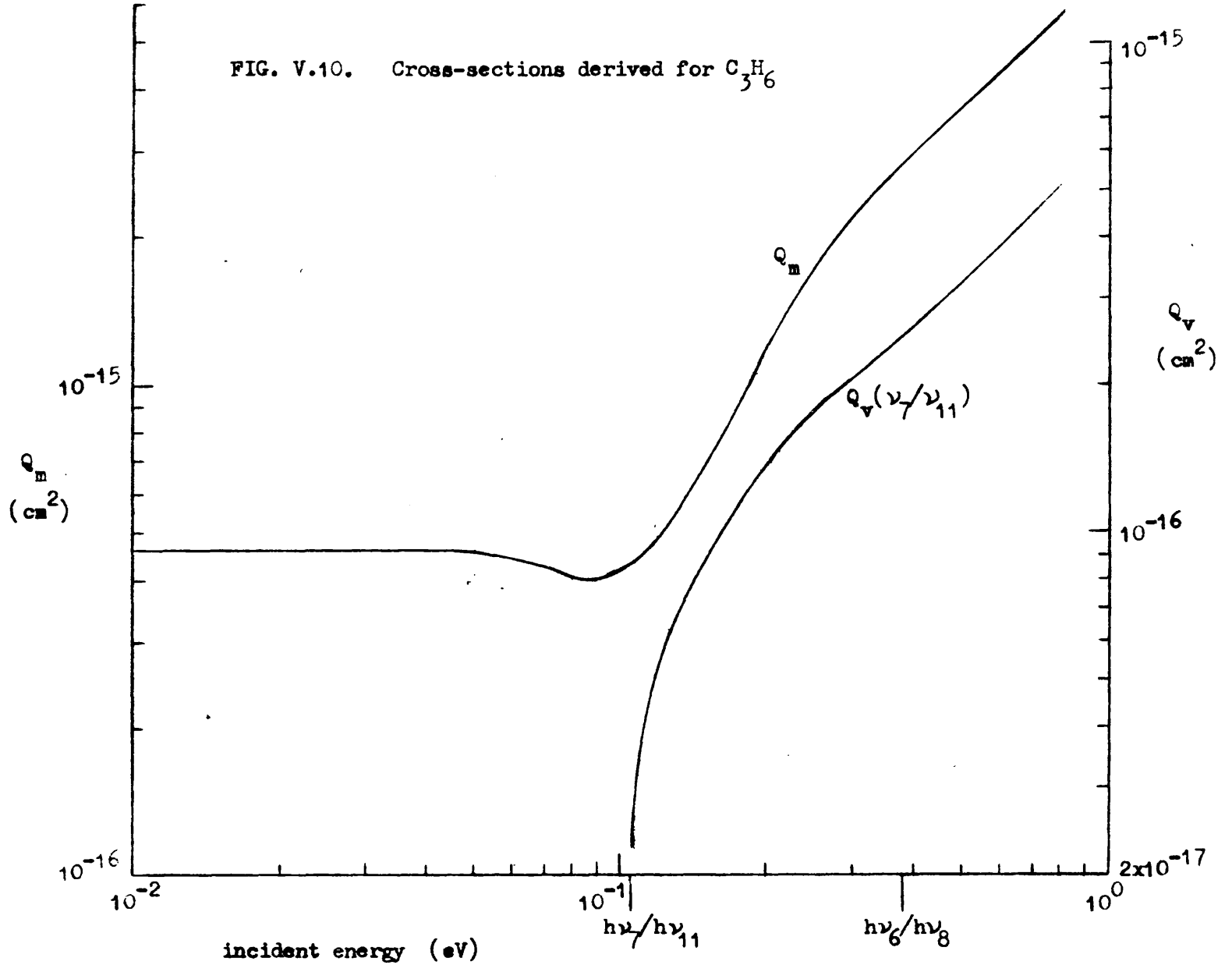

FIG. V.10. Cross-sections derived for C_3H_6

ν_{11}	(vs)	868 cm^{-1}	(.108 eV)	ring deformation
ν_7	(vs)	872 cm^{-1}	(.108 eV)	CH_2 rock
ν_{10}	(s)	1028 cm^{-1}	(.127 eV)	CH_2 bend
ν_9	(s)	1432 cm^{-1}	(.178 eV)	CH_2 deformation
ν_8	(vs)	3024 cm^{-1}	(.375 eV)	C-H stretch
ν_6	(vs)	3103 cm^{-1}	(.385 eV)	C-H stretch

There is little hope of distinguishing between these in a swarm experiment, except possibly to verify that excitation must be occurring at the lower thresholds. No attempt has been made at this stage to include more than one Q_v. As with C_2H_2, a single cross-section was used to represent inelastic processes, with a threshold at .108 eV corresponding to excitation of either or both of ν_{11} and ν_7. Using this Q_v the fitting procedure was carried out for transport data in the range $.05 \leq E/P \leq 3$ V $cm^{-1}torr^{-1}$. Two energy ranges were used, the lower having a step-length of 1.69 meV and the upper extending to 0.84 eV. Final cross-sections are presented in Table V.7 and Fig. V.10, and the calculated transport coefficients in Table V.8 and Fig. V.11. The calculated D/μ values appear to be about 10% low at low E/P and 10-15% high at the higher E/P. Further cross-section adjustments could be made to achieve a better fit but in view of the uncertainty of the experimental data, particularly the W values, and the computational time involved, further refinement was not considered to be justified.

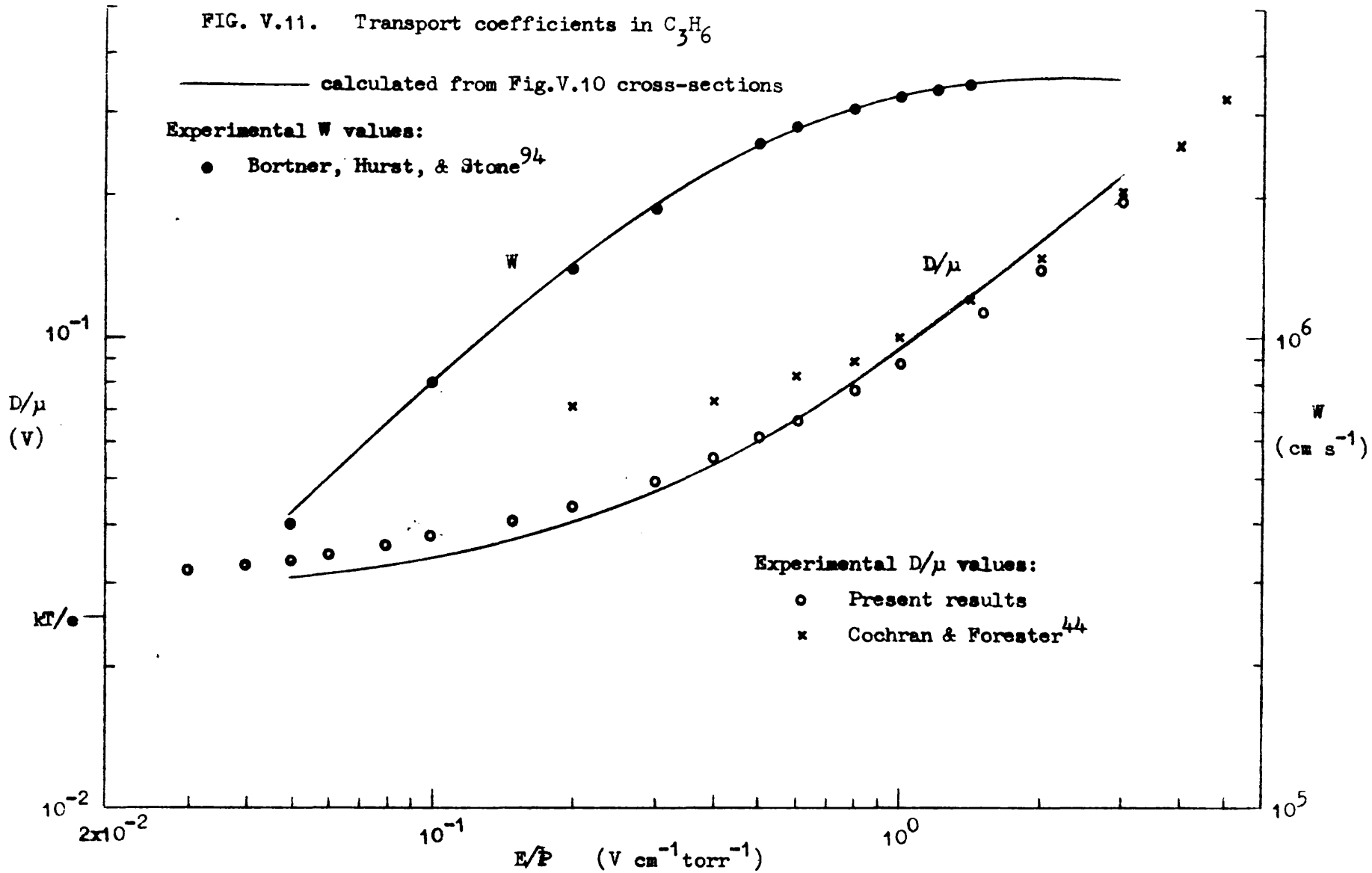
FIG. V.11. Transport coefficients in C_3H_6
calculated from Fig.V.10 cross-sections
Experimental W values:
Bortner, Hurst, & Stone[94]
W
D/μ
Experimental D/μ values:
Present results
Cochran & Forester[44]
10^{-1}
D/μ
(V)
kT/e
10^{-2}
$2x10^{-2}$
10^{-1}
10^{0}
E/P (V cm^{-1} $torr^{-1}$)
10^{6}
W
(cm s^{-1})
10^{5}

V.4.3. Final cross-sections

Q_m again appears to be constant at low energy, taking the value 4.6×10^{-16} cm^2 for $E/P \lesssim .05$ eV, quite close to the ethylene result. At higher energies, Q_m seems to rise much more sharply than in the ethylene case.

The Q_v derived here differs from the preceding cases in rising rather more slowly from threshold. In fact, if the present D/μ data is correct, the true rate of rise is possibly even less than that shown in Fig. V.10. However, if as suspected the experimental W data is too low, the effect would be to lower the overall magnitude of the derived Q_v (since $\lambda \propto W^2$). Again, the continued rise after threshold could be due to excitation of several higher modes. Brongersma and Oosterhoff[98] have obtained trapped-electron spectra showing unresolved energy losses between 1 and 6 eV (the onset of the first triplet state) but extension of swarm data to higher E/P is necessary before processes in this energy region can be studied.

V.5. HYDROGEN SULPHIDE

V.5.1. Experimental data

The present D/μ results are the only known swarm measurements in pure H_2S. Drift velocities have only been measured in low-concentration mixtures with C_2H_4[93,22]. By studying the drift velocity vs concentration dependence over various concentration ranges, Christophorou et al.[22]

concluded that the drift velocity W_P for a pure polar molecule could be related to that for ethylene (W_E) by

$$W_P = A.W_E$$

over the E/P range where the swarms are thermal. For H_2S, they gave A = .0176. However these authors assumed a thermal swarm in ethylene for E/P < 0.1 V $cm^{-1}torr^{-1}$, which has been found to be untrue (see V.2.4.). Nevertheless, if this value of A is combined with the thermal $\mu_t P$ for ethylene reported by Nelson and Davis[29], the resulting estimate of $\mu_t P$ for H_2S (= 0.191 $cm^2V^{-1}\mu s^{-1}torr$) can be taken to be reasonably accurate. This allows calculation of W values in H_2S for E/P $\lesssim$ 1 V $cm^{-1}torr^{-1}$, where according to the present work the swarm is practically thermal.

V.5.2. Applicability of cross-section analysis

The present method of cross-section analysis cannot be applied to H_2S for the following reasons:

(1) W values are only available for a thermal swarm, thus denying access to the energy variable in the usual way.

(2) As the gas is polar, the rotational excitation cross-sections are expected to be high, and a large proportion of momentum transfer collisions may involve exchange of rotational energy[50]. Since D/μ is close to thermal over most of the E/P range studied, the continuous approximation is inapplicable in this case. Exact

solution of the Boltzmann equation would be difficult owing to

(a) the close spacing of rotational levels, and

(b) the existence of three different rotational constants as H_2S is an asymmetric top.

In the previous gases studied, neglect of rotation was justifiable as the higher vibrational energy losses would be expected to dominate. However, for a polar gas, the rotational cross-sections might be considerably larger than those for vibrational excitation and this assumption would not be justified. However, a few sample calculations were made in order to assess whether the expected cross-section magnitude could explain the present D/μ results.

V.5.3. Calculations assuming elastic scattering only

If the Altshuler form (I.60) for the momentum-transfer cross-section is assumed, Christophorou et al. give the constant A to be 4.52 $cm^4 s^2$. This leads to a cross-section

$$Q_m = 12.9 \times 10^{-16}/\epsilon \qquad (V.8)$$

where ϵ is the energy in eV. Calculations were made for ϵ up to 0.5 eV, E/P up to 10 V $cm^{-1} torr^{-1}$, leading to the D/μ values shown by the dotted line in Fig. V.12, which are plainly far higher than the observed values. It is therefore, not surprisingly, essential to take inelastic collisions into account.

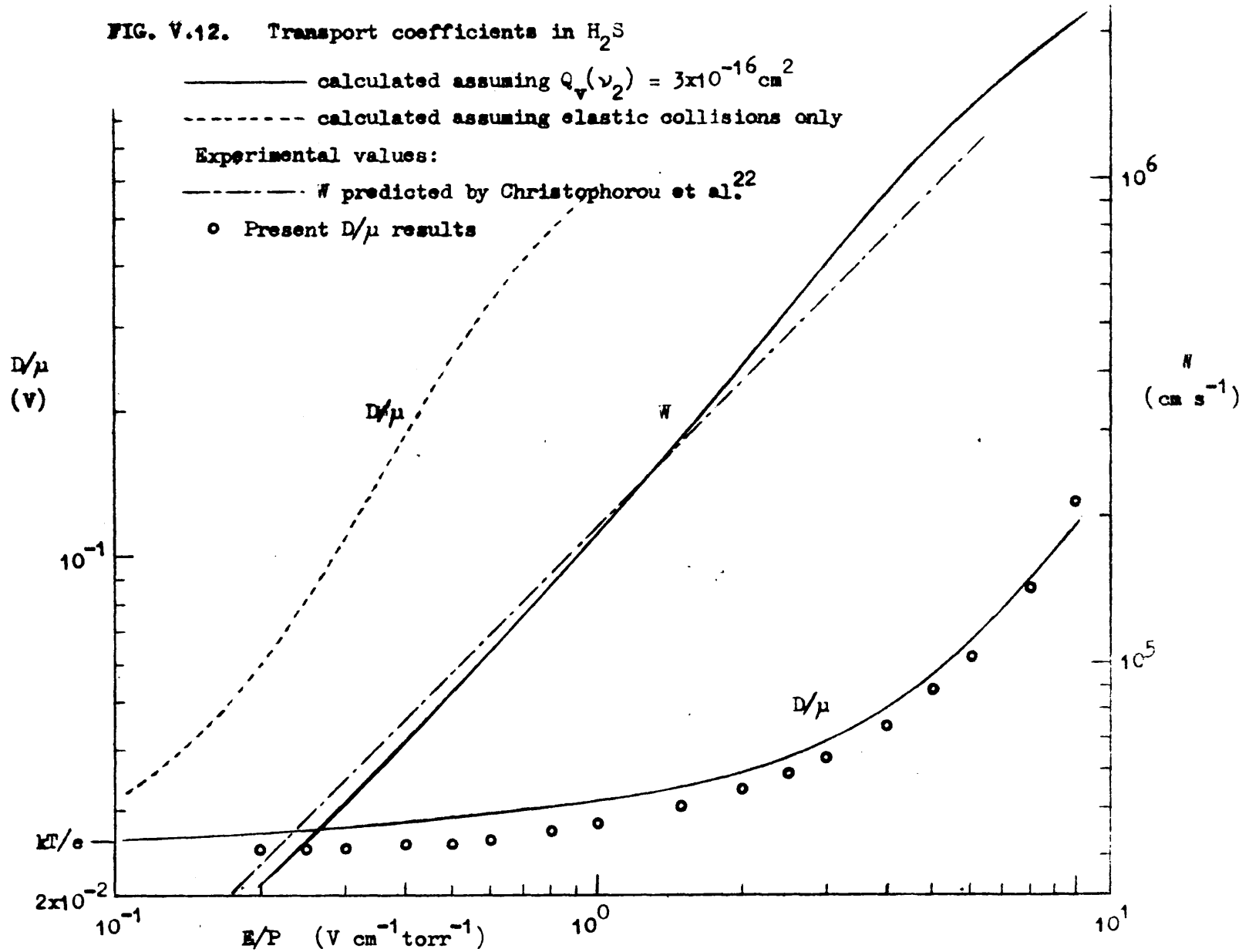
FIG. V.12. Transport coefficients in H_2S
calculated assuming $Q_v(\nu_2) = 3\times10^{-16}$ cm^2
calculated assuming elastic collisions only
Experimental values:
W predicted by Christophorou et al.[22]
Present D/μ results
D/μ (V)
W (cm s^{-1})
D/μ
W
D/μ
10^{-1}
10^6
10^5
kT/e
2×10^{-2}
10^{-1}
10^0
10^1
E/P (V cm^{-1} torr^{-1})

V.5.4. Calculations assuming vibrational excitation only

To account for the observed values of D/μ, an inelastic cross-section was introduced corresponding to single excitation of the ν_2 bending mode (threshold 0.160 eV). A constant value for this of $\sim 3 \times 10^{-16}$ cm^2 in the range $0.16 < \epsilon < 0.5$ eV was found to give a fair prediction of the observed D/μ. This is the rough order of magnitude expected for such a cross-section, but is probably an overestimate due to neglect of rotation and other vibrations. The transport coefficients obtained are shown in Fig. V.12.

V.5.5. Calculations assuming rotational excitation only

As stated, inclusion of rotational excitation presents difficulties in the case of H_2S. However for $D/\mu >> kT/e$ the continuous approximation should give a reasonable order-of-magnitude result.

In considering CO, Hake and Phelps[27] derived the particular form of the Boltzmann equation resulting from Takayanagi's expression for the rotational excitation cross-section of a dipolar molecule (I.62). However the form of the equation involving the "net rotational cross-section" Q'_r (see IV.2.3.) is more flexible since any given energy dependence can be incorporated in the trial values of Q'_r.

Takayanagi's theory gives

$$\sigma_{J\to J+1}(\epsilon) = \frac{R_y \sigma_r}{\epsilon} \cdot \frac{J+1}{2J+1} \ln \frac{\left[\epsilon^{\frac{1}{2}} + (\epsilon - \epsilon_J)^{\frac{1}{2}}\right]}{\left[\epsilon^{\frac{1}{2}} - (\epsilon - \epsilon_J)^{\frac{1}{2}}\right]} \qquad (V.9)$$

$$\sigma_{J\to J-1}(\epsilon) = \frac{R_y \sigma_r}{\epsilon} \cdot \frac{J}{2J+1} \ln \frac{\left[(\epsilon + \epsilon_{-J})^{\frac{1}{2}} + \epsilon^{\frac{1}{2}}\right]}{\left[(\epsilon + \epsilon_{-J})^{\frac{1}{2}} - \epsilon^{\frac{1}{2}}\right]} \qquad (V.10)$$

where $\sigma_r = 8\pi\mu^2 a_o^2/3$ and R_y is the Rydberg. Using the approximation given by Hake and Phelps[27] for the logarithmic terms, euqation (IV.20) for Q'_r becomes

$$Q'_r = 2^{\frac{3}{4}} B_o^{-\frac{1}{4}} R_y \sigma_r \epsilon^{-\frac{3}{4}} \sum_J \left[(J+1)^{7/4} - J^{7/4}\right] \exp\left[-J(J+1)B_o/kT\right]/P_J \qquad (V.11)$$

where P_J is the rotational partition function. For J values of interest, $(J+1)^{7/4} - J^{7/4}$ may be roughly approximated by $(2J+1)/2$, which simplifies (V.11) to

$$Q'_r \simeq 2^{\frac{1}{4}} B_o^{-\frac{1}{4}} R_y \sigma_r \epsilon^{-\frac{3}{4}} \qquad (V.12)$$

The above derivation has assumed a single rotational constant as in the heteronuclear diatomic case. H_2S however is an asymmetric top and therefore has three rotational constants, two of which (A_o and C_o) are associated with rotation of the total molecular dipole μ, whilst the third (B_o) is optically inactive. As the above expression for Q'_r is relatively insensitive to the value of the rotational constant, the constant A_o (10.39 cm^{-1}) was used here as it is associated with a greater energy exchange. The resulting estimate for Q'_r is

$$Q'_r \simeq 7.9\epsilon^{-\frac{3}{4}} \qquad (V.13)$$

A few trial calculations were carried out starting from this expression. In all cases no vibrational cross-section was incorporated, and Q_m was held at its previous value. A general finding was that the calculated D/μ was much more strongly dependent on E/P than observed. At low E/P ($\lesssim 2$ V $cm^{-1}torr^{-1}$) subthermal D/μ values resulted, a consequence

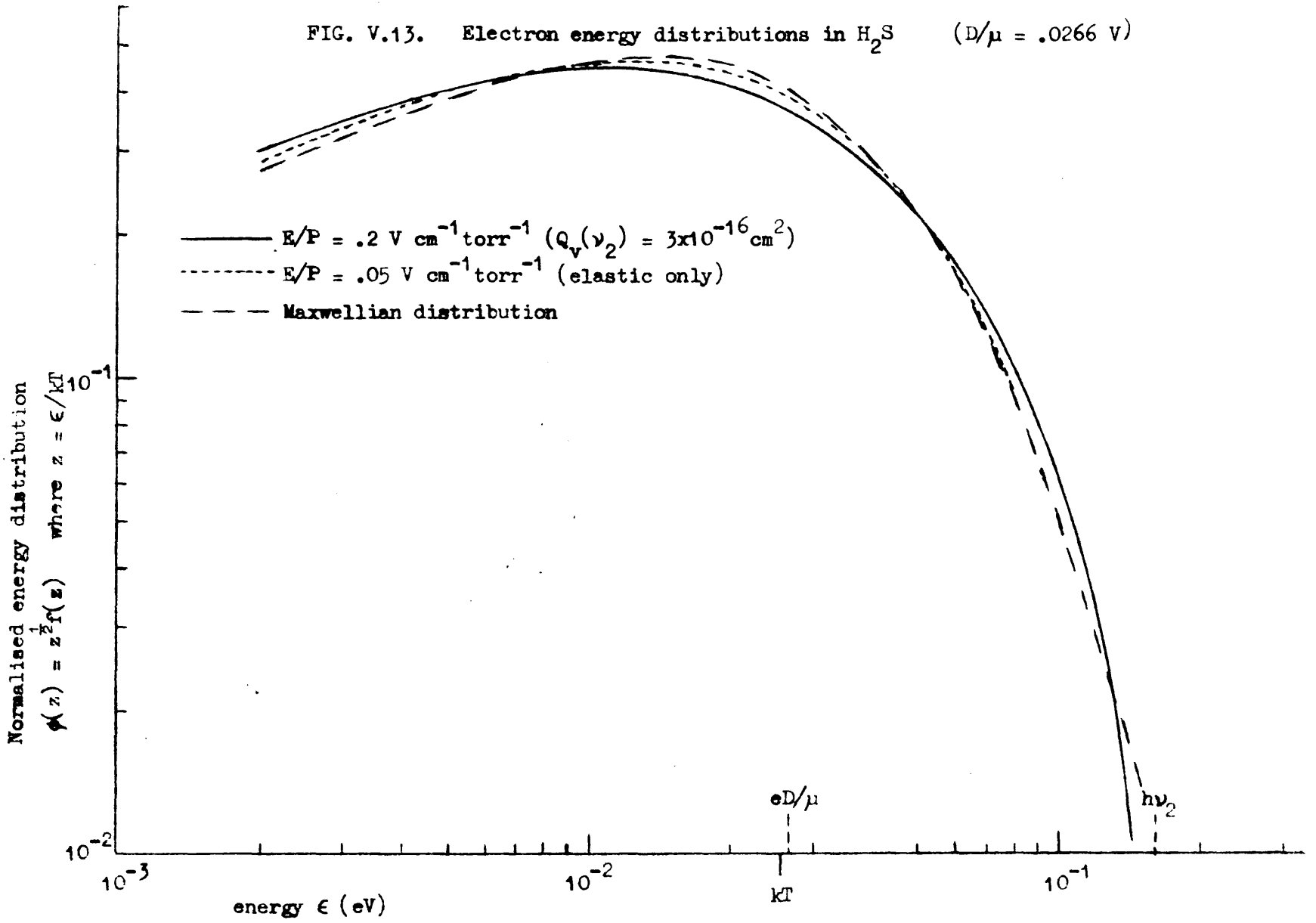
FIG. V.13. Electron energy distributions in H_2S (D/μ = .0266 V)
E/P = .2 V cm^{-1}torr^{-1} ($Q_v(\nu_2)$ = 3x10^{-16}cm^2)
E/P = .05 V cm^{-1}torr^{-1} (elastic only)
Maxwellian distribution
Normalised energy distribution
$\phi(z) = z^{\frac{1}{2}}f(z)$ where $z = \epsilon/kT$
10^{-1}
10^{-2}
10^{-3}
10^{-2}
10^{-1}
energy ϵ (eV)
eD/μ
kT
$h\nu_2$

of the breakdown of the continuous approximation as $D/\mu \rightarrow kT/e$. Results of the correct order of magnitude were obtained using (V.13) at $E/P \simeq 5$, but at $E/P = 10$ the calculated values are $\sim 60\%$ high. This suggests either that Q_r' decreases more rapdily than $\epsilon^{-\frac{3}{4}}$ (ϵ^{-1} was tried but gave insignificant improvement); or that vibrational excitation is serving to reduce D/μ. With the present limited information it is impossible to examine the situation in any detail, or even to assess the relative contribution of rotational and vibrational excitation.

V.5.6. Energy distribution in H_2S

Using the Q_v of V.5.4. (3×10^{-16} cm^2), the energy distribution function was calculated at $E/P = 0.2$ and is shown in Fig. V.13. Although it must be emphasised that the lack of unique cross-sections leads to lack of unique $f(\epsilon)$ (and particularly the neglect of rotational excitation gives an exaggerated departure from the Maxwellian), Fig. V.13 illustrates an important point: namely that a near-thermal D/μ does not necessarily imply a Maxwellian distribution.

V.5.7. Further remarks

The momentum-transfer cross-section given by Christophorou et al. appears to be consistent with the swarm data at low E/P, requiring the inclusion of inelastic cross-sections to explain the D/μ results at higher E/P. This value of Q_m has been noted[93,50] to be considerably

in excess of that given by Altshuler's theory (I.59), as is the case with several other inorganic hydrides[65,67]. Crawford et al.[50] stated that Altshuler's theory is unlikely to be reliable for molecules with low dipole moments such as H_2S, owing to the neglect of relatively important higher order interaction terms, but made no quantitative estimate of this. The postulate of temporary negative ion formation has been until recently contradicted by calculations of the critical binding moment (I.4.1.), but such theories based on simple point-dipole models are no longer held to be realistic and discussion of the implications of real potentials are continuing in the literature[69,106]. Bardsley and Mandl[52] have pointed out that the combination of the dipolar field with the short range forces may support low-energy bound states. The scattering of electrons by weakly polar molecules such as H_2S is thus probably not conducive to simple dominant-potential treatment such as that of Altshuler's theory.

V.6. CONCLUSIONS

It is evident from the foregoing attempts to analyse swarm data that the results as they stand are far from conclusive, and in the absence of evidence from more direct sources can only be regarded as a suggestion of what collision processes might reasonably be occurring. The variety of possible inelastic processes in the polyatomic species under study drastically reduces the degree of uniqueness in the derived cross-sections relative to that attainable for diatomic molecules.

Nevertheless, some tentative conclusions can be drawn. The results of the hydrocarbon analysis point to near-threshold single-level excitation as being the dominant vibrational process. Furthermore, the rate of energy loss can be satisfactorily explained by the excitation of infrared active modes, using cross-sections of the order of magnitude suggested by current theory[92]. However there are no definite grounds, experimental or theoretical, for completely discounting any contribution from excitation of inactive modes, particularly at threshold.

The uniqueness problem might be tackled further by adopting particular forms for the cross-section energy dependence, but such assumptions cannot readily be drawn from existing theory which is clearly inadequate in this energy region. It is not felt that the adoption of a series of peaks as used by Hake and Phelps would be relevant, as this approach was based on the postulate of narrow resonances.

There are no grounds at present for postulating near-threshold excitation through an intermediate resonant state. In fact the present results do not appear to be easily reconcilable with this picture, certainly as far as relatively long-lived resonances are concerned.

At impact energies below vibrational thresholds, few conclusions can be drawn from swarm analysis as collision effects are largely masked by the thermal motion of the gas. Thus rotational processes cannot easily be accounted for in the analysis - and even if they could, the insensitivity of transport coefficients to cross-sections in a near-thermal swarm would give a high uncertainty in the result.

Low-temperature experiments are the only foreseeable way of improving on this situation. Similarly, the anomalies in the apparent momentum-transfer cross-sections for CH_4 and H_2S will not be readily resolved by room-temperature experiments.

The correspondence between theory and experiment in this field was for many years unsatisfactory, principally as a result of over-simplified theory. There is now a large and rapidly expanding body of complex theory pertaining to electron-molecule collisions, although a mere fraction of the effort has been directed towards polyatomic molecules. In spite of the increasing complication of the theoretical models, it remains possible to distinguish between "resonance" and "direct" approaches. The former focus attention on the molecular state, regarding the colliding electron as a time-dependent component of the state; while the latter centre on the wavefunctions of the projectile and regard the molecular field primarily as a perturbing potential. However there are no rigid barriers between theories. For example, the early classification of resonances, while useful from an empirical viewpoint, has become hazy with increasing sophistication of treatment. Mittleman[110] has remarked that the resonant state is ill-defined and the classification is only qualitative. The tendency in "direct" theories is to take increasingly greater account of contributions from excited molecular states and electron exchange, emphasising the role of the "intermediate" state. The close similarity of the broad short-lived resonance model to direct scattering has already been mentioned (I.43). It is probably best to

regard the two types of scattering as alternative theoretical starting points for examining a complete spectrum of physical phenomena, the models representing the extreme cases which are not found in reality.

As an example of this flexibility in approach, the work of Gryzinski[111] must be mentioned. This author has taken a completely independent approach using classical mechanics in preference to wave mechanics. He treats the atom or molecule as a dynamic system of point charges moving in classical orbits, interacting with the projectile through the resulting oscillating multipole moments. In this way he has succeeded in explaining the Ramsauer effect, long held to be proof of the omnipotence of wave mechanics - mainly because of the failure of early classical descriptions based on static fields. In some ways Gryzinski's theory appears more closely related to physical reality than the quantum approaches.

There is a danger in collision physics, as in the wave mechanics of atomic and molecular structure, of the theories becoming increasingly abstract and less physically meaningful. In such a paradise of mathematics it should constantly be borne in mind that the relevance of any theory lies in its ability to predict observed phenomena, and that where two or more theories have equal merit in this respect, preference should be given to that which is most closely identified with the physical picture.

Table V.1. Cross-sections derived for CH_4 (Set 2)

ϵ (eV)	Q_m (10^{-16} cm^2)	$Q_v(\nu_4)$ (10^{-16} cm^2)	$Q_v(\nu_3)$ (10^{-16} cm^2)
0.010	100	0	0
0.015	42	0	0
0.020	23	0	0
0.030	9.0	0	0
0.050	3.6	0	0
0.070	1.24	0	0
0.10	1.62	0	0
0.15	1.22	0	0
0.20	1.04	0.35	0
0.30	1.04	0.62	0
0.50	1.68	0.24	0.64
0.70	2.2	0.19	0.28
1.0	2.8	0.20	0.19
1.5	3.8	0.23	0.22
2.0	5.1	0.28	0.27
3.0	7.2	0.31	0.30
5.0	13.6	0.30	0.30

Table V.2. Transport coefficients in CH_4

E/P ($V\ cm^{-1}\ torr^{-1}$)	W(calc.) ($cm\ s^{-1}$)	D/μ(calc.) (V)	$\frac{q_m^*(obs.)}{q_m^*(calc.)}$	$\frac{q_i^*(obs.)}{q_i^*(calc.)}$
0.04	5.00×10^{5}	3.50×10^{-2}	1.20	0.85
0.05	6.46	3.64	1.11	0.93
0.06	7.86	3.75	1.11	0.93
0.08	1.11×10^{6}	4.03	1.12	0.92
0.10	1.44	4.31	1.20	0.86
0.15	2.32	5.03	1.18	0.88
0.20	3.21	5.78	1.11	0.94
0.30	4.89	7.35	1.06	0.97
0.40	6.36	8.97	1.01	1.02
0.50	7.59	1.06×10^{-1}	0.97	1.04
0.60	8.60	1.23	0.97	1.01
0.80	1.00×10^{7}	1.57	0.97	0.98
1.0	1.07	1.96	1.00	0.96
1.5	1.07	3.13	1.01	0.93
2.0	9.83×10^{6}	4.57	0.99	0.93
3.0	8.19	7.95	0.97	0.96
4.0	7.21	1.15×10^{0}	1.00	0.99
5.0	6.57	1.50	1.00	0.98
6.0	6.10	1.84	0.99	1.01

Table V.3. Cross-sections derived for C_2H_4 (Set 2)

ϵ (eV)	Q_m (10^{-16} cm^2)	$Q_v(\nu_7)$ (10^{-16} cm^2)	$Q_v(\nu_2)$ (10^{-16} cm^2)
0.010	3.7	0	0
0.015	3.75	0	0
0.020	3.8	0	0
0.030	3.9	0	0
0.050	4.2	0	0
0.070	4.2	0	0
0.10	4.1	0	0
0.15	5.0	1.10	0
0.20	6.8	0.96	0
0.30	7.8	0.77	0
0.40	10.5	0.37	1.5
0.50	13.5	0.37	0.92
0.70	16	0.45	0.36
1.0	18	0.57	0.42
1.5	20	0.74	0.64
2.0	22	0.87	0.78
3.0	27	1.10	1.05
4.0	22	1.30	1.25

Table V.4. Transport coefficients in C_2H_4

E/P ($V\ cm^{-1}torr^{-1}$)	W(calc.) ($cm\ s^{-1}$)	D/μ(calc.) (V)	$\frac{q_m^*(obs.)}{q_m^*(calc.)}$	$\frac{q_i^*(obs.)}{q_i^*(calc.)}$
0.02	1.94×10^{5}	3.01×10^{-2}	1.01	1.07
0.03	2.89	3.06	1.02	1.03
0.04	3.83	3.09	1.00	1.03
0.05	4.76	3.13	1.00	1.02
0.06	5.67	3.16	1.02	1.00
0.08	7.45	3.24	1.03	0.99
0.10	9.18	3.32	1.00	0.99
0.15	1.33×10^{6}	3.53	0.97	1.01
0.20	1.70	3.76	0.98	0.97
0.30	2.34	4.31	0.99	0.97
0.40	2.89	4.87	0.98	0.97
0.50	3.32	5.48	1.00	0.96
0.60	3.66	6.14	1.00	0.99
0.80	4.12	7.56	1.00	1.03
1.0	4.41	9.06	1.01	1.05
1.5	4.83	1.27×10^{-1}	1.01	1.05
2.0	5.01	1.62	1.01	1.04
3.0	5.27	2.25	1.02	0.94
5.0	5.04	3.71	1.01	0.89
6.0	4.91	4.49	0.98	0.89
8.0	4.70	6.16	0.96	0.96
10	4.59	7.92	0.95	1.05
14	4.53	1.16×10^{0}	0.92	1.28

Table V.5. Cross-sections derived for C_2H_2

ϵ (eV)	Q_m (10^{-16} cm^2)	$Q_v(\nu_5)$ (10^{-16} cm^2)
0.01	9.5	0
0.015	9.5	0
0.02	9.5	0
0.03	9.5	0
0.05	10.3	0
0.07	12.5	0
0.10	15.5	4.8
0.15	17	4.9
0.20	18	4.9
0.30	19	5.3
0.40	20	5.7
0.50	21	5.9
0.70	23	6.2
1.0	26	6.3
1.5	30	6.3
2.0	34	6.2
2.5	38	6.2

Table V.6. Transport coefficients in C_2H_2

E/P ($V\ cm^{-1}\ torr^{-1}$)	W(calc.) ($cm\ s^{-1}$)	D/μ(calc.) (V)	$\frac{q_m^*(obs.)}{q_m^*(calc.)}$	$\frac{q_i^*(obs.)}{q_i^*(calc.)}$
0.15	5.51×10^5	2.83	0.98	1.07
0.20	7.25	2.95×10^{-2}	0.97	1.07
0.30	1.04×10^6	3.11	0.99	1.06
0.40	1.34	3.27	1.00	1.07
0.50	1.61	3.42	1.01	1.06
0.60	1.87	3.57	1.00	1.07
0.80	2.33	3.88	1.02	1.06
1.0	2.74	4.19	1.04	1.03
1.5	3.55	4.99	1.05	1.04
2.0	4.15	5.85	1.06	1.04
3.0	4.92	7.82	1.07	1.02
4.0	5.35	1.01×10^{-1}	1.03	0.97
5.0	5.51	1.30	1.00	0.96
6.0	5.66	1.61	1.01	0.94
8.0	5.68	2.36	1.02	0.97
10	5.69	3.18	1.04	1.00
14	5.53	5.14	0.91	1.04
19	5.87	8.23	0.97	1.05

Table V.7. Cross-sections derived for C_3H_6

ϵ (eV)	Q_m (10^{-16} cm^2)	$Q_v(\nu_7/\nu_{11})$ (10^{-16} cm^2)
0.010	4.6	0
0.015	4.6	0
0.020	4.6	0
0.030	4.6	0
0.050	4.5	0
0.070	4.3	0
0.10	4.3	0
0.15	7.3	0.89
0.20	12.5	1.45
0.30	23	2.1
0.50	38	3.2
0.70	52	4.5

Table V.8. Transport coefficients in C_3H_6

E/P ($V\ cm^{-1}torr^{-1}$)	W(calc.) ($cm\ s^{-1}$)	D/μ(calc.) (V)	$\frac{q_m^*(obs.)}{q_m^*(calc.)}$	$\frac{q_i^*(obs.)}{q_i^*(calc.)}$
0.05	4.25×10^5	3.05×10^{-2}	1.01	0.89
0.08	6.55	3.26	0.97	0.92
0.10	8.00	3.39	0.94	0.94
0.20	1.43×10^6	4.04	0.98	0.94
0.30	1.93	4.71	0.99	0.96
0.50	2.59	6.15	0.99	1.00
0.80	3.14	8.26	1.04	1.01
1.0	3.34	9.66	1.05	1.03
1.4	3.52	1.24×10^{-1}	1.07	1.06
2.0	3.59	1.64	1.08	1.09
3.0	3.55	2.26	1.09	1.06

REFERENCES

1. N.F. Mott & H.S.W. Massey, "The Theory of Atomic Collisions", 3rd ed., O.U.P., (1965)
2. H.S,W. Massey & E.H.S. Burhop, "Electronic & Ionic Impact Phenomena", 2nd ed., Vol.I, O.U.P. (1969)
3. H.S.W. Massey, "Electronic & Ionic Impact Phenomena", 2nd ed., Vol.II, O.U.P. (1969)
4. D.E. Golden & H.W. Bandel, Phys.Rev. 138, A14 (1965)
5. J.S. Townsend & V.A. Bailey, Phil.Mag. 44, 1033 (1922)
6. S. Trajmar, J.K. Rice, & A. Kuppermann, Advan.Chem.Phys. 18, 15 (1970)
7. H. Ehrhardt & F. Linder, Phys.Rev.Letters 21, 419 (1968)
8. E.N. Lassettre & S.A. Francis, J.Chem.Phys. 40, 1208 (1964)
9. E.N. Lassettre, A. Skerbele, & V.D. Meyer, J.Chem.Phys. 45,3214 (1966)
10. P.S.P. Wei, Thesis, California Institute of Technology (1967)
11. G.J. Schulz, Phys.Rev. 112, 150 (1958)
12. C.R. Bowman & W.D. Miller, J.Chem.Phys. 42, 681 (1965)
13. G.J. Schulz, Phys.Rev.Letters 10, 104 (1963)
14. N.E. Bradbury & R.A. Nielsen, Phys.Rev. 49, 388 (1936)
15. G.S. Hurst, L.B. O'Kelly, E.B. Wagner, & J.A. Stockdale, J.Chem.Phys. 39, 1341 (1963)
16. G. Cavalleri, E. Gatti, & P. Principi, Nuov.Cim. 31, 302 (1964)
17. T.L. Cottrell & I.C. Walker, Quart.Rev. 20, 153 (1966)
18. R. Grünberg, Z.Phys. 204, 12 (1967)
19. W.P. Allis, in 'Handbuch der Physik' (ed. S.Flügge) Vol.21, Springer-Verlag, Berlin (1956)
20. J.L. Pack & A.V. Phelps, Phys.Rev. 121, 798 (1961)
21. J.L. Pack, R.E. Voshall, & A.V. Phelps, Phys.Rev. 127, 2084 (1962)
22. L.G. Christophorou, G.S. Hurst, & W.G. Hendrick, J.Chem.Phys. 45, 1081 (1966)
23. C.R. Bowman & D.E. Gordon, J.Chem.Phys. 46, 1878, (1967)
24. L.S. Frost & A.V. Phelps, Phys.Rev. 127, 1621 (1962)

25. A.G. Engelhardt & A.V. Phelps, Phys.Rev. 131, 2115 (1963)
26. A.G. Engelhardt, A.V. Phelps, & C.G. Risk, Phys.Rev. 135, A1566 (1964)
27. R.D. Hake & A.V. Phelps, Phys.Rev. 158, 70 (1967)
28. H.R. Skullerud, J.Phys.B 2, 696 (1969)
29. D.R. Nelson & F.J. Davis, J.Chem.Phys. 51, 2322 (1969)
30. K. Takayanagi, Prog.Theor.Phys.Suppl.(Japan) 40, 216 (1967)
31. L.G.H. Huxley & R.W. Crompton, in 'Atomic & Molecular Processes' (ed. Bates), Academic, N.Y. (1962)
32. R.W. Crompton & R.L. Jory, Aust.J.Phys. 15, 451 (1962)
33. R.W. Crompton, M.T. Elford, & J. Gascoigne, Aust.J.Phys. 18, 409 (1965)
34. J.H. Parker & J.J. Lowke, Phys.Rev. 181, 290 & 302 (1969)
35. J.H. Parker & R.W. Warren, Rev.Sci.Instr. 33, 948 (1961)
36. J.H. Parry, in 'Methods in Paleomagnetism'(ed. Collinson, Crier, & Runcorn), Elsevier
37. J.L. Moruzzi, Rev.Sci.Instr. 38, 1284 (1967)
38. B.S. Liley, Aust.J.Phys. 20, 527 (1967)
39. R.W. Crompton, M.T. Elford, & A.I. McIntosh, Aust.J.Phys. 21, 43 (1968)
40. R.W. Warren & J.H. Parker, Phys.Rev. 128, 2661 (1962)
41. L.G.H. Huxley & R.W. Crompton, Proc.Phys.Soc. B68, 381 (1955)
42. J.L.A. Francey, J.Phys.B 2, 669 & 680 (1969)
43. T.L. Cottrell & I.C. Walker, Trans.Faraday Soc. 63, 549 (1967)
44. L.W. Cochran & D.W. Forester, Phys.Rev. 126, 1785 (1962)
45. W.J. Pollock, Thesis, Edinburgh University (1967)
46. J.A. Rees, Aust.J.Phys. 18, 41 (1965)
47. E.B. Wagner, F.J. Davis, & G.S. Hurst, J.Chem.Phys. 47, 3138 (1967)
48. L.G. Christophorou, E.L. Chaney, & A.A. Christodoulides, Chem.Phys.Letters 3, 363 (1969)
49. T.L. Cottrell & I.C. Walker, Trans.Faraday Soc. 61, 1585 (1965)
50. O.H. Crawford, A. Dalgarno, & P.B. Hays, Molec.Phys. 13, 181 (1967)
51. J.D. Craggs & H.S.W. Massey, in 'Handbuch der Physik'(ed. S. Flügge), Vol.37/1,Springer-Verlag (1959)

52. J.N. Bardsley & F. Mandl, Rep.Progr.Phys. 31, 471 (1968)
53. H.S. Taylor, Advan.Chem.Phys. 18, 91 (1970)
54. G.V. Nazaroff, Chem.Phys.Letters 6, 138 (1970)
55. A. Herzenberg & F. Mandl, Proc.Roy.Soc. A270, 48 (1962)
56. J.C.Y. Chen, J.Chem.Phys. 40, 3507 & 3513 (1964)
57. J.B. Fisk, Phys.Rev. 49, 167 (1936)
58. H.S.W. Massey & R.O. Ridley, Proc.Phys.Soc. A69, 659 (1956)
59. D.G. Truhlar, J.K. Rice, S. Trajmar, & D.C. Cartwright, Chem.Phys.Letters 9, 299 (1971)
60. E. Brüche, Ann.Phys. 4, 387 (1930)
61. W.J. Pollock, Trans.Faraday Soc. 64, 2919 (1968)
62. R.A. Buckingham, H.S.W. Massey, & S.R. Tibbs, Proc.Roy.Soc. A178, 119 (1941)
63. S. Altshuler, Phys.Rev. 107, 114 (1957)
64. M.H. Mittleman & R.E. von Holdt, Phys.Rev. 140, A726 (1965)
65. T.L. Cottrell, W.J. Pollock, & I.C. Walker, Trans.Faraday Soc. 64, 2260 (1968)
66. J.A. Stockdale, L.G. Christophorou, J.E. Turner, & V.E. Anderson, Phys.Rev.Letters 25A, 510 (1967)
67. L.G. Christophorou & A.A. Christodoulides. J.Phys.B 2, 71 (1969)
68. W.R. Garrett, Chem.Phys.Letters 5, 393 (1970)
69. C. Bottcher, Chem.Phys.Letters 9, 57 (1971)
70. K. Takayanagi & Y. Itikawa, J.Phys.Soc.Japan 24, 160 (1968)
71. E. Gerjuoy & S. Stein, Phys.Rev. 97, 1671 (1955)
72. E. Gerjuoy & S. Stein, Phys.Rev. 98, 1848 (1955)
73. R.W. Crompton, D.K. Gibson, & A.I. McIntosh, Aust.J.Phys. 22,715 (1969)
74. S. Geltman & K. Takayanagi, Phys.Rev. 143, 25 (1966)
75. N.F. Lane & S. Geltman, Phys.Rev. 160, 53 (1967)
76. R.J.W. Henry & N.F. Lane, Phys.Rev. 183, 221 (1969)
77. R.A. Abram & A. Herzenberg, Chem.Phys.Letters 3,187 (1969)
78. G.J. Schulz, Phys.Rev. 135, A988 (1964)

79. J.N. Bardsley, A. Herzenberg, & F. Mandl, Proc.Phys.Soc. 89, 305 & 321 (1966)

80. H. Ehrhardt, L. Langhans, F. Linder, & H.S. Taylor, Phys.Rev. 173, 222 (1968)

81. P.D. Burrow & G.J. Schulz, Phys.Rev. 187, 97 (1969)

82. G.J. Schulz, Phys.Rev. 125, 229 (1962)

83. J.C.Y. Chen, J.Chem.Phys. 45, 2710 (1966)

84. V.N. Soshnikov, Opt.Spectrosc. 28, 457 (1970)

85. E.L. Breig & C.C. Lin, J.Chem.Phys. 43, 3839 (1965)

86. M.J.W. Boness & G.J. Schulz, Phys.Rev.Letters 21, 1031 (1968)

87. Y. Singh, J.Phys.B 3, 1222 (1970)

88. J.C.D. Brand & J.C. Speakman, "Molecular Structure", Arnold (1964)

89. A. Skerbele, M.A. Dillon, & E.N. Lassettre, J.Chem.Phys.49, 5042 (1968)

90. J. Geiger & K. Wittmaack, Z.Phys. 187, 433 (1967)

91. R.A. Bonham & J. Geiger, J.Chem.Phys. 51, 5246 (1969)

92. C.R. Claydon, G.A. Segal, & H.S. Taylor, J.Chem.Phys. 52, 3387 (1970)

93. G.S. Hurst, J.A. Stockdale, & L.B. O'Kelly, J.Chem.Phys. 38,2572 (1963)

94. T.E. Bortner, G.S. Hurst & W.G. Stone, Rev.Sci.Instr. 28, 103 (1957)

95. J. Bannon & H.L. Brose, Phil.Mag. 6, 817 (1928)

96. L. Frommhold, Phys.Rev. 172, 118 (1968)

97. D.J. Kouri, W.N. Sams, & L. Frommhold, Phys.Rev. 164, 285 (1969)

98. H.H. Brongersma & L.J. Oosterhoff, Chem.Phys.Letters 3, 437 (1969)

99. M.J.W. Boness, J.B. Hasted, L. Moore, & I.W. Larkin, Chem.Phys.Letters 1, 292 (1967)

100. M.-J. Hubin-Franskin & J.E. Collin Intern.J.Mass Spectrom.Ion Phys. 5, 163 (1970)

101. A.A. Christodoulides & L.G. Christophorou, J.Chem.Phys.54, 4691 (1971)

102. L.G. Christophorou, D.L. McCorkle, & J.G. Carter, J.Chem.Phys. 54, 253 (1971)

103. G. Herzberg, "I.R. & Raman Spectra of Polyatomic Molecules", Van Nostrand, Princeton (1945)

104. A. Stamatovic & G.J. Schulz, Phys.Rev. 188, 213 (1969)

105. Y. Itikawa, Phys.Rev.A 3, 831 (1971)
106. W.R. Garrett, Phys.Rev.A 3, 961 (1971)
107. R.W. Crompton & A.G. Robertson, Aust.J.Phys. (to be published)
108. W. Legler, Phys.Letters 31A, 129 (1970)
109. H. Lehning, Phys.Letters 29A, 719 (1969)
110. M.H. Mittleman, Phys.Rev. 182, 128 (1969)
111. M. Gryzinski, Institute of Nuclear Research, Warsaw, Report No.1217/SLFP/PP
112. T. Holstein, Phys.Rev. 70, 367 (1946)
113. D.K. Gibson, Aust.J.Phys. 23, 683 (1970)
114. H. Myers, J.Phys.B 2, 393 (1969)
115. G. Cavalleri & G. Sesta, Phys.Rev. 170, 286 (1968)
116. G. Cavalleri, Phys,Rev.Letters 23, 907 (1969)
117. J.H. Parker, Phys.Rev. 132, 2096 (1963)

ACKNOWLEDGEMENTS

I wish to record my sincere thanks to Dr. Isobel Walker for initiating and supervising this project, and for her continued advice and support. I also wish to thank Don Dance, Andy Barrie and Hamish Porter for many useful discussions; Brian Povey for invaluable technical advice; John Dyer, Campbell Chesterman and Bill Stirling for assistance and co-operation; and Professor R.P. Bell for providing financial support.